JACS
JOURNAL OF THE AMERICAN CHEMICAL SOCIETY

Article

pubs.acs.org/JACS

Architecture Mapping of the Inner Mitochondrial Membrane Proteome by Chemical Tools in Live Cells

Song-Yi Lee,[†] Myeong-Gyun Kang,[†] Sanghee Shin,[‡,§] Chulhwan Kwak,[†] Taejoon Kwon,[∥] Jeong Kon Seo,[*,⊥] Jong-Seo Kim,[*,‡,§] and Hyun-Woo Rhee[*,†]

[†]Department of Chemistry and [∥]Department of Biomedical Engineering, [⊥]UNIST Central Research Facilities (UCRF), Ulsan National Institute of Science and Technology (UNIST), Ulsan 44919, Korea

[‡]Center for RNA Research, Institute of Basic Science (IBS), Seoul 08826, Korea

[§]School of Biological Sciences, Seoul National University, Seoul 08826, Korea

Supporting Information

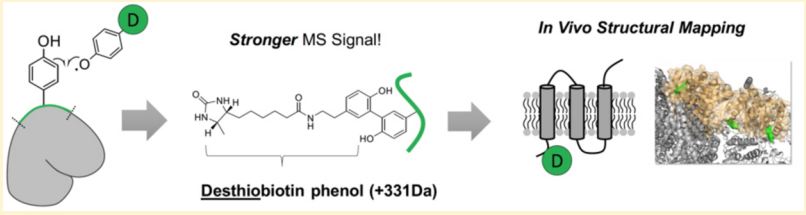

ABSTRACT: The inner mitochondrial membrane (IMM) proteome plays a central role in maintaining mitochondrial physiology and cellular metabolism. Various important biochemical reactions such as oxidative phosphorylation, metabolite production, and mitochondrial biogenesis are conducted by the IMM proteome, and mitochondria-targeted therapeutics have been developed for IMM proteins, which is deeply related for various human metabolic diseases including cancer and neurodegenerative diseases. However, the membrane topology of the IMM proteome remains largely unclear because of the lack of methods to evaluate it in live cells in a high-throughput manner. In this article, we reveal the in vivo topological direction of 135 IMM proteins, using an in situ-generated radical probe with genetically targeted peroxidase (APEX). Owing to the short lifetime of phenoxyl radicals generated in situ by submitochondrial targeted APEX and the impermeability of the IMM to small molecules, the solvent-exposed tyrosine residues of both the matrix and intermembrane space (IMS) sides of IMM proteins were exclusively labeled with the radical probe in live cells by Matrix-APEX and IMS-APEX, respectively and identified by mass spectrometry. From this analysis, we confirmed 58 IMM protein topologies and we could determine the topological direction of 77 IMM proteins whose topology at the IMM has not been fully characterized. We also found several IMM proteins (e.g., LETM1 and OXA1) whose topological information should be revised on the basis of our results. Overall, our identification of structural information on the mitochondrial inner-membrane proteome can provide valuable insights for the architecture and connectome of the IMM proteome in live cells.

INTRODUCTION

The inner mitochondrial membrane (IMM) is one of the most active sites for cellular metabolism.[1,2] The IMM proteome conducts various essential biochemical reactions such as oxidative phosphorylation, metabolite production, and mitochondrial biogenesis. Many IMM proteins form macromolecular complexes at the IMM (e.g., OxPhos complex,[3−6] TIM/TOM complex,[7] MICOS complex,[8] MCU complex,[9] and mitochondrial nucleoid complex[10]), and the IMM proteins in each complex are often coupled with each other to regulate mitochondrial physiology.[11,12] Because abnormal functionality of IMM protein complexes are directly connected to various human metabolic diseases including cancer, diabetes, aging and neurodegenerative diseases,[13−15] it is crucial to understand the correct architecture of the IMM proteome in live cells for efficient development of mitochondria-targeted therapeutics.[16,17] However, there has been no method to reveal the topology of mitochondrial membrane proteins in live cells until now.

Conventional biochemical assays for the topological identification of mitochondrial membrane proteins have been applied only to purified organelle, and the results were often controversial.[18] Furthermore, this method could not be employed in a high-throughput manner. Additionally, several three-dimensional (3D) protein structure analysis methods (e.g., X-ray crystallography and NMR spectroscopy) have been employed only for ultrapurified samples.[3−6] However, these techniques are also limited by the quantity, solubility, and crystallizability of the protein required for the analyses for other membrane protein complexes.[19] Furthermore, all of these in vitro samples are evaluated under nonphysiological conditions; thus, the structures determined by these methods might not

Received: October 10, 2016
Published: February 3, 2017

DOI: 10.1021/jacs.6b10418
J. Am. Chem. Soc. 2017, 139, 3651−3662

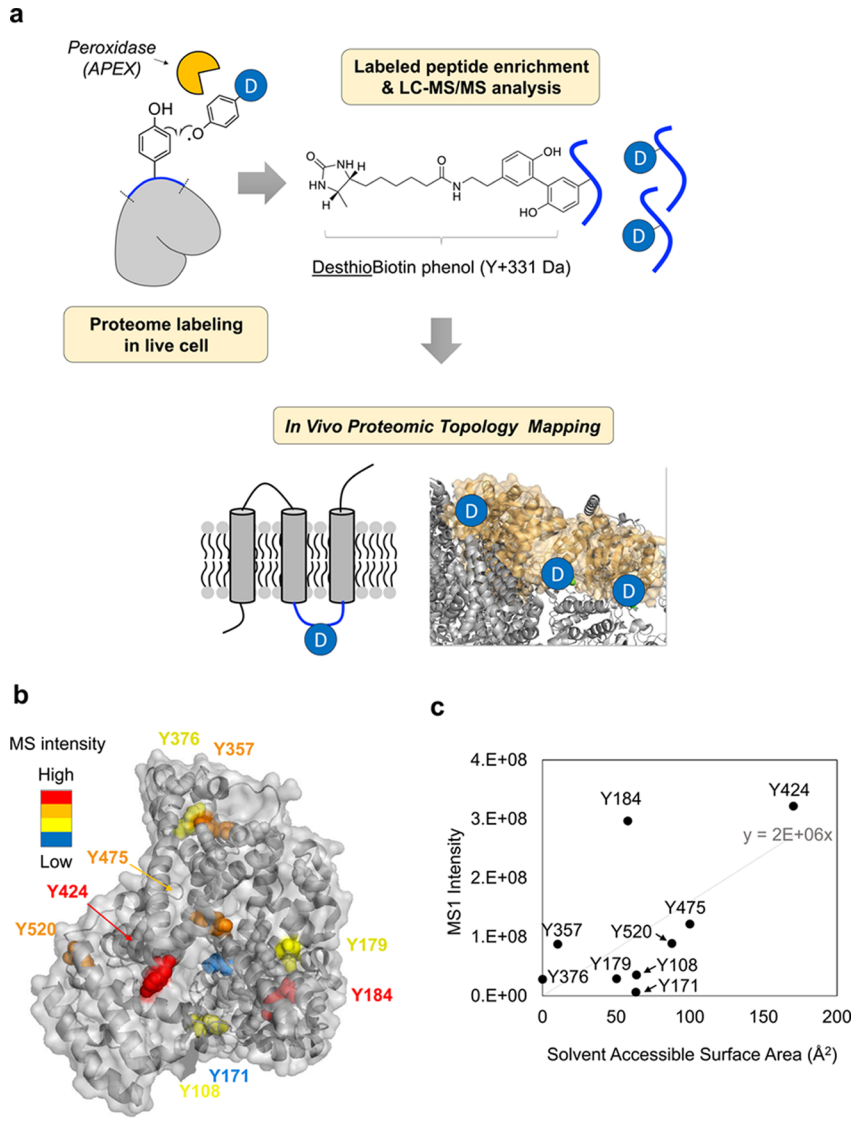

Figure 1. In vivo proteomic topology mapping by LC−MS/MS analysis. (a) Scheme of DBP-labeling method and the identification of labeled site for topology mapping. (b) Mapping of DBP-labeled sites on BSA (PDB ID: 3 V03). The labeled sites are marked with different colors according to the MS1 intensity of the labeled peptides. (c) Correlation graph between solvent accessible surface area (Å^2, *x*-axis) and MS1 intensity of labeled peptide per labeled sites on BSA.

perfectly reflect the endogenous protein structure under the heterogeneous conditions of live cells (e.g., protein−protein interactions, post-translational modifications).[20] Thus, another tool that can orthogonally provide in vivo structural information on proteins is required.

In this article, we introduce a new proteomic architecture mapping method by in situ-generated phenoxyl radical probe. Owing to the short lifetime (<1 ms) of phenoxyl radical in aqueous solution,[21] the radical-labeled tyrosine residues may reflect the solvent-exposed sites on the endogenous proteins. Moreover, this radical probe can be in situ generated by genetically targeted peroxidase (APEX) in subcompartmental space of mitochondrion. Thus, the mass spectrometry (MS) identification of labeled tyrosine residues provides topological information on the labeled proteins at each subcompartmental space of the mitochondrion. It is noteworthy that previous analyses by using APEX labeling could not resolve structural identification because these analyses performed based on the unlabeled peptide detection.[21−24]

Topological information can be obtained only by the mass spectrometric analysis of directly modified peptides by phenoxyl radicals. In previous studies, however, only a handful of the labeled peptide were identified mainly due to poor recovery of biotinylated peptides from streptavidin (SA)-beads.[21,22] Consequently, with those lacking number of the labeled sites, a thorough investigation about the correlation between the MS intensity and the solvent exposure level of the labeled peptides could not be carried out. Thus, we designed a new chemical probe, desthiobiotin-phenol that enabled more efficient recovery and stronger MS intensity of the labeled peptides, and applied it to topological mapping of IMM proteome. Our new method resulted in significantly comprehensive identification of labeled sites (Spot-ID) from in situ labeling of mitochondrial matrix and IMM proteome. With the most comprehensive labeled site information so far, we expanded and corrected the topological annotation of mitochondrial membrane proteins, providing a proteomic architecture of IMM proteome in live mammalian cells.

DOI: 10.1021/jacs.6b10418
J. Am. Chem. Soc. 2017, 139, 3651−3662

RESULTS

Characterization of the Desthiobiotin-phenol (DBP)-Labeling by LC−MS/MS Analysis. The thioether of conventional probe, biotin-phenol (BP), in labeled peptides is easily oxidized to the sulfoxide group during the radical generation reaction,[25,26] which may reduce the signal intensity of the labeled peptides and consequently compromises the identification of low-abundant or inefficiently labeled proteins. In fact, the LC−MS intensity of the oxidized BP-labeled peptides on the tyrosine residue (+377 Da) amounted up to ∼20% of the BP-labeled, original peptides (+361 Da) in human cell lines (Supporting Figure S1). However, the significant sulfur oxidation of BP might be solved by using nonsulfurated biotin or desthiobiotin,[27] as desthiobiotin also has a sufficient binding affinity to SA. Thus, we synthesized desthiobiotin-phenol (DBP) and analyzed its labeled peptides on tyrosine residue (+331 Da) in BSA by LC−MS/MS (Figure 1a). Several DBP-labeled peptides were identified without any further oxidation on DBP, whereas BP-labeled peptides showed an oxidized product at the same sequence (Supporting Figure S1a and Supporting Data Set S1). Notably, LC−MS/MS analysis also indicated that both DBP- and BP-labeled peptides are shown multiple times on the chromatogram, suggesting that heterogeneous products form during the radical coupling reaction (Supporting Figure S1b).

Before SA-enrichment, DBP-labeled peptides showed comparable MS1 intensity to BP-labeled peptides with the identically labeled sites in the 1:1 mixture of BP- and DBP-labeled BSA digests (Supporting Figure S2a). This result indicates that the global labeling efficiency of DBP-labeling is similar to that of BP-labeling. After SA-enrichment, however, the relative intensity of DBP-labeled BSA peptides was enhanced to ∼30% over that of BP-labeled BSA peptides (Supporting Figure S2b), whereas the MS2 response of both labeled peptides with the identical sequence was very similar in terms of fragmentation pattern (Supporting Figure S2c). These results from BSA suggest that the improved MS sensitivity of DBP-labeling might be mainly attributed to the increased elution efficiency of DBP than BP from the SA-beads, not to increased labeling efficiency. The relative affinity difference in both biotin and desthiobiotin to SA also supports this hypothesis. The solid binding affinity (K_a = 10^{15} M^{-1}) of biotin to SA might be too strong to allow detergent-free elution of the biotin-labeled peptides even in the harsh elution condition.[28] However, the lower binding affinity (K_a = 10^{12} M^{-1}) of desthiobiotin toward SA not only appears to be sufficient to bind the labeled peptides to the SA-beads but may also enable the labeled peptides to be easily released from the SA-beads in the detergent-free elution condition (e.g., formamide elution), which is friendly for LC−MS/MS analysis. This result supports that the topology mapping based on the proximity of labeled sites would be practical in proteomic scale using APEX with a DBP probe.

Furthermore, we found there was a positive correlation between the MS1 signal intensity of peptides containing DBP-labeled tyrosine and solvent accessible surface area (SASA, Å^2) of the labeled tyrosine in crystal structure of BSA (Figure 1b and c). Among the labeled tyrosine residues of BSA, we noted solvent-exposed tyrosine residues (Y424, Y475) showed higher MS1 labeling intensity compared with other buried tyrosine residues (Y357, Y376) of BSA. This result implies that DBP radical more efficiently reacts with more exposed tyrosine residues and the MS1 intensity level of labeled peptides can be used for the rough estimation or comparison of solvent exposed surface area of labeled tyrosine. It is noteworthy that Y376, which is completely buried Tyr residue (SASA = 0 Å^2) in BSA crystal structure, was also labeled by DBP (Figure 1b and c). This result suggests that Y376 might be temporally solvent-exposed and could be reacted with DBP radical during dynamic structural changes in solution at room temperature.[29]

Submitochondrial Proteome Mapping by Spot-ID. To investigate the reactivity of DBP with subcellularly expressed APEX in living cells, we treated various APEX2[30] conjugate-expressing cells with BP (500 μM) and DBP (500 μM). As shown in Supporting Figure S3a, BP and DBP generated remarkably similar labeled-protein band patterns, indicating that DBP retains comparable membrane permeability and reactivity with APEX, and its phenoxyl radical efficiently reacted with endogenous proteins as well. To monitor the SA-bead-enrichment property of DBP-labeled proteins, BP- and DBP-labeled proteome by SCO1-APEX2 were analyzed by SA-HRP Western blots before and after enrichment using much more harsh elution condition containing SDS detergent than that condition for LC−MS/MS analysis, in which both the enriched proteome showed similarly strong intensity in SA-HRP Western blots (Supporting Figure S3b). This data confirms that the binding affinity of DBP is practically sufficient for the SA-bead enrichment of labeled protein and the differential LC−MS sensitivity of DBP over BP surely comes from the difference of elution efficiency between the probes on SA-beads, not labeling efficiency, as we described.

Next, the mitochondrial matrix-targeted (Matrix-APEX2) and IMS-targeted LACTB-APEX2 were coupled with DBP-labeling to map the labeled sites (Spot-ID). Previously, these APEX2s were employed for the proteome mapping of submitochondrial spaces based on unlabeled peptide ID; hence, the labeling specificity and the coverage of Spot-ID in our method could be compared with the previous data set.[21,22] Furthermore, we employed a new IMS-targeted APEX2, SCO1-APEX2, which is localized in the IMS and interacting with the cytochrome oxidase complex (Complex IV) as an assembly factor.[31] Thus, we attempted to examine whether SCO1-APEX2 could generate a different set of labeled sites from those of LACTB-APEX2. The expression patterns of Matrix-APEX2, and SCO1-APEX2 were imaged by transmission electron microscope and each DAB/OsO_4 staining pattern was well-matched to the expected submitochondrial space (Supporting Figure S4b).[32]

The transiently expressed samples with Matrix-APEX2, LACTB-APEX2, SCO1-APEX2 by Lipofectamine 2000 (L2K) transfection and the untransfected sample were labeled with DBP. From the analysis of this transiently expressed sample analysis, we found not only a distinct cluster of labeled sites from each submitochondrial targeted APEX2 but also a considerable number of labeled peptides from cytosolic proteins, which might be labeled during APEX2 translocation from cytoplasm to the mitochondria (Supporting Figure S4 and Supporting Data Set S2). The labeled sites overlapped between Matrix-APEX2 and IMS-APEX2 are practically important as "background" labeled sites (e.g., CYP51A1) for other APEX-labeled site identifications (see Supporting Information). We expected that these "background" sites could be diminished when APEX expression and the concentration of DBP would be stringently controlled at low levels in stable cell lines for less spurious phenoxyl radical labeling.

DOI: 10.1021/jacs.6b10418
J. Am. Chem. Soc. 2017, 139, 3651−3662

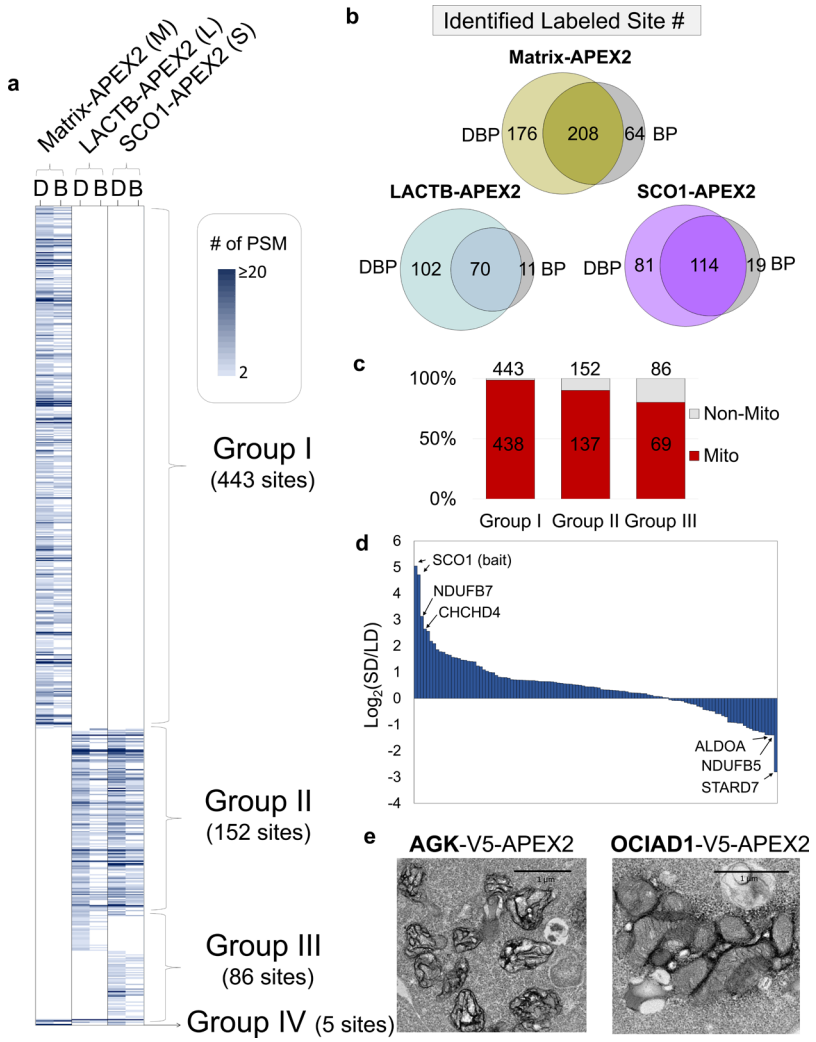

Figure 2. Identified DBP-labeled sites by APEX2. (a) Overview of 686 DBP- and BP-labeled sites of mitochondrial Matrix-APEX2, LACTB-APEX2 and SCO1-APEX2 stable cell lines. The table shows the findings for each reproducibly labeled site per biological replicate experiment. The color intensity represents number of peptide spectra match (PSM) of the labeled peptides per unique labeled site over replicate experiments with various APEX2s. Detailed information is shown in the Supporting Data Set S3. (b) Overlaps of identified DBP- and BP-labeled unique sites in parallel experiments for Matrix-, LACTB-, and SCO1-APEXs. (c) Mitochondrial specificity check of Groups I to III. The number of total labeled sites is depicted over the column. (d) Differential MS1 intensity of respectively labeled peptide between SCO1- and LACTB-APEX2 sample. *x*-axis: labeled site, *y*-axis: log2 value of differential peptide MS1 intensity of SCO1 (S) over LACTB (L). (e) Electron microscopic imaging of AGK-V5-APEX2 and OCIAD1-V5-APEX2. Scale bar: 1 μm.

We generated Flp-In T-REx 293 stable cell lines with Matrix-APEX2, LACTB-APEX2, and SCO1-APEX2 and performed Spot-ID with these cell lines. Labeled sites were assigned when they were reproducibly observed in each biological replicate. From the analysis of DBP-labeled peptides from six independently labeled samples, we identified 608 unique DBP-labeled sites, which were reproducibly discovered in each replicate of APEX2-labeled samples. We also confirmed that DBP showed better depth of coverage (e.g., peptide spectrum match and unique labeled site number) than by using the previous probe (BP) in the parallel experiments by using Matrix-APEX2, LACTB-APEX2 and SCO1-APEX2 (Figure 2b and Supporting Data Set S3). We clustered four exclusively labeled sets (Groups I–IV) of DBP- and BP-labeled tyrosine residues (total 686 sites) from the three APEX2s results (Figure 2a, Supporting Data Set S3). Group I sites (443 sites) were exclusively labeled only by Matrix-APEX2, and Group II sites (152 sites) were labeled by both LACTB-APEX2 and SCO1-APEX2, but not by Matrix-APEX2. Over 98% of Group I and over 90% Group II sites were mapped on the mitochondrial proteins with high mito-specificity (Figure 2c).

Furthermore, the majority of Group I's mitochondrial proteins were mapped onto mitochondrial matrix or IMM proteins (Supporting Data Set S3). Only two IMS proteins, PNPT1 (also known as PNPase)[33] and STOML2[34] were assigned to Group I. However, PNPT1 has been recently reidentified as a mitochondrial matrix protein with supporting evidence of EM imaging in the previous study.[21] Since we could not find any labeled sites of STOML2 by IMS-APEX2, this peripheral membrane protein should be localized in the mitochondrial matrix. In contrast, we found two matrix proteins (NDUFA4 and NDUFB10, known as matrix-side subunits of OxPhos Complex,[35,36]) were reproducibly labeled by IMS-APEX2 (Group II, Supporting Data Set S3). From the immunoprecipitation experiment, we confirmed that NDUFB10 and STOML2 were exclusively DBP-modified in

DOI: 10.1021/jacs.6b10418
J. Am. Chem. Soc. 2017, 139, 3651−3662

IMS- and Matrix-APEX2 sample, respectively (Supporting Figure S5a). This result indicates that our MS-identification of these proteins based on the modification site is not false positive. Because NDUFA4, NDUFB10 and STOML2 contain no predicted transmembrane domain, their submitochondrial localization should be revised according to their labeled sites by APEXs.

We also found that CLPB, a known mitochondrial matrix chaperone protein,[37] were exclusively labeled by IMS-APEX2. For confirmation of CLPB's localization in mitochondrion, we prepared CLPB-APEX2 and examined its biotinylation pattern which can tell its submitochondrial localization.[38] We could observe very diffusive biotinylated pattern of CLPB-APEX2 from mitochondria, which supports that CLPB should not be localized within the mitochondrial matrix (Supporting Figure S5b). Furthermore, analysis of correlations between CLPB-APEX2's biotinylated protein pattern with that of other standard submitochondrial-targeted APEX2 constructs (e.g., Matrix, SCO1 and TOM20-APEX2s), using Western blot with SA-HRP (Supporting Figure S5c and d) revealed a high correlation with the pattern observed with SCO1 (0.89) and low correlations with TOM20 (0.64) and Matrix (0.67), indicating that the CLPB C-terminus localized to the IMS (Supporting Figure S5e). Thus, our data suggest that CLPB should be located at IMS and its function as molecular chaperone should be rediscussed in the IMS not in the mitochondrial matrix.[37]

A distinct cluster of labeled sites by either LACTB-APEX2 (28 sites) or SCO1-APEX2 (58 sites) was also detected in Group III (Figure 2a). LACTB-APEX2 exclusively labeled more number of cytosolic proteins (e.g., YBX1, YWHAQ), whereas SCO1-APEX2 labeled inner mitochondrial membrane proteins such as OPA1, TIMM17B and MICU1. Among the respectively DBP-labeled peptides by SCO1-APEX2 and LACTB-APEX2 in Group II, several peptides showed distinctively differential MS1 signal intensities (Figure 2d). For example, SCO1 (bait, Y216, Y244), NDUFB7 (Y89) and CHCHD4/MIA40 (Y105) PTGES2 (Y263) and AIFM1 (Y347) showed reproducibly higher MS1 intensity in SCO1-APEX2 than LACTB-APEX2, whereas STARD7 (Y171), NDUFB5 (Y171) and ALDOA (Y364) showed higher MS1 intensity in LACTB-APEX2 than SCO1-APEX2. Since the stronger MS1 signal intensity should be originated from more efficient DBP labeling which is dependent on proximity, we postulated that these differentially labeled proteins including exclusively labeled proteins might be considered as a clustered proteome that is proximal to SCO1-APEX2 or to LACTB-APEX2 in IMS.

Among the labeled proteins by IMS-APEXs (LACTB-APEX2 or SCO1-APEX2), we found several mito-orphan proteins (e.g., ACOT1, SMIM4 and TMEM223, Supporting Data Set S3) and a considerable number of mitochondrial proteins still have no any submitochondrial annotation, which were labeled either by Matrix-APEX2 (Matrix-orphan, Supporting Data Set S3) or IMS-APEX2 (IMS-orphan, Supporting Data Set S3). For example, AGK is known as a mitochondrial protein without submitochondrial annotation and it is exclusively labeled by IMS-APEX2, which suggests that AGK should be an IMS protein or at least an IMS-exposed domain containing protein.

For the confirmation of their submitochondrial location, AGK-V5-APEX2 and OCIAD1-V5-APEX2 (C-term tagged APEX2 at the target protein) were constructed and used for imaging by electron microscope (EM). The EM images showed that AGK-V5-APEX2 was clearly localized to IMS, while OCAID1-V5-APEX2 was localized to outer mitochondrial membrane (OMM) (Figure 2e), indicating its C-terminus headed for OMM. Considering the labeled sites (Y25, Y128, Y129, Y199, Y210) of OCIAD1 by IMS-APEX2, we postulated that OCIAD1 should contain plausible transmembrane domain through OMM.

TMEM261 Is a Newly Identified Mitochondrial Protein in IMS. Notably, we reproducibly found DBP-labeled Y12 of TMEM261 (also known as C9orf123) in LACTB-APEX2 and SCO1-APEX2 samples, which is a transmembrane (TM) protein without subcellular annotation. To confirm its subcellular localization, we cloned TMEM261-V5-APEX2 and checked its expression and biotin-labeled pattern. Although this protein is not currently annotated as a mitochondrial protein,[39] TMEM261-V5-APEX2 showed a clear mitochondrial pattern, which overlaid well with the mitochondrial marker protein, mito-BFP (Figure 3a). Furthermore, its biotinylation pattern was not restricted to mitochondria, indicating the biotinylated proteins by TMEM261-APEX2 were diffused from the porous outer mitochondrial membrane and this result implies that C-terminus of TMEM261 might be localized to IMS or OMM.[38] We also performed transmission electron microscopy (TEM) imaging of TMEM261-V5-APEX2, which clearly localized in IMS (Figure 3b). This result indicates that the C-terminus of TMEM261 is exposed in the IMS (Figure 3c). Considering its two expected TM domains, the labeled site (Y12) by IMS-APEX2 and EM imaging result of C-term tagged APEX2 at TMEM261-APEX2, TMEM261 is likely to be an IMM or OMM protein, with its N- and C-terminus exposed to the IMS (Figure 3c).

To understand its role in the mitochondria, we also performed Spot-ID experiments with TMEM261-APEX2 stable cell line. We collected 470 DBP-labeled sites in TMEM261-APEX2 (Supporting Data Set S4) and among these labeled sites, ~39% of sites (182 sites) were overlapped with labeled sites of IMS-APEX2 (Group II, Figure 3d). In this analysis, we could observe again that DBP showed much better depth of coverage of labeled sites (total 470 sites) than by using the previous probe (BP, total 284 sites) in the parallel experiments (Figure 3e and Supporting Data Set S4). Interestingly, distinctly labeled sites of endoplasmic reticulum (ER) lumen or secretory pathway proteins such as CALU, RCN1, RCN2, HSP90B1, PDIA3, and PDIA6 were observed in its exclusively labeled sites of TMEM261-APEX2 (Group III, Figure 3d and f). The labeled sites of these ER lumen proteins were not covered by other IMS-APEX2s or Matrix-APEX2. In further analysis, these labeled sites on ER-lumen proteins were also identified by ss-APEX2-KDEL whose APEX2 is localized at the ER lumen, whereas these labeled sites were not covered by APEX2-NES whose APEX2 is localized at the cytoplasm (Supporting Data Set S5). This result implies that TMEM261 might be very proximate to the ER-mitochondrion tethered junction;[40,41] thus, its generated DBP radical can diffuse efficiently into the ER lumen through OMM (Figure 3g). We also found that several DBP-labeled nuclear proteins (e.g., DDX3X and RUVBL1) in Group III have known mitochondrial functions.[42,43] Thus, it might be intriguing to investigate whether functions of nuclear proteins labeled by TMEM261-APEX2 are related to mitochondria and nuclear crosstalk[44,45] in future studies.

Interestingly, a recent report suggested this gene is significantly overexpressed in human breast cancer in the

DOI: 10.1021/jacs.6b10418
J. Am. Chem. Soc. 2017, 139, 3651−3662

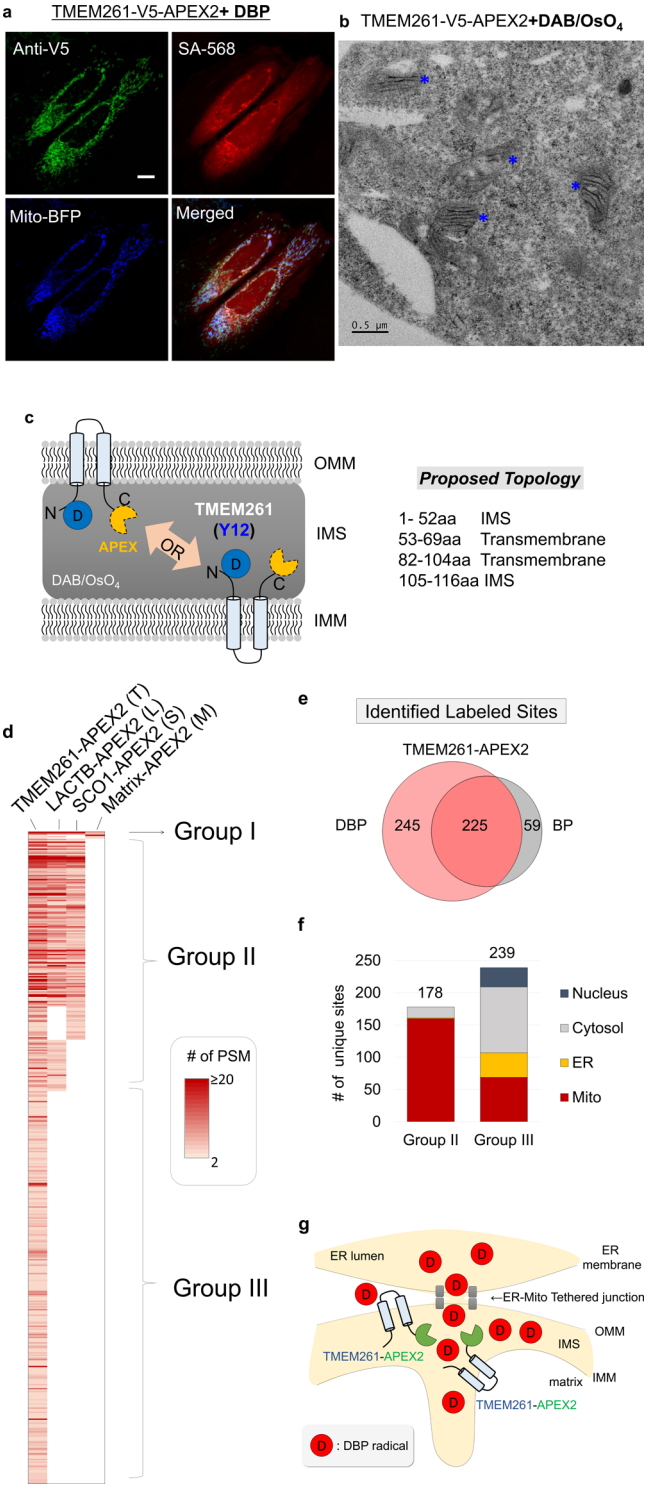

Figure 3. TMEM261 is a newly identified mitochondrial protein. (a) TMEM261-V5-APEX2 labeling imaging; the green channel (anti-V5) is for enzyme expression pattern; the red channel (SA-568), for the DBP labeling pattern; and the blue channel is for the mitochondrial marker mito-BFP. HeLa cell was used for this imaging experiment. Scale bar = 10 μm. (b) Electron microscopic imaging of TMEM261-V5-APEX2. TMEM261-V5-APEX2 labeling sites are depicted by blue asterisks. Scale bar: 500 nm. (c) The proposed membrane topology of TMEM261 in the mitochondrion. (d) Overview of 470 DBP-labeled sites of TMEM261-APEX2. The table shows the findings of each reproducibly labeled site per biological replicate experiment. The color intensity represents number of peptide spectra match of the labeled peptides per unique labeled site over replicate experiments. Detailed information is shown in the Supporting Data Set S4. (e) Overlaps of identified DBP- and BP-labeled unique sites in parallel experiments for TMEM261-APEX2. (f) Suborganelle specificity of labeled sites in Group II and Group III. The number of total identified sites with subcellular information is depicted over the column. (g) Schematic representation of TMEM261 localization in IMS near the ER-mitochondrial junction based on the Spot-ID result.

context of gene copy number amplification.[46] Moreover, we found the possibility of TMEM261 as an oncogene in prostate cancer from bioinformatics analysis (Supporting Information). Thus, further study is required to investigate its physiological role related to mitochondrial function in cancer tissues in the future.

In Vivo Membrane Protein Topology Determination by Spot-ID. Our Spot-ID results provided valuable information on the topological direction of membrane proteins; due to the short lifetime of in situ-generated phenoxyl radicals and the high impermeability property of the IMM, the labeled sites should be in the same direction as that of targeted APEX. For instance, MIC60/IMMT (also known as mitofilin) is a core IMM protein component of the MICOS complex,[47] and the N-terminus domain (1−46 aa) is localized in the matrix, and the C-terminus domain (65−758 aa) is localized in the IMS. The 33rd tyrosine residue of MIC60 was labeled by Matrix-APEX2 (Group I), and the 95th, 358th, 543rd and 578th tyrosine residues of MIC60 were labeled by IMS-APEX2s (Group II and III) (Figure 4a). The topological direction of 16 TM including MIC60 proteins at IMM were also well-matched with labeled sites either by Matrix-APEX2 or IMS-APEX2 (SCO1-APEX2 and LACTB-APEX2) (Figure 4b and Supporting Figure S6a). For peripheral membrane proteins, 26 matrix-localized proteins were exclusively labeled by Matrix-APEX2, and 16 IMS-localized proteins were exclusively labeled by IMS-APEX2s (Figure 4c and Supporting Figure S7a). Given that our labeled site accurately reflected its sublocalized spaces, we determined the topology of 44 mitochondrial TM proteins at the IMM (Figure 4d, h and Supporting Figure S6b) and membrane-localized direction of 33 mitochondrial peripheral membrane proteins at the IMM (Figure 4e, h and Supporting Figure S7b).

Interestingly, we found that Y17 of UQCRQ was reproducibly labeled by Matrix-APEX2 while Y60 and Y78 of UQCRQ was reproducibly labeled by IMS-APEX2. Although UQCRQ contains no reported TM domain in Uniprot, our results strongly suggest that UQCRQ should be a TM protein at the IMM. Similarly, we also found Y38 of COX4I1 was labeled by Matrix-APEX2, whereas Y126 of COX4I1 was labeled by IMS-APEX2. This result also suggests that COX4I1 should have a single TM domain between 38 and 126 aa at IMM. It is noteworthy that the Dense Alignment Surface (DAS)-TM analysis[48] predicted a single transmembrane domain for both COX4I1 and UQCRQ, consistent with our result (Supporting Figure S6c and d). The proposed topologies of these proteins are shown in Figure 4d.

Among the labeled sites, we observed several OMM proteins labeled by IMS-APEX2. For example, MUL1, an OMM transmembrane protein with both N- and C-termini exposed to the cytosol,[49] was labeled by IMS-APEX2 at Y173, which is exposed to IMS (Figure 4f). We also found that several beta-barrel OMM proteins such as VDAC1, VDAC2, VDAC3, and SAMM50 were labeled by IMS-APEX2. Intriguingly, all four

DOI: 10.1021/jacs.6b10418
J. Am. Chem. Soc. 2017, 139, 3651−3662

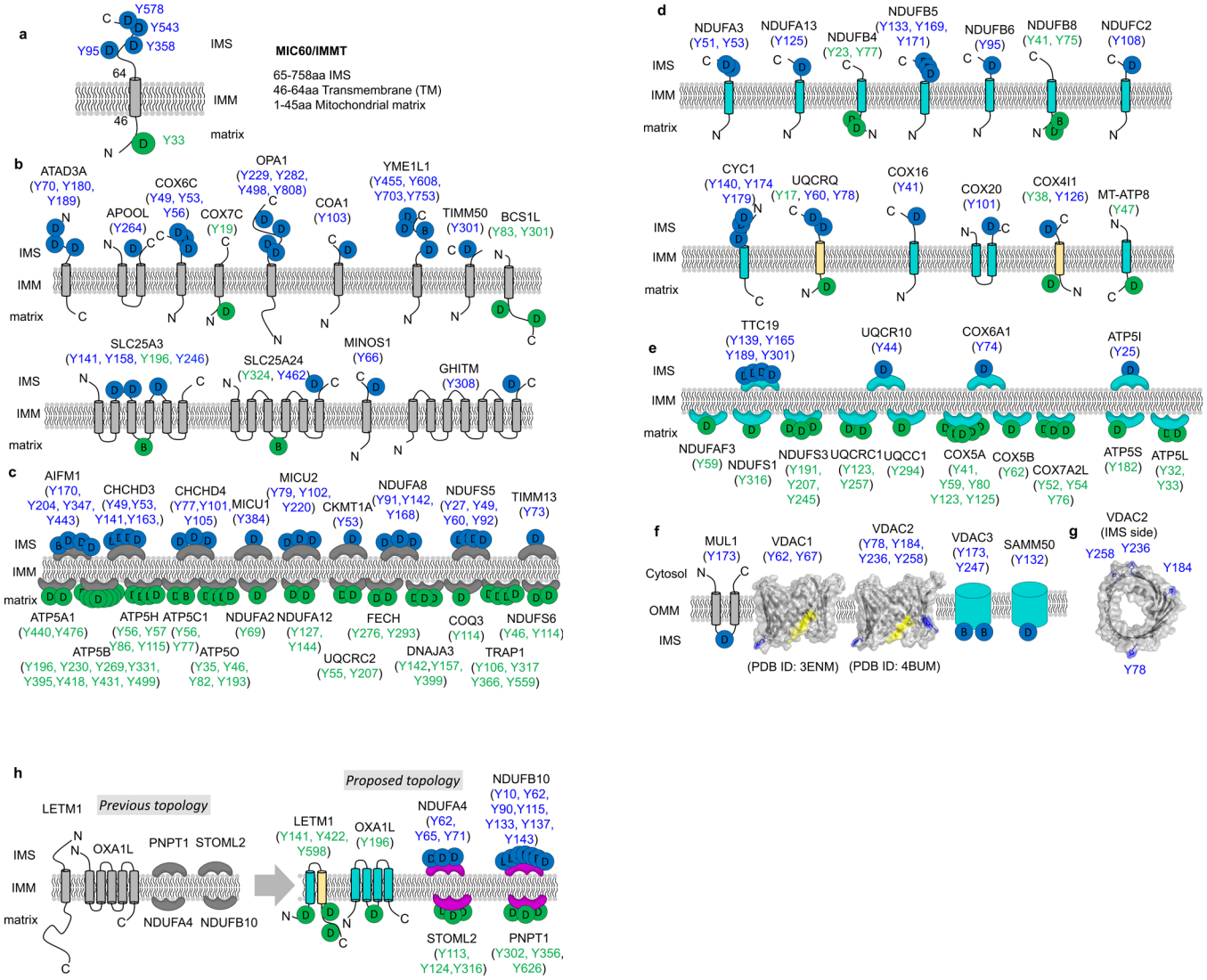

Figure 4. Labeled sites for in vivo protein topology determination. (a) MIC60/IMMT protein topology confirmation by our labeled sites. (b) IMM-TM protein topology confirmation. Other confirmed IMM-TM proteins are shown in Supporting Figure S6a. (c) Peripheral membrane protein-binding face confirmation by our results. Other confirmed IMM-peripheral membrane proteins are shown in Supporting Figure S7a. (d) Proposed membrane topology of IMM-TM proteins of OxPhos complex by our labeled site result. Other proposed IMM-TM proteins are shown in Supporting Figure S6b. (e) Proposed membrane-binding face of several peripheral membrane OxPhos complex proteins at the IMM based on the labeled sites. Other proposed IMM-peripheral membrane proteins are shown in Supporting Figure S7b. (f) Confirmed and proposed orientation of OMM proteins based on the sites labeled by IMS-APEX2. N- and C-termini of VDAC1 (PDB ID: 3ENM) and VDAC2 (PDB ID: 4BUM) are shown in yellow, and tyrosine residues labeled by IMS-APEX2 are in blue. (g) IMS side of VDAC2 protein. (h) Proposed membrane topology of LETM1, OXA1L, STOML2, NDUFA4, and NDUFB10 by our labeled site results. The proposed TM direction is shown in blue. The proposed newly identified TM domain is shown in yellow. Either DBP- or BP-labeled sites by Matrix-APEX2 are marked by green circles with "D" or "B" respectively, and DBP- or BP-labeled sites by IMS-APEX2 are marked with blue circles with "D" or "B" respectively. Detailed information is shown in the Supporting Data Set S3.

DBP-labeled tyrosine residues (Y78, Y184, Y236, and Y258) of VDAC2 were positioned at the same side of the protein (Figure 4f and g), indicating that this side of VDAC2 is exposed to IMS. Additionally, we could determine that the N- and C-termini of VDAC1 were exposed to IMS based on the labeled site (Y62, Y67). Our data proposed that these two VDAC proteins have the same orientation based on the sites labeled by IMS-APEX2 (Figure 4f). Considering that the orientation of VDAC protein is still under debate,[50] it is noteworthy that our proposed orientation of VDAC1 is consistent with the previously determined orientation of tagged VDAC1[51,52] and a dynamic simulation study of VDAC1.[53] Similarly, for the first time, we proposed the orientation of VDAC3[54] and SAMM50[55] at OMM based on our labeled sites. Furthermore, the labeled sites of VDAC1 and VDAC2 in our data set, which are located at the same side of the structure, supports that these crystal structures of VDAC1[56] and VDAC2[57] are close to their native conformation in live cells.[58]

We also found some results conflicting with previously established topologies of IMM membrane proteins such as LETM1 (Uniprot ID: O95202)[59] and OXA1L (Uniprot ID: Q15070).[60] To confirm that the N-terminus domain of LETM1 containing Y141 is exposed in the mitochondrial matrix, we prepared a V5-APEX2-LETM1 construct, in which APEX2 is inserted between 151-aa and 152-aa of LETM1 (Supporting Figure S8a). We checked the expressed and biotinylated

DOI: 10.1021/jacs.6b10418
J. Am. Chem. Soc. 2017, 139, 3651−3662

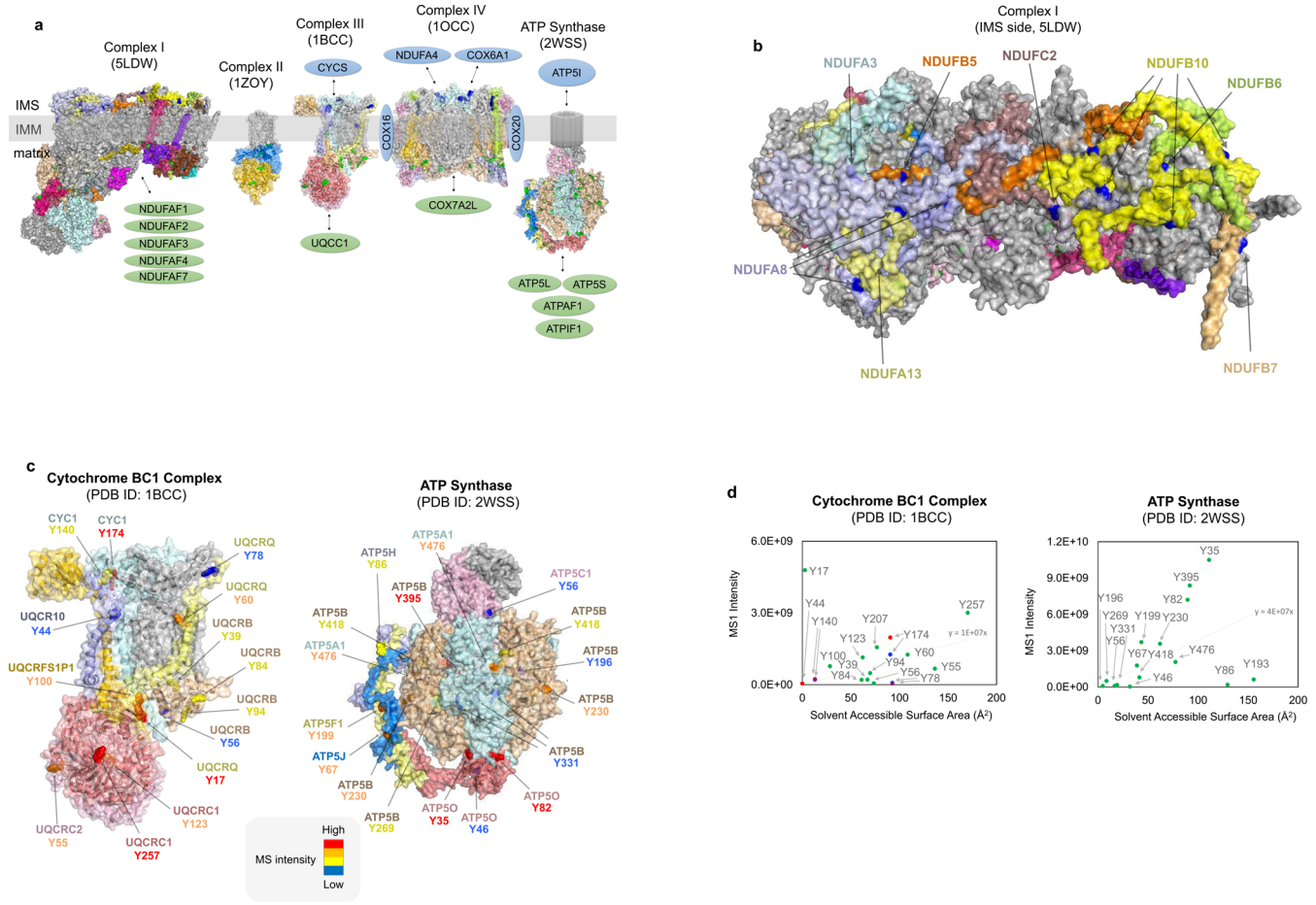

Figure 5. Labeled sites on the OxPhos complex. (a) Crystal or EM structures of Complex I (PDB ID: 5LDW), Complex II (PDB ID: 1ZOY), Complex III (PDB ID: 1BCC), Complex IV (PDB ID: 1OCC), and ATP synthase (PDB ID: 2WSS). The MS-identified subunits were colored with different colors, the tyrosine residues labeled by Matrix-APEX2 were colored in green, and the residues labeled by IMS-APEX2 were colored in blue. The supernumerary subunits of OxPhos complex that were not characterized by the crystal or EM structures but were identified by either Matrix-APEX2 or IMS-APEX2 are shown. (b) IMS side of Complex I (PDB ID: 5LDW). Labeled IMS-side-exposed subunits of Complex I are colored with various colors and the sites labeled by IMS-APEX2 are colored in blue. The sites labeled by Matrix-APEX2 were shown in Supporting Figure S10. (c) Cytochrome BC1 complex (Complex III, left) and mitochondrial ATP synthase complex (right). The labeled sites are marked with different colors according to the MS1 intensity of the labeled peptides. (d) Correlation between solvent-accessible surface area (Å^2, *x*-axis) and MS1 intensity of labeled peptides per labeled site on the crystal structures shown in (c). The sites labeled by Matrix-APEX2 are colored in green and those by SCO1-APEX2 or LACTB-APEX2 are colored in red or blue, respectively. Correlation factor was included in the graph. When the labeled sites are shown in multiple times at identical chains, the highest solvent accessible surface area among the identical sites was selected for this graph Detailed information on the labeled subunits and labeled residues of theses mitochondrial complexes were shown in Supporting Data Set S6.

patterns in HEK293T cells, and it showed a good mitochondrial pattern and very restricted biotinylated pattern (Supporting Figure S8b), which implies APEX2 in this construct should be positioned in the mitochondrial matrix.[38] In addition, we performed EM imaging[32] of V5-APEX2-LETM1, which very clearly showed mitochondrial matrix staining (Supporting Figure S8c and d). Thus, we can correct that LETM1's N-terminus stretched out to the matrix, not to IMS, which concurs with its labeled site (Y141) by Matrix-APEX2. When considering the two predicted TM domains (204−232 aa and 413−421 aa, Supporting Figure S8e) along with its DBP-labeled sites (Y141, Y422, Y598) by Matrix-APEX2, we propose that LETM1 exhibits the membrane topology shown in Supporting Figure S8f.

Interestingly, the DAS-TM prediction program also indicates that OXA1L may contain 4 TM domains (Supporting Figure S9a), whereas 5 annotated TM domains are shown in Uniprot. The number of TM domains is important in membrane topology because the odd or even number of TM domains indicates cross-membrane localization or colocalization of N- and C-termini of OXA1L, respectively. Thus, we sought to determine whether OXA1L's N-terminal and C-terminal domains localized to the mitochondrial matrix by APEX-EM.[61] For this, we prepared OXA1L(1−435 aa)-V5-APEX2 where V5-APEX2 was conjugated to the C-terminus of full-length OXA1L (Supporting Figure S9b). Notably, APEX-EM imaging showed clear mitochondrial matrix staining (Supporting Figure S9c). This finding was subsequently confirmed by bioinformatics analysis with Mitoprot,[62] which predicted that N-terminal domain of OXA1L (1−72 aa) harbors a strong mitochondrial targeting sequence with over 97% confidence that would be cleaved after mitochondrial translocation. Following this result, we prepared OXA1L(1−73 aa)-V5-APEX2 where V5-APEX2 was conjugated to the C-terminus of the N-terminal OXA1L(1−73 aa) domain construct (Supporting Figure S9b) and found obvious mitochondrial matrix localization with APEX2-EM (Supporting Figure S9d). Thus, EM imaging with Spot-ID results (Y196) proposed a topology

DOI: 10.1021/jacs.6b10418
J. Am. Chem. Soc. 2017, 139, 3651−3662

with 4 TM domains (Supporting Figure S9e). We also identified that cleavage of OXA1L N-terminal signal peptide (1−72aa) occurred by Western blotting (Supporting Figure S9f). Our proposed topology of LETM1 and other membrane proteins (OXA1L, PNPT1, STOML2, NDUFA4, and NDUFB10) are displayed in Figure 4h.

In Vivo Structural Identification of Mitochondrial Protein by Spot-ID. In our data set, numerous tyrosine residues of OxPhos subunits were identified as labeled sites by Matrix- or IMS-APEX2. On the basis of the resulting labeling information in matrix or in IMS, the orientation of these subunits was proposed (Figure 4). Our proposed topology of the OxPhos complex is consistent with the crystal or EM structure of these complexes (Figure 5). For example, Complex I in mammalian mitochondria, whose structure was recently reported by the Hirst group,[6] comprises 45 proteins, including 31 supernumerary subunits. Among these proteins, 21 proteins were mapped by both Matrix- and IMS-APEX2, and their labeled sites exactly matched either matrix-side or IMS-side exposed tyrosine residues on the complex (Figure 5a). Interestingly, NDUFB10, which was annotated as a matrix protein in Uniprot but was labeled by IMS-APEX2 in our data, was positioned at the IMS side in a recently reported Complex I structure (Figure 5b).[6] In other mitochondrial complexes (e.g., Complex II, III, and IV and ATP Synthase),[3−5,63] the discovered labeled sites were well-matched with the determined protein structure in terms of the orientation of the tyrosine residue at IMM (Figure 5 and Supporting Figure S10). Given that some of our identified protein topology of OxPhos complex subunits are indeed well-supported by identified crystal structures of OxPhos complex, our proposed membrane topologies of other IMM and OMM proteins should be considered as a true positive resource (Supporting Data Set S7).

We also found that the labeled sites were primarily localized at the surface-exposed subunits of the complexes. For instance, none of the core membrane subunit proteins (e.g., ND1, ND2, ND3, and ND4) of Complex I were labeled by either APEX, but the supernumerary subunits (e.g., NDUFA3, NDUFA8, NDUFA13, NDUFAB1, NDUFB4, NDUFB5, NDUFB6, NDUFB7, NDUFB8, NDUFB9, NDUFB10, and NDUFC2), which are components for building a cage structure around the core membrane subunits, were found to be labeled by APEX2 (Figure 5b and Supporting Figure S10). This result indicates that the solvent-accessible protein subunits were preferentially labeled by APEX over the structurally buried protein subunits in the complex. There are several supernumerary subunits of OxPhos complex that were not characterized by the atomic structures but identified in our study. The topological direction of those accessory subunits (e.g., NDUFAF1, NDUFAF2, NDUFAF3, NDUFAF4, NDUFAF7, TIMMDC1/C3orf1, TMEM126B for Complex I; UQCC1 for Complex II; TTC19 for Complex III, NDUFA4, COX6A1, COX7A2L, SCO1, SCO2, CMC2, TACO1, LRPPRC for Complex IV; ATP5I, ATP5L, ATP5S, ATPAF1, ATPAI1 for ATP Synthase) are proposed in Figure 5a and Supporting Figure S11.

As we described in Figure 1c, the short-lived phenoxyl radical tends to react on the protein surface tyrosine residue in a simple in vitro experiment. We further examined a correlation between the surface exposure level and the MS intensity of labeled peptides in the living cells by matching several identified sites with the crystal structure of mitochondrial macromolecular protein complexes. As shown in Figure 5, we marked the identified tyrosine residues on the ATP Synthase and cytochrome BC1 complex (also known as Complex III) with differential color codes according to the MS1 intensity (Figure 5c). We observed that more exposed residues (e.g., Y35 and Y82 of ATP5O; Y257 of UQCRC1) were more strongly labeled than other tyrosine residues. In this macromolecular complex, a positive correlation between MS1 signal intensity of the labeled sites and its exposure level (solvent accessible surface area, Å^2) was also observed (Figure 5d). Interestingly, a couple of the labeled sites with considerably high MS1 intensity were not fully exposed on the surface. For example, Y17 of UQCRQ possesses a negligible solvent accessible surface area (2.7 Å^2) in the crystal structure, however, its labeled peptide showed the highest MS1 intensity (4.8×10^8) among the labeled tyrosine residues of cytochrome BC complex. Since the protein structure can be dynamically changed by interaction with other proteins or post-translational modification, we postulated that this site might be exposed to solvent in their dynamic native structure and followed by phenoxyl radical labeling. Thus, we postulated that the MS intensity of our Spot-ID peptides can reflect the native dynamic structure of protein in a living cellular context.[64,65]

DISCUSSION

We found our proposed topologies of mitochondrial membrane proteins can provide insights for physically interacting domain within certain mitochondrial complexes. For example, it was reported that OXA1L interacted with mitochondrial ribosome in the matrix with its C-terminus;[60] however, our identified topologies of OXA1L propose that its N-terminus should interact with mitochondrial ribosome (Supporting Figure S12). Because OXA1L plays a major role in nuclear-encoded protein translocation from the cytosol,[66] our result supports that C-terminus of OXA1L should interact with its substrate proteins at the IMS side. Interestingly, our proposed topologies of PHB (IMS-side) and STOML2 (matrix-side) hypothesizes whether these two protein interaction[34] should be mediated by a IMM-TM protein (e.g., ATAD3A) at IMM. Our proposed connectome of protein subunits in other mitochondrial macromolecular complexes at IMM (e.g., TIM23 complex, MICOS complex, PHB complex) are shown in Supporting Figure S12.

Compared to previous identification results based on SILAC ratio of the unlabeled peptides,[21,22] our Spot-ID approach showed lower numbers of identified proteins (Supporting Figure S13b); however, previously identified results contain false positives due to the indirect determination of proximity labeled proteins, as we described. For example, CHCHD3 is a mitochondrial peripheral membrane protein at IMS-side, however, it was previously identified as a mitochondrial matrix protein by Matrix-APEX.[21] In current study, we did not observe any labeled peptide of CHCHD3 reported by Matrix-APEX2, while multiple labeled peptides of CHCHD3 were detected by LACTB-, SCO1-, or TMEM261-APEX2s, with strong MS1 intensity. From the immunoprecipitation experiment, we confirmed that CHCHD3 was not labeled in the Matrix-APEX2 sample, whereas it was strongly labeled by either LACTB-APEX2 or SCO1-APEX2 (Supporting Figure S13c). It is possible that CHCHD3 was mis-annotated as a matrix protein in previous study via the strong interaction with biotinylated transmembrane protein (e.g., MIC60)[67] at the matrix-side by Matrix-APEX (Supporting Figure S13d). Likewise other peripheral IMM proteins (e.g., ATP5J, COX5A and

DOI: 10.1021/jacs.6b10418
J. Am. Chem. Soc. 2017, 139, 3651−3662

COX5B) with labeled sites from Matrix-APEX2 in this study, but previously annotated as IMS proteins,[22] should be regarded as matrix proteins. Overall, this analysis supports that our proposed submitochondrial localization of ~250 mito-orphan proteins should be considered as a true resource for the spatial-resolved clustered proteome within the mitochondrion (Supporting Data Set S3). We also found that the coverage of labeled peptides by Spot-ID workflow with DBP (Supporting Figure S13e) were significantly higher than that of previously identified BP-labeled peptides with low false discovery rate (Supporting Figure S13).

The MS signal enhancement after enrichment in DBP-labeling over BP-labeling was observed in APEX2-labeled human cell line sample. The MS signal gain of DBP-labeled peptides was ranging up to >10-fold higher than that of BP-labeled peptides for ~80% of labeled peptides and was not dependent on protein abundance (Supporting Figure S14a). Overall, the DBP-labeling clearly resulted in a higher number of identified spectra (+35−97%), and unique labeled sites (+41−112%) than BP-labeling method in human cell lines (Supporting Figure S14b). In addition, the MS signal intensity of the DBP-labeled peptides was highly reproducible between the replicates (Supporting Figure S14c).

We also performed a Spot-ID analysis by using ss-APEX2-KDEL and found that various ER luminal proteins were labeled by this construct (Supporting Figure S15 and Supporting Data Set S5). This result indicates that our DBP-APEX method universally works in other subcellular compartments, in contrast to other proximity labeling methods using promiscuous biotin ligase (pBirA), which is less active in the secretory pathway.[21] Compared with the same mitochondrial targeting sequence of Matrix-APEX2, we also found that translocation of pBirA to the mitochondrial matrix was not efficient (Supporting Figure S16). Other in vivo membrane topology identification methods using enzymatic glycosylation[68] are limited to the secretory pathway and cannot be employed in other subcellular spaces such as the mitochondrion.

Notably, conventional biochemical analysis by proteinase K digestion and digitonin treatment showed that NDUFB10 and STOML2 localized to the mitochondrial matrix and IMS, repectively, and this results are inconsistent with that determined by Spot-ID (Supporting Figure S17). However, the recently characterized Complex I[6] atomic structure provided clear evidence that NDUFB10 is located in the IMS. In addition, the proteinase K/digitonin preparation method may have also resulted in incorrect conclusions on the number of transmembrane domains in OXA1L characterized in a previous study.[69] Thus, we assert that our Spot-ID method may provide more reliable results for submitochondrial protein localization and membrane topology analysis than conventional biochemical assays.

Technically, our Spot-ID approach is conceptually similar to chemical modification methods that have been employed for membrane protein topology identification[70] or for probing solvent accessible residues on the protein surface[71] using reactive biotin-probes.[19] In contrast to the radical probe in the APEX system, however, conventional probes such as biotin ester or biotin maleimide have a much longer lifetime in aqueous solution ($t_{1/2}$ = 15 min to 2 h),[72] thus, these probes are not compatible for spatiotemporal protein labeling in a specific intracellular compartment of the live cell. Therefore, to the best of our knowledge, our approach might be the only currently available method to identify the proteomic topology of mitochondrial membrane proteins in a high-throughput manner. Furthermore, our Spot-ID method can be potentially employed to map other types of subcellular proteomic topology in live cells.

In conclusion, we developed a new approach to map phenoxyl-radical labeled sites using a newly designed chemical probe for APEX labeling. We found that our new method, Spot-ID, provided unbiased mapping results with higher spatial resolution than the previous indirect identification approach. Furthermore, the labeled sites on the protein provided valuable structural information, such the topological orientation of membrane proteins or surface-exposed residues of endogenous proteins in live cells, which was largely unobtainable by traditional chemical or biological methods. In this study, we were able to confirm and propose the membrane topologies of 135 IMM proteins and 4 beta-barrel OMM proteins. Our proposed topology of subunits of OxPhos complex are consistent with that of macromolecular complexes previously identified by EM or X-ray crystallography, which supports our proposed topologies for other mitochondrial proteins. We also found a positive correlation between the MS intensity of labeled peptides and their solvent-exposed level in the crystal structure. Overall, all of these data support that our approach can identify the in vivo structural topology of the subcellular proteome in live cells.

EXPERIMENTAL PROCEDURES

Desthiobiotin-Phenol Synthesis. Desthiobiotin (100 mg) was dissolved in 2 mL DMSO (dimethyl sulfoxide) at room temperature. 1.1 equiv of HATU (2-(7-aza-1H-benzotriazole-1-yl)-1,1,3,3-tetramethyluronium hexafluorophosphate) and 2.0 equiv of DIPEA (*N*,*N*-diisopropylethylamine) were added into the solution. The mixture was stirred for 10 min at room temperature. Then 2.0 equiv of the tyramine was added. The reaction mixture was stirred overnight at room temperature. Detail product purification method and chemical characterization data are shown in Supporting Information.

Stable Cell Line Selection and Culturing. Flp-In T-REx 293 cells (Life Technologies) were transfected using Lipofectamine 2000 (Life Technologies), typically with 20 μL Lipofectamine 2000 and 4000 ng plasmid (9:1 = pOG44:pCDNA5) per T25 flask. After 24 h, cells were cultured and selected with hygromycin B (100−200 μg/mL) for 2−3 weeks. To induce the protein expression in stable cells, cells were treated with 100 ng/mL doxycycline. Cells were desthiobiotin-phenol-labeled and lysed 18−24 h after induction. Detail information is shown in Supporting Information.

Desthiobiotin-Phenol Labeling in Stably Expressed APEX Cell Line. The stable cells were incubated with 250 μM desthiobiotin-phenol or biotin-phenol. at 37 °C under 5% CO_2 for 30 min. Afterward, 750 μL of 10 mM H_2O_2 (diluted from 30% H_2O_2, Sigma-Aldrich H1009) was added to each flask, for a final concentration of 1 mM H_2O_2, and the flasks were gently agitated for 1 min at room temperature. The reaction was then quenched by adding 7.5 mL of DPBS containing 10 mM Trolox, 20 mM sodium azide, and 20 mM sodium ascorbate to each flask. Then, cells were washed three times with cold quenching solution (DPBS containing 5 mM Trolox, 10 mM sodium azide, and 10 mM sodium ascorbate) and lysed with 1.5 mL RIPA lysis buffer (50 mM Tris, 150 mM NaCl, 0.1% SDS, 0.5% sodium deoxycholate, 1% Triton X-100), 1 × protease cocktail, 1 mM PMSF (phenylmethylsulfonyl fluoride), 10 mM sodium azide, 10 mM sodium ascorbate, and 5 mM Trolox for 10 min at 4 °C. Lysates were clarified by centrifugation at 15 000*g* for 10 min at 4 °C. Detail information is shown in Supporting Information.

Labeled Peptide Enrichment. For removal of unreacted free desthiobiotin-phenol or biotin-phenol, cell lysates was moved into Amicon filter (Merck Millipore, 10 kDa-off) followed by centrifugation at 7500*g* for 15 min at 4 °C. PBS (phosphate-buffered saline) containing 1 mM PMSF and 1 × protease cocktail was added up to 4

DOI: 10.1021/jacs.6b10418
J. Am. Chem. Soc. 2017, 139, 3651−3662

mL followed by centrifugation three more times. Finally, the cell lysates was transferred to an Eppendorf tube and mixed with 300 μL of streptavidin beads (Pierce). The sample was rotated for 1 h at room temperature and washed twice with PBS. After removing the PBS, 100 μL of denaturing solution (6 M urea, 2 M thiourea, 10 mM HEPES) was added and reduced using 20 μL of 100 mM DTT (dithiothreitol) in 50 mM ammonium bicarbonate (ABC) buffer for 60 min at 56 °C using a Thermomixer (Eppendorf). Protein alkylation was performed by adding 35 μL of 300 mM iodoacetamide in 50 mM ABC buffer with shaking in the dark for 30 min. Afterward, trypsin gold (Promega) was added.to the solution and incubated at 37 °C with shaking for overnight. Afterward, formic acid was added to terminate the trypsin reaction and the beads were washed with PBS four times and eluted by boiling at 95 °C for 10 min after adding 250 μL of 95% formamide, 10 mM EDTA, pH 8.2. Eluted peptide samples was desalted with Varian Bond ELUT (Agilent, 12109301) and home-made column. Detailed information for desalting and LC−MS/MS is described in Supporting Information.

LC−MS/MS Data Processing. All MS/MS data were searched by MS-GF+ algorithm[73,74] (v.9979) and MaxQuant (version 1.5.3.30) with Andromeda[75] search engine at 10 ppm of precursor ion mass tolerance against the SwissProt *Homo sapiens* proteome database (20199 entries, UniProt (http://www.uniprot.org/)). The False discovery rate (FDR) was set at <1% for peptide spectrum match including unlabeled peptides for both search algorithms. FDR less than 1% was obtained for unique labeled peptide and unique labeled protein level as well. The extracted ion chromatogram (XIC) was plotted by Qual Browser in Xcalibur software (Thermo Scientific). Detail information is described in Supporting Information.

■ ASSOCIATED CONTENT

Supporting Information

The Supporting Information is available free of charge on the ACS Publications website at DOI: 10.1021/jacs.6b10418.

Detail information on plasmid constructs, bioinformatics analysis of TMEM261, transiently expressed APEX2 sample preparation, Supporting result, Supporting analysis and discussion; Representative spectra of DBP-labeled peptides (PDF)
Data Set S1 (XLSX)
Data Set S2 (XLSX)
Data Set S3 (XLSX)
Data Set S4 (XLSX)
Data Set S5 (XLSX)
Data Set S6 (XLSX)
Data Set S7 (XLSX)

■ AUTHOR INFORMATION

Corresponding Authors

*jkseo6998@unist.ac.kr
*jongseokim@snu.ac.kr
*rhee@unist.ac.kr

ORCID

Hyun-Woo Rhee: 0000-0002-3817-3455

Notes

The authors declare the following competing financial interest(s): Ulsan National Institute of Science and Technology and Institute of Basic Science are seeking to file a patent application covering part of the information contained in the paper.

■ ACKNOWLEDGMENTS

This work was supported by the Korea Health Technology R&D Project through the Korea Health Industry Development Institute (KHIDI) funded by the Ministry of Health & Welfare of Korea (HI16C0091). J.-S. K. gratefully acknowledges the funding from the Institute for Basic Science from the Ministry of Science, ICT, and Future Planning of Korea (IBS-R008-D1). LTQ-Orbitrap Elite MS analysis was supported by UCRF. The authors thank Prof. Jongsun Park (Chungnam National University) for the generous gift of LETM1 gene and Ms. Myeong-Seon Jeong (Korea Basic Science Institute) for TEM imaging.

■ REFERENCES

(1) Cogliati, S.; Frezza, C.; Soriano, M. E.; Varanita, T.; Quintana-Cabrera, R.; Corrado, M.; Cipolat, S.; Costa, V.; Casarin, A.; Gomes, L. C.; Perales-Clemente, E.; Salviati, L.; Fernandez-Silva, P.; Enriquez, J. A.; Scorrano, L. *Cell* **2013**, *155*, 160−171.
(2) Cogliati, S.; Enriquez, J. A.; Scorrano, L. *Trends Biochem. Sci.* **2016**, *41*, 261−273.
(3) Tsukihara, T.; Aoyama, H.; Yamashita, E.; Tomizaki, T.; Yamaguchi, H.; ShinzawaItoh, K.; Nakashima, R.; Yaono, R.; Yoshikawa, S. *Science* **1996**, *272*, 1136−1144.
(4) Zhang, Z. L.; Huang, L. S.; Shulmeister, V. M.; Chi, Y. I.; Kim, K. K.; Hung, L. W.; Crofts, A. R.; Berry, E. A.; Kim, S. H. *Nature* **1998**, *392*, 677−684.
(5) Sun, F.; Huo, X.; Zhai, Y. J.; Wang, A. J.; Xu, J. X.; Su, D.; Bartlam, M.; Rao, Z. H. *Cell* **2005**, *121*, 1043−1057.
(6) Zhu, J.; Vinothkumar, K. R.; Hirst, J. *Nature* **2016**, *536*, 354−8.
(7) Neupert, W. *Annu. Rev. Biochem.* **1997**, *66*, 863−917.
(8) Harner, M.; Korner, C.; Walther, D.; Mokranjac, D.; Kaesmacher, J.; Welsch, U.; Griffith, J.; Mann, M.; Reggiori, F.; Neupert, W. *EMBO J.* **2011**, *30*, 4356−4370.
(9) Kamer, K. J.; Mootha, V. K. *Nat. Rev. Mol. Cell Biol.* **2015**, *16*, 545−553.
(10) Bogenhagen, D. F.; Rousseau, D.; Burke, S. *J. Biol. Chem.* **2008**, *283*, 3665−3675.
(11) Chen, X. J.; Wang, X. W.; Kaufman, B. A.; Butow, R. A. *Science* **2005**, *307*, 714−717.
(12) Lewis, S. C.; Uchiyama, L. F.; Nunnari, J. *Science* **2016**, *353*, aaf5549.
(13) Wallace, D. C. *Nat. Rev. Cancer* **2012**, *12*, 685−698.
(14) Gerbitz, K. D.; Gempel, K.; Brdiczka, D. *Diabetes* **1996**, *45*, 113−126.
(15) Lin, M. T.; Beal, M. F. *Nature* **2006**, *443*, 787−795.
(16) Fulda, S.; Galluzzi, L.; Kroemer, G. *Nat. Rev. Drug Discovery* **2010**, *9*, 447−464.
(17) Arce, P. M.; Khdour, O. M.; Goldschmidt, R.; Armstrong, J. S.; Hecht, S. M. *ACS Med. Chem. Lett.* **2011**, *2*, 608−613.
(18) Foskett, J. K.; Madesh, M. *Biochem. Biophys. Res. Commun.* **2014**, *449*, 377−383.
(19) Bennett, K. L.; Matthiesen, T.; Roepstorff, P. *Methods Mol. Biol.* **2000**, *146*, 113−131.
(20) Deribe, Y. L.; Pawson, T.; Dikic, I. *Nat. Struct. Mol. Biol.* **2010**, *17*, 666−672.
(21) Rhee, H. W.; Zou, P.; Udeshi, N. D.; Martell, J. D.; Mootha, V. K.; Carr, S. A.; Ting, A. Y. *Science* **2013**, *339*, 1328−1331.
(22) Hung, V.; Zou, P.; Rhee, H. W.; Udeshi, N. D.; Cracan, V.; Svinkina, T.; Carr, S. A.; Mootha, V. K.; Ting, A. Y. *Mol. Cell* **2014**, *55*, 332−341.
(23) Mick, D. U.; Rodrigues, R. B.; Leib, R. D.; Adams, C. M.; Chien, A. S.; Gygi, S. P.; Nachury, M. V. *Dev. Cell* **2015**, *35*, 497−512.
(24) Jing, J.; He, L.; Sun, A.; Quintana, A.; Ding, Y.; Ma, G.; Tan, P.; Liang, X.; Zheng, X.; Chen, L.; Shi, X.; Zhang, S. L.; Zhong, L.; Huang, Y.; Dong, M. Q.; Walker, C. L.; Hogan, P. G.; Wang, Y.; Zhou, Y. *Nat. Cell Biol.* **2015**, *17*, 1339−1347.
(25) Ghesquiere, B.; Jonckheere, V.; Colaert, N.; Van Durme, J.; Timmerman, E.; Goethals, M.; Schymkowitz, J.; Rousseau, F.; Vandekerckhove, J.; Gevaert, K. *Mol. Cell. Proteomics* **2011**, *10*, M110.006866.

DOI: 10.1021/jacs.6b10418
J. Am. Chem. Soc. 2017, 139, 3651−3662

(26) Nam, J. S.; Kang, M. G.; Kang, J.; Park, S. Y.; Lee, S. J.; Kim, H. T.; Seo, J. K.; Kwon, O. H.; Lim, M. H.; Rhee, H. W.; Kwon, T. H. *J. Am. Chem. Soc.* **2016**, *138*, 10968−10977.
(27) Melville, D. B.; Dittmer, K.; Brown, G. B.; Vigneaud, D. U. V. *Science* **1943**, *98*, 497−499.
(28) Hirsch, J. D.; Eslamizar, L.; Filanoski, B. J.; Malekzadeh, N.; Haugland, R. P.; Beechem, J. M.; Haugland, R. P. *Anal. Biochem.* **2002**, *308*, 343−357.
(29) Burnley, B. T.; Afonine, P. V.; Adams, P. D.; Gros, P. *eLife* **2012**, *1*, e00311.
(30) Lam, S. S.; Martell, J. D.; Kamer, K. J.; Deerinck, T. J.; Ellisman, M. H.; Mootha, V. K.; Ting, A. Y. *Nat. Methods* **2015**, *12*, 51−54.
(31) Leary, S. C.; Cobine, P. A.; Kaufman, B. A.; Guercin, G. H.; Mattman, A.; Palaty, J.; Lockitch, G.; Winge, D. R.; Rustin, P.; Horvath, R.; Shoubridge, E. A. *Cell Metab.* **2007**, *5*, 9−20.
(32) Martell, J. D.; Deerinck, T. J.; Sancak, Y.; Poulos, T. L.; Mootha, V. K.; Sosinsky, G. E.; Ellisman, M. H.; Ting, A. Y. *Nat. Biotechnol.* **2012**, *30*, 1143−1148.
(33) Wang, G.; Chen, H. W.; Oktay, Y.; Zhang, J.; Allen, E. L.; Smith, G. M.; Fan, K. C.; Hong, J. S.; French, S. W.; McCaffery, J. M.; Lightowlers, R. N.; Morse, H. C.; Koehler, C. M.; Teitell, M. A. *Cell* **2010**, *142*, 456−467.
(34) Hajek, P.; Chomyn, A.; Attardi, G. *J. Biol. Chem.* **2007**, *282*, 5670−5681.
(35) Balsa, E.; Marco, R.; Pereles-Clemente, E.; Szklarczyk, R.; Calvo, E.; Landazuri, M. O.; Enriquez, J. A. *Cell Metab.* **2012**, *16*, 378−386.
(36) Hebert-Chatelain, E.; Jose, C.; Cortes, N. G.; Dupuy, J. W.; Rocher, C.; Dachary-Prigent, J.; Letellier, T. *Biochim. Biophys. Acta, Bioenerg.* **2012**, *1817*, 718−725.
(37) Rottgers, K.; Zufall, N.; Guiard, B.; Voos, W. *J. Biol. Chem.* **2002**, *277*, 45829−45837.
(38) Lee, S. Y.; Kang, M. G.; Park, J. S.; Lee, G.; Ting, A. Y.; Rhee, H. W. *Cell Rep.* **2016**, *15*, 1837−1847.
(39) Calvo, S. E.; Clauser, K. R.; Mootha, V. K. *Nucleic Acids Res.* **2016**, *44*, D1251−1257.
(40) Chandra, N. C.; Spiro, M. J.; Spiro, R. G. *J. Biol. Chem.* **1998**, *273*, 19715−19721.
(41) Rowland, A. A.; Voeltz, G. K. *Nat. Rev. Mol. Cell Biol.* **2012**, *13*, 607−615.
(42) Galluzzi, L.; Kepp, O.; Kroemer, G. *Nat. Rev. Mol. Cell Biol.* **2012**, *13* (12), 780−788.
(43) Kim, S. G.; Hoffman, G. R.; Poulogiannis, G.; Buel, G. R.; Jang, Y. J.; Lee, K. W.; Kim, B. Y.; Erikson, R. L.; Cantley, L. C.; Choo, A. Y.; Blenis, J. *Mol. Cell* **2013**, *49*, 172−185.
(44) Cagin, U.; Enriquez, J. A. *Int. J. Biochem. Cell Biol.* **2015**, *63*, 10−15.
(45) Tan, K.; Fujimoto, M.; Takii, R.; Takaki, E.; Hayashida, N.; Nakai, A. *Nat. Commun.* **2015**, *6*, 6580.
(46) Wu, J.; Liu, S.; Liu, G.; Dombkowski, A.; Abrams, J.; Martin-Trevino, R.; Wicha, M. S.; Ethier, S. P.; Yang, Z. Q. *Oncogene* **2012**, *31*, 333−341.
(47) Zerbes, R. M.; Bohnert, M.; Stroud, D. A.; von der Malsburg, K.; Kram, A.; Oeljeklaus, S.; Warscheid, B.; Becker, T.; Wiedemann, N.; Veenhuis, M.; van der Klei, I. J.; Pfanner, N.; van der Laan, M. *J. Mol. Biol.* **2012**, *422*, 183−191.
(48) Cserzo, M.; Eisenhaber, F.; Eisenhaber, B.; Simon, I. *Protein Eng., Des. Sel.* **2002**, *15*, 745−752.
(49) Jenkins, K.; Khoo, J. J.; Sadler, A.; Piganis, R.; Wang, D.; Borg, N. A.; Hjerrild, K.; Gould, J.; Thomas, B. J.; Nagley, P.; Hertzog, P. J.; Mansell, A. *Immunol. Cell Biol.* **2013**, *91*, 321−330.
(50) Marques, E. J.; Carneiro, C. M.; Silva, A. S.; Krasilnikov, O. V. *Biochim. Biophys. Acta, Biomembr.* **2004**, *1661*, 68−77.
(51) McDonald, B. M.; Wydro, M. M.; Lightowlers, R. N.; Lakey, J. H. *FEBS Lett.* **2009**, *583*, 739−742.
(52) Tomasello, M. F.; Guarino, F.; Reina, S.; Messina, A.; De Pinto, V. *PLoS One* **2013**, *8*, e81522.
(53) Choudhary, O. P.; Paz, A.; Adelman, J. L.; Colletier, J. P.; Abramson, J.; Grabe, M. *Nat. Struct. Mol. Biol.* **2014**, *21*, 626−632.
(54) Michaud, M.; Ubrig, E.; Filleur, S.; Erhardt, M.; Ephritikhine, G.; Marechal-Drouard, L.; Duchene, A. M. *Proc. Natl. Acad. Sci. U. S. A.* **2014**, *111*, 8991−8996.
(55) Kozjak, V.; Wiedemann, N.; Milenkovic, D.; Lohaus, C.; Meyer, H. E.; Guiard, B.; Meisinger, C.; Pfanner, N. *J. Biol. Chem.* **2003**, *278*, 48520−48523.
(56) Ujwal, R.; Cascio, D.; Colletier, J. P.; Faham, S.; Zhang, J.; Toro, L.; Ping, P. P.; Abramson, J. *Proc. Natl. Acad. Sci. U. S. A.* **2008**, *105*, 17742−17747.
(57) Schredelseker, J.; Paz, A.; Lopez, C. J.; Altenbach, C.; Leung, C. S.; Drexler, M. K.; Chen, J. N.; Hubbell, W. L.; Abramson, J. *J. Biol. Chem.* **2014**, *289*, 12566−12577.
(58) Hiller, S.; Abramson, J.; Mannella, C.; Wagner, G.; Zeth, K. *Trends Biochem. Sci.* **2010**, *35*, 514−521.
(59) Dimmer, K. S.; Navoni, F.; Casarin, A.; Trevisson, E.; Endele, S.; Winterpacht, A.; Salviati, L.; Scorrano, L. *Hum. Mol. Genet.* **2008**, *17*, 201−14.
(60) Haque, M. E.; Elmore, K. B.; Tripathy, A.; Koc, H.; Koc, E. C.; Spremulli, L. L. *J. Biol. Chem.* **2010**, *285*, 28353−28362.
(61) Martell, J. D.; Deerinck, T. J.; Sancak, Y.; Poulos, T. L.; Mootha, V. K.; Sosinsky, G. E.; Ellisman, M. H.; Ting, A. Y. *Nat. Biotechnol.* **2012**, *30*, 1143−8.
(62) Claros, M. G.; Vincens, P. *Eur. J. Biochem.* **1996**, *241*, 779−786.
(63) Rees, D. M.; Leslie, A. G. W.; Walker, J. E. *Proc. Natl. Acad. Sci. U. S. A.* **2009**, *106*, 21597−21601.
(64) Chong, S. H.; Ham, S. *Acc. Chem. Res.* **2015**, *48*, 956−965.
(65) Dickson, A.; Brooks, C. L. *J. Am. Chem. Soc.* **2013**, *135*, 4729−4734.
(66) Stiller, S. B.; Hopker, J.; Oeljeklaus, S.; Schutze, C.; Schrempp, S. G.; Vent-Schmidt, J.; Horvath, S. E.; Frazier, A. E.; Gebert, N.; van der Laan, M.; Bohnert, M.; Warscheid, B.; Pfanner, N.; Wiedemann, N. *Cell Metab.* **2016**, *23*, 901−908.
(67) Darshi, M.; Mendiola, V. L.; Mackey, M. R.; Murphy, A. N.; Koller, A.; Perkins, G. A.; Ellisman, M. H.; Taylor, S. S. *J. Biol. Chem.* **2011**, *286*, 2918−2932.
(68) Kim, H.; Melen, K.; Osterberg, M.; von Heijne, G. *Proc. Natl. Acad. Sci. U. S. A.* **2006**, *103*, 11142−11147.
(69) Sato, T.; Mihara, K. *J. Biol. Chem.* **2009**, *284*, 14819−14827.
(70) Song, J. M.; Midson, C.; Blachly-Dyson, E.; Forte, M.; Colombini, M. *J. Biol. Chem.* **1998**, *273*, 24406−24413.
(71) Suckau, D.; Mak, M.; Przybylski, M. *Proc. Natl. Acad. Sci. U. S. A.* **1992**, *89*, 5630−5634.
(72) Grumbach, I. M.; Veh, R. W. *J. Immunol. Methods* **1991**, *140*, 205−210.
(73) Kim, S.; Mischerikow, N.; Bandeira, N.; Navarro, J. D.; Wich, L.; Mohammed, S.; Heck, A. J.; Pevzner, P. A. *Mol. Cell. Proteomics* **2010**, *9*, 2840−2852.
(74) Kim, S.; Pevzner, P. A. *Nat. Commun.* **2014**, *5*, 5277.
(75) Cox, J.; Neuhauser, N.; Michalski, A.; Scheltema, R. A.; Olsen, J. V.; Mann, M. *J. Proteome. Res.* **2011**, *10*, 1794−1805.

DOI: 10.1021/jacs.6b10418
J. Am. Chem. Soc. 2017, 139, 3651−3662

Supporting Information

Architecture Mapping of the Inner Mitochondrial Membrane Proteome by Chemical Tools in Live Cells

Song-Yi Lee[1], Myeong-Gyun Kang[1], Sanghee Shin[2,3], Chulhwan Kwak[1], Taejoon Kwon[4], Jeong Kon Seo[5,*] Jong-Seo Kim[2,3,*], and Hyun-Woo Rhee [1,*]

[1]Department of Chemistry and [4]Department of Biomedical Engineering, [5]UNIST Central Research Facilities (UCRF), Ulsan National Institute of Science and Technology (UNIST), Ulsan, 44919, Korea [2]Center for RNA Research, Institute of Basic Science (IBS), Seoul, 08826, Korea [3]School of Biological Sciences, Seoul National University, Seoul, 08826, Korea.

*Corresponding authors:

rhee@unist.ac.kr, jongseokim@snu.ac.kr, jkseo6998@unist.ac.kr

Supporting Table 1. Construct Information

Name (expected size)	Features	Promotor / Vector	Details
Mito-V5-APEX2 (unprocessed: 32 kDa, processed: 29 kDa)	*NotI*-Mito-*BamHI*-V5-APEX2-Stop-*XhoI*	CMV/ pcDNA3	Mito-: MLATRVFSLVGKRAISTSVCVRAH (matrix targeting sequence, Fornuskova et al., 2010)
Mito-V5-APEX2 (unprocessed: 32 kDa, processed: 29 kDa)	*KpnI*-Mito-*BamHI*-V5-APEX2-Stop-*NotI*	CMV/ pcDNA5	Mito-: MLATRVFSLVGKRAISTSVCVRAH (matrix targeting sequence, Fornuskova et al., 2010)
LACTB-Flag-APEX2* (unprocessed: 35 kDa, processed: 29 kDa)	*NotI*-LACTB-*BamHI*-Flag-APEX2-Stop-*XhoI*	CMV/ pcDNA3	$LACTB_{(1-68)}$: MYRLLSSVTARAAATAGPAWD GGRRGAHRRPGLPVLGLGWAG GLGLGLGLALGAKLVVGLRGA VPIQS (IMS targeting signal, Polianskyte et al., 2009)
LACTB-V5-APEX2 (unprocessed: 35 kDa, processed: 29 kDa)	*KpnI*-LACTB-*BamHI*-V5-APEX2-Stop-*NotI*	CMV/ pcDNA5	$LACTB_{(1-68)}$: MYRLLSSVTARAAATAGPAWD GGRRGAHRRPGLPVLGLGWAG GLGLGLGLALGAKLVVGLRGA VPIQS (IMS targeting signal, Polianskyte et al., 2009)
ScoI-V5-APEX2* (unprocessed: 62 kDa, processed: 59 kDa)	*KpnI*-ScoI-*BamHI*-V5-APEX2-Stop-*XhoI*	CMV/ pcDNA3	Sco1 (NM_004589)
ScoI-V5-APEX2 (unprocessed: 62 kDa, processed: 59 kDa)	*HindIII*-ScoI-*BamHI*-V5-APEX2-Stop-*XhoI*	CMV/ pcDNA5	Sco1 (NM_004589)
TMEM261-V5-APEX2 (unprocessed: 42.8 kDa)	*HindIII*-TMEM261-*BamHI*-V5-APEX2-Stop-*XhoI*	CMV/ pcDNA5	TMEM261 (NM_033428.2)
Tom20-V5-APEX2*	*NotI*-Tom20-10 aa linker-*NheI*-	CMV/ pcDNA3	10 aa linker : GGSGDPPVAT

(45.7 kDa)	V5-APEX2-Stop-*XhoI*		Tom20 (NM_014765.2)
TRMT61B-V5-APEX2* (81.5 kDa)	*NotI*-TRMT61B-*NheI*-V5-APEX2-Stop-*XbaI*	CMV/ pcDNA3	TRMT61B (NM_017910),
ATP5J-V5-APEX2 (unprocessed: 41.2 kDa, processed: 37.2 kDa)	*NotI*-ATP5J-*BamHI*-V5-APEX2-Stop-*XhoI*	CMV/ pcDNA3	ATP5J (NM_001685),
MGST3-V5-APEX2* (45.1 kDa)	*NotI*-MGST3-*BamHI*-V5-APEX2-Stop-*XhoI*	CMV/ pcDNA3	MGST3 (NM_004528)
Pdk1-V5-APEX2* (unprocessed, 81.5 kDa, processed: 76.0 kDa)	*NotI*-Pdk1-10 aa linker-*NheI*-V5-APEX2-Stop-*XhoI*	CMV/ pcDNA3	Pdk1 (NM_002610)
V5-APEX2-Sec61B* (38.6 kDa)	*NotI*-V5-APEX2-*NheI*-Sec61B-Stop-*XhoI*	CMV/ pcDNA3	Sec61B (NM_006808)*
Sec61B-V5-APEX2* (38.5 kDa)	*NotI*-Sec61B-*NheI*-V5-APEX2-Stop-*XbaI*	CMV/ pcDNA3	Sec61B (NM_006808)*
ss-APEX2-V5-KDEL* (unprocessed: 31.8 kDa, processed: 29.5 kDa)	*EcoRV-ss-HA-ApaI*-APEX2-V5-KDEL-Stop-*NotI*	CMV/ pDisplay	ss: METDTLLLWVLLLWVPGSTGD (IgK chain leader sequence for ER lumen) KDEL: ER retention motif*
V5-APEX2-NES* (29.8 kDa)	*NotI*-V5-APEX2-NES-Stop-*XhoI*	CMV/ pcDNA3	NES: LQLPPLERLTLD (nuclear exclusion signal)*
V5-APEX2-LETM1 (112.9 kDa)	*HindIII*-LETM (1-151 aa)-*NotI*-V5-APEX2-*NheI*-10aa linker-LETM1(152-739 aa)-Stop-*XhoI*	CMV/ pcDNA5	LETM1 (1-151 aa): MASILLRSCRGRAPARLPPPPRYTVPRGSPGDPA HLSCASTLGLRNCLNVPFGCCTPIHPVYTSSRG DHLGCWALRPECLRIVSRAPWTSTSVGFVAVGP QCLPVRGWHSSRPVRDDSVVEKSLKSLKDKNK KLEEGGPVYSPPAEVVVKK (LETM1 N-terminal domain)
OCIAD1-V5-APEX2-AP (58.2 kDa)	*HindIII*-OCIADI-*BamHI*-V5-APEX2-AP-	CMV/ pcDNA5	AP : GLNDIFEAQKIEWHE (Acceptor peptide)

	Stop-*XhoI*		
CLPB-V5-APEX2-AP (109.3 kDa)	*HindIII*-CLPB-*BamHI*-V5-APEX2-AP-Stop-*XhoI*	CMV/ pcDNA5	AP : GLNDIFEAQKIEWHE (Acceptor peptide)
Mito-pBirA-HA (unprocessed: 39 kDa, processed: 36 kDa)	*HindIII*-Mito-*BamHI*-BirA-HA-Stop-*XhoI*	CMV/ pcDNA5	Mito-: MLATRVFSLVGKRAISTSVCVRAH (matrix targeting sequence, Fornuskova et al., 2010)
OXA1L(1-73 aa)-V5-APEX2 (unprocessed: 37 kDa, processed: 29 kDa)	*KpnI*-OXA1L(1-73 aa)-*NheI*-V5-APEX2-Stop-*NotI*	CMV/ pcDNA5	NM_005015.3
OXA1L(1-435 aa)-V5-APEX2 (unprocessed: 77 kDa, processed: 69 kDa)	*KpnI*-OXA1L(1-435 aa)-V5-APEX2-Stop-*NotI*	CMV/ pcDNA5	NM_005015.3

The nuclear export sequence, NES (LQLPPLERLTLD), was derived from residues 6–17 of the HIV-1 Rev protein30. The ER-targeted C1 sequence was derived from the N-terminal 27 amino acids of rabbit P450 C1 (MDPVVVLGLCLSCLLLLSLWKQSYGGG). Protein processed size during translocation was obtained by programs: Mitoprot[1] (http://ihg.gsf.de/ihg/mitoprot.html or Mitoprot software is available by: ftp://ftp.biologie.ens.fr/pub/molbio) and SignalP 4.1 Server[2] (http://www.cbs.dtu.dk/services/SignalP/) .

*The imaging pattern of these constructs was previously characterized in Lee et al, Cell Rep. 2016, 15, 1837-1847.

Supporting Experimental Procedures

Desthiobiotin-phenol synthesis: Desthiobiotin (100 mg) was dissolved in 2 mL DMSO (dimethyl sulfoxide) at room temperature. 1.1 equivalents of HATU (2-(7-aza-1H-benzotriazole-1-yl)-1,1,3,3-tetramethyluronium hexafluorophosphate) and 2.0 equivalents of DIPEA (*N*,*N*-diisopropylethylamine) were added into the solution. The mixture was stirred for 10 min at room temperature. Then 2.0 equivalent of the tyramine was added. The reaction mixture was stirred overnight at room temperature. Products were purified by preparative HPLC using a C18 reverse phase column with a 5–95% gradient of acetonitrile in water for 40 min. Products eluted around 20 min. Product yields were ~70%. ^{1}H-NMR (400 MHz, d4-Methanol):δ 1.10 (3H,d,J = 6.5 Hz), 1.30–1.46 (8H,m), 1.57 (2H,m), 2.14(2H,t,J = 7.5 Hz), 2.68 (2H,t,J = 7.5 Hz), 3.35 (2H,m), 3.77 (1H,m), 3.81 (1H,m), 6.70 (2H, d, J = 8 Hz), 7.02 (2H, d, J = 8 Hz). ^{13}C-NMR (100 MHz, d6-DMSO): δ 15.508, 25.212, 25.591, 28.710, 29.522, 34.439, 35.371, 40.433, 50.259, 55.016, 115.049, 129.450, 129.564, 155.581, 162.865, 171.963, HMRS m/z ($C_{18}H_{28}N_3O_3$): theoretical: 334.2131, observed: 334.2136,

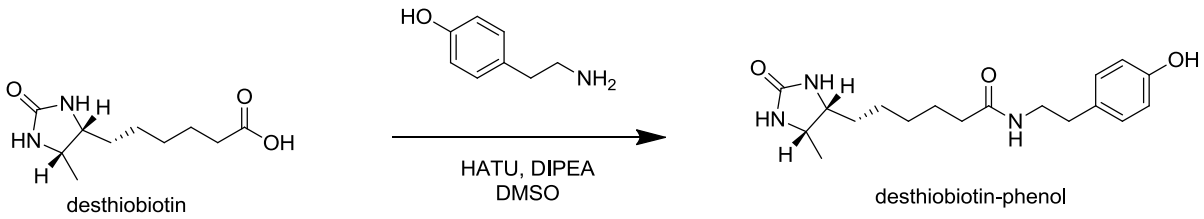

Biotin-phenol was synthesized and characterized by following reported procedure (Rhee and Zou et al, *Science*, **2013**, *339*, 1328-1331). All chemicals and reagents were purchased from Sigma-Aldrich and Alfa Aesar.

Stable cell line selection and culturing. Flp-In™ T-REx™ 293 cells (Life Technologies) were cultured in DMEM (Gibco) supplemented with 10% FBS, 2 mM L-glutamine, 50 units/mL penicillin, and 50 μg/ml streptomycin at 37°C under 5% CO_2. Cells were grown in a T25 flask. Stable cell lines were generated by co-transfection with the pcDNA™5/FRT/TO expression construct and the pOG44 plasmid. Cells were transfected at 60–80% confluence using Lipofectamine 2000 (Life Technologies), typically with 20 μL Lipofectamine 2,000 and 4,000 ng plasmid (9:1 = pOG44:pcDNA5) per T25 flask. After 24 h, cells were split into a 90 mm cell culture dish (SPL, 11090) with the proper concentration of hygromycin B (100–200 μg/mL). Media containing hygromycin B were changed every 3–4 days. After 2–3 weeks, 3–4 colonies were selected and transferred to a 24-well plate. Cells were continuously split into larger plates, and a cell stock was made. After splitting the cells into a 6-well plate, separate samples were prepared for expression testing. To induce the protein expression in stable cells, cells at 60-80% confluence were treated with 100 ng/mL doxycycline (Sigma Aldrich). Cells were desthiobiotin-phenol-labeled and lysed 18–24 h after induction.

Desthiobiotin-phenol (and biotin-phenol) labeling in stably expressed APEX cell line. Stable cells were grown in four T75 flasks. Cells were induced with doxycycline at 60–80% confluence. After 18–24 h, the medium in each flask was changed to 7.5 mL of fresh growth medium containing 250 μM desthiobiotin-phenol or biotin-phenol. All DBP and BP parallel experiments were performed

simultaneously with same protocol. The flasks were incubated at 37°C under 5% CO_2 for 30 min according to previously published protocols. Afterwards, 750 µL of 10 mM H_2O_2 (diluted from 30% H_2O_2, Sigma Aldrich H1009) was added to each flask, for a final concentration of 1 mM H_2O_2, and the flasks were gently agitated for 1 min at room temperature. The reaction was then quenched by adding 7.5 mL of DPBS containing 10 mM Trolox, 20 mM sodium azide, and 20 mM sodium ascorbate to each flask. Then, the solution was removed, and the cells were washed three times with cold quenching solution (DPBS containing 5 mM Trolox, 10 mM sodium azide, and 10 mM sodium ascorbate). Cells were detached using of cold quenching solution and centrifuged at 1,500 × *g* for 5 min at 4°C. Cells were resuspended with fresh cold quenching solution and centrifuged again. Cells from one flask were lysed with 1.5 mL RIPA lysis buffer (50 mM Tris, 150 mM NaCl, 0.1% SDS, 0.5% sodium deoxycholate, 1% Triton X-100), 1 × protease cocktail (Sigma Aldrich, P8849), 1 mM PMSF (phenylmethylsulfonyl fluoride), 10 mM sodium azide, 10 mM sodium ascorbate, and 5 mM Trolox for 10 min at 4°C. Lysates were clarified by centrifugation at 15,000 × *g* for 20 min at 4°C. Then, the four T75 flask samples were combined (~6 mL).

Labeled peptide enrichment. For removal of unreacted free desthiobiotin-phenol or biotin-phenol, 6 mL of cell lysates was divided into two Amicon filter (Merck Millipore, UFC801096) followed by centrifugation at 7500 × *g* for 15 min at 4 °C. PBS (phosphate-buffered saline) containing 1 mM PMSF and 1 × protease cocktail was added up to 4 mL followed by centrifugation three more times. Finally, the volume of the cell lysates was reduced to ~1 mL and transferred to an Eppendorf tube. Then, 300 µL of streptavidin beads (Pierce) was washed with PBS three times and added to the sample. The sample was rotated for 1 h at room temperature. The flow-through fraction was kept, and the beads were washed twice with PBS. After removing the PBS, 100 µL of denaturing solution (6 M urea, 2 M thiourea, 10 mM HEPES) was added. The solution was reduced using 20 µL of 100 mM DTT (dithiothreitol) in 50 mM ammonium bicarbonate (ABC) with shaking at 900 rpm for 60 min at 56°C using a Thermomixer (Eppendorf). Protein alkylation was performed by adding 35 µL of 300 mM iodoacetamide in 50 mM ABC with shaking at 900 rpm in the dark for 30 min. The final reaction volume was adjusted with 50 mM ABC to 1,000 µL. Then, 8 µL of 1 mg/mL trypsin gold in acetic acid (Promega, V5280) was added. The solution was incubated at 37°C with shaking at 900 rpm overnight. The supernatant was transferred to another Eppendorf tube, and 1 µL of formic acid was added to terminate the reaction. The beads were washed with PBS four times and eluted by boiling at 95°C for 10 min after adding 250 µL of 95% formamide, 10 mM EDTA, pH 8.2. Then, divided samples were combined into one e-tube and 1 ml of 3% acetonitrile/0.1% formic acid (v/v) was added. The solution was desalted with Varian Bond ELUT (Agilent, 12109301) and home-made column.

Desalting. Varian Bond ELUT was activated with 1 mL 3% acetonitrile/0.1% formic acid, 1 mL 100% acetonitrile, and 2 mL 3% acetonitrile/0.1% formic acid (v/v). Then, the sample was added to the column for binding (× 2). The column was washed using 2 mL 3% acetonitrile/0.1% formic acid (v/v). It was then eluted with 1.4 mL 70% acetonitrile/0.1% formic acid (v/v) and 500 µL of 100% acetonitrile. The eluted fraction was dried. Dried samples were redissolved in the 0.1% formic acid.

A home-made column was used for obtaining more clean samples. The end of a 200-µL Eppendorf tip was blocked with a 3M Empore C8 disk (3M Bioanalytical Technologies, 2214) and ~5 mg of POROS Oigo R2 reversed phase resin (Applied Biosystems, 1-1159-06) was added. The column was

activated by sequential centrifugation at 1000 × g with 100 µL of 3 % acetonitrile/0.1 % formic acid (v/v), 100 µL of 100 % acetonitrile, and 200 µL of 3 % acetonitrile/0.1 % formic acid (v/v). Then, the samples in the 0.1 % formic acid were added to the column. The column was washed using 200 µL of 3 % acetonitrile/0.1 % formic acid (v/v) three times. The column was then eluted with 200 µL of 70 % acetonitrile/0.1 % formic acid (v/v) twice and then with 50 µL of 100 % acetonitrile. The eluted fraction was dried in a speed-vac and kept in the refrigerator.

LC-MS/MS. Analytical capillary columns (100 cm x 75 µm i.d.) and trap columns (2 cm x 150 µm i.d) were packed in-house with 3 µm Jupiter C18 particles (Phenomenex, Torrance, CA). The long analytical column was placed in a column heater (Analytical Sales and Services, Pompton Plains, NJ) regulated to a temperature of 45 °C. Dionex Ultimate 3000 RSLC nano-system (Thermo Scientific, Sunnyvale, CA) was operated at a flow rate of 350 nL/min over 2 hours with linear gradient ranging from 95 % solvent A (H_2O with 0.1% formic acid) to 40% of solvent B (acetonitrile with 0.1% formic acid).

The enriched samples were analyzed on an Orbitrap Fusion Lumos mass spectrometer (Thermo Scientific) equipped with an in-house customized nanoelectrospray ion source. Precursor ions were acquired (m/z 400 – 1600 at 120 K resolving power and the isolation of precursor for MS/MS analysis was performed with a 1.4 Th. Higher-energy collisional dissociation (HCD) with 30% collision energy was used for sequencing with a target value of 1e5 ions determined by automatic gain control. Resolving power for acquired MS2 spectra was set to 30 k at m/z 200 with 150 ms maximum injection time.

LTQ-Orbitrap Elite mass spectrometer (Thermo Scientific) equipped with a nanoelectrospray ion source was also used. A C18 reverse-phase HPLC column (150 mm × 75 µm i.d.) was used to separate the peptide mixture using a 10–24% acetonitrile/0.1% formic acid gradient for 90 min at a flow rate of 300 nL/min. For MS/MS analysis, precursor ion scan MS spectra (m/z 400 - 2000) were acquired using the Orbitrap spectrometer at a resolution of 60 K at 400 m/z with an internal lock mass. The 20 most intensive ions were isolated and fragmented in the linear ion trap by collisionally induced dissociation (CID).

LC-MS/MS data processing. All MS/MS data were searched by MS-GF+ algorithm (v.9979) and MaxQuant (version 1.5.3.30) with Andromeda search engine at 10 ppm of precursor ion mass tolerance against the SwissProt Homo sapiens proteome database (20199 entries, UniProt (http://www.uniprot.org/)). The following search parameters were applied: semi-tryptic digestion, fixed carbamidomethylation on cysteine, dynamic oxidation of methionine, and dynamic BP (delta monoisotopic mass: 361.146), Oxidized BP (delta monoisotopic mass: 377.1409), and DBP (delta monoisotopic mass: 331.1896) of tyrosine residue. The False discovery rate (FDR) was set at < 1 % for peptide spectrum match including unlabeled peptides for both search algorithm. FDR less than 1% was obtained for unique labeled peptide and unique labeled protein level as well. The extracted ion chromatogram (XIC) was plotted by Qual Browser in Xcalibur™ software (Thermo Scientific).

Western blot analysis of desthiobiotin-phenol labeling. Whole cell lysates (10 µl) were separated on a 10% SDS-PAGE gel. For blotting analysis, gels were transferred to nitrocellulose membrane, stained by Ponceau S (10 min in 0.1% (w/v) Ponceau S in 5% acetic acid/water), and

blocked with 2% (w/v) dialyzed BSA and 0.1% Tween-20 in Tris-buffered saline (TBST) at 4°C overnight or at room temperature for 1 h. The blots were immersed in streptavidin-HRP in blot blocking buffer (1:10,000 dilution, Thermo Scientific, cat. no. 21126) at room temperature for 30 min and then rinsed with blot blocking buffer four times for 5 min (4 × 5 min) before development with Clarity reagent (Bio-Rad) and imaging on an LAS 4000. For assessing comparative enzyme expression level, the membrane was stripped with stripping buffer (100 mM 2-Mercapto-ethanol, 2% SDS, 62.5 mM Tris-HCl pH 6.8). Blots were washed 4 × 5 min in TBST buffer, and incubated into 5% blot blocking buffer for 1–2 h. Blots blocked again using blot blocking buffer, and then incubated in 10 mL of primary antibodies (mouse-anti-V5 or mouse-anti-Flag) for 1–2 h at room temperature. Blots were washed 4 × 5 min in TBST buffer before incubation in 10 mL of secondary antibody (anti-mouse-HRP) in blot blocking buffer for 30–60 min at room temperature. The membranes were then washed again 4 × 5 min in TBST buffer before imaging with Clarity reagent (Bio-Rad) as described above.

Fluorescence microscope imaging. For imaging experiments, DBP- or BP-labeled cells were fixed with 4% paraformaldehyde solution in DPBS at room temperature for 15 min. Cells were then washed with DPBS three times and permeabilized with cold methanol at –20°C for 5 min. Cells were washed again three times with DPBS and blocked for 1 h with 2% BSA in DPBS ("blocking buffer") at room temperature.

To detect APEX2-fusion expression, cells were incubated with mouse anti-V5 antibody (Invitrogen, cat. no. R960-25, 1:5000 dilution) for 1 h at room temperature. After washing four times with TBST each 5 min, cells were simultaneously incubated with secondary Alexa Fluor 488-goat anti-mouse IgG (Invitrogen, cat. no. A-11001, 1:1000 dilution) and streptavidin–Alexa Fluor 568 IgG (Invitrogen, cat. no. S11226, 1:1000 dilution) for 30 min at room temperature. Cells were then washed four times with TBST each for 5 min and maintained in DPBS on ice for imaging by FV1000SPD (Olympus) of UOBC in UNIST, Korea.

Transmission electron microscope (TEM) imaging Transiently expressed cells or stably expressed cells were grown in plastic 6-well plates (Falcon, 353078) to 90% confluence. Cells were fixed using 2% glutaraldehyde (Electron Microscopy Sciences) and 2% paraformaldehyde in 0.1 M in sodium cacodylate buffer, pH 7.4. After 30–60 min, the cells were treated for 3 x 5 min in buffer containing 20 mM glycine to quench the unreacted glutaraldehyde and then washed again in cold buffer 2 x 5 min. DAB staining was initiated by adding freshly diluted 1 mg/mL (2.8 mM) DAB (Sigma Aldrich; from a stock of the free base dissolved in 0.1 M HCl) and 10 mM H_2O_2 in PBS. After 20 min, the reaction was stopped by removing the DAB solution, and the cells were again washed with PBS 3 × 5 min each. Post-fixation was performed using 2% (w/v) osmium tetroxide (Electron Microscopy Sciences) for 40 min on the ice and cells were rinsed 5 × 2 min each in chilled distilled water. Cells were brought to room temperature, washed in distilled water, and then carefully scraped off from the plastic, resuspended, and centrifuged at 1500 × g for 1 min to generate a cell pellet. The supernatant was removed and the pellet was dehydrated in a graded ethanol series (50%, 60%, 70%, 80%, 90%, 100%, 100%, 100%) for 15 min each time; then, it was infiltrated into EMBED-812 (Electron Microscopy Sciences) using 1:1 (v/v) resin and anhydrous ethanol for 1 h. The second change of 2:1 (v/v) resin and anhydrous ethanol was incubated overnight. After removing the resin, the sample was exchanged once more with 100% resin for 2 h before transferring the sample to fresh resin, followed by polymerization at 60°C for 24 h. Embedded cell pellets were cut with a diamond knife into 50-nm

sections and imaged on a FEI-Tecnai G2 Spirit bio transmission electron microscope (operated at 120 kV) at the Korea Basic Science Institute in Daejeon and Chuncheon, Korea.

Plasmids and Cloning

Plasmids and cloning. Genes were cloned into the specified vectors using standard enzymatic restriction digest and ligation with T4 DNA ligase. To generate constructs where short tags (e.g., V5 or Flag epitope tag) or signal sequences were appended to the protein, the tag was included in the primers used to PCR-amplify the gene. PCR products were digested with restriction enzymes and ligated into cut vectors (e.g., pcDNA3, and pcDNA5). In all cases, the CMV promoter was used for expression in mammalian cells. The genetic constructs cloned and used for this study are summarized in **Supporting Table 1**.

Analysis of DBP- and BP-labeled Sites from Bovine Serum Albumin (BSA) 250 μg of BSA was labeled with 250 μM DBP (or BP) with 1 μM of HRP and 1 mM H_2O_2 in PBS at room temperature. After 30 min, the mixture was placed on Amicon filter unit (Merck Millipore, UFC801096) followed by centrifugation at 7500 × g for 15 min at 4 °C. PBS was added up to 4 mL followed by centrifugation three more times. Finally, the mixture was concentrated up to 20 – 30 μL with 0.5 mL Amicon filter unit (Merck Millipore, UFC501024). After transferred to new e-tube, 100 μL of denaturing solution (6 M urea, 2 M thiourea, 10 mM HEPES) was added. The solution was reduced using 20 μL of 100 mM DTT (dithiothreitol) in 50 mM ammonium bicarbonate (ABC) with shaking at 800 rpm for 60 min at 56 °C using a Thermomixer (Eppendorf). Protein alkylation was performed by adding 35 μL of 300 mM iodoacetamide in 50 mM ABC with shaking at 800 rpm in the dark for 30 min. The final reaction volume was adjusted with 50 mM ABC to 1 mL. Then, 8 μL of 1 mg/mL trypsin gold in acetic acid (Promega, V5280) was added. The solution was incubated at 37 °C with shaking at 400 rpm overnight. 1 μl of formic acid was added for reaction stop. The solution was desalted with Varian Bond ELUT (Agilent, 12109301).

To characterize the mass spectrometric advantages of DBP- over BP- labeling method, DBP- and BP-labeled BSA digest samples were mixed together with equimolar ratio. The equimolar mixture was analyzed by LC-MS/MS at identical condition, before and after enrichment of the labeled peptides. For enrichment, 30 - 50 μg of equimolar mixture was incubated with 50-150 μL of streptavidin magnetic bead (Pierce, 88817) in 25 mM ABC at room temperature. After 1 h, beads were washed with PBS three times and eluted by boiling at 95 °C for 10 min after adding 30 μL of 95 % formamide, 10 mM EDTA, pH 8.2. The eluent was diluted with 120 μL of 3 % acetonitrile/0.1 % formic acid (v/v) followed by SPE clean-up; C-18 SPE cartridge (Sigma, cat # 52601-U) was pre-activated with 3 mL of MeOH and rinsed with 2 mL of acidified water (0.1 % TFA). The diluted eluent was slowly loaded into the cartridge (1 mL/min). After washing the cartridge with 4 mL of 95 % H_2O/ 5 % ACN /0.1 % TFA, the cleaned peptides was collected by 1 mL of 80 % ACN/ 20 % H_2O/ 0.1 % TFA, followed by lyophilization in speed-vac. The dried samples were reconstituted with 25 mM ABC for LC-MS/MS analysis.

Mammalian cell culturing and transfection. HEK-293T cells from ATCC (passages < 30) were cultured in a MEM (Gibco) supplemented with 10 % FBS, 50 units/mL penicillin, and 50 µg/mL streptomycin at 37 °C under 5 % CO_2. Cells were grown on two T75 flasks. Cells were transfected at 60 – 80 % confluence using Lipofectamine 2000 (Life Technologies), typically with 60 µL Lipofectamine 2,000 and 12,000 ng plasmid per T75 flask. Cells were desthiobiotin-phenol-labeled and lysed 18 – 24 h after transfection.

Desthiobiotin-phenol labeling in live transiently expressed cells (M, L, S, U, ss-APEX2-KDEL, APEX2-NES). Cells were grown in two T75 flasks. Cells were transfected or induced at 60 – 80 % confluence. After 18 – 24 h, the medium in each flask was changed to 7.5 mL of fresh growth medium containing 500 µM (or 250 µM for the APEX2-KDEL and APEX2-NES sample) desthiobiotin-phenol. The flasks were incubated at 37 °C under 5 % CO_2 for 30 min according to previously published protocols. Afterwards, 750 µL of 10 mM H_2O_2 (diluted from 30 % H_2O_2, Sigma Aldrich H1009) was added to each flask, for a final concentration of 1 mM H_2O_2, and the flasks were gently agitated for 1 min at room temperature. The reaction was then quenched by adding 7.5 mL of DPBS containing 10 mM Trolox, 20 mM sodium azide, and 20 mM sodium ascorbate. Then, the solution was removed, and the cells were washed three times with cold quenching solution (DPBS containing 5 mM Trolox, 10 mM sodium azide, and 10 mM sodium ascorbate). Cells were detached using 7 mL of cold quenching solution and centrifuged at 1,500 × g for 5 min at 4 °C. Cells were resuspended with fresh cold quenching solution and centrifuged again. Cells in each flasks were lysed with 1.5 mL RIPA lysis buffer (50 mM Tris, 150 mM NaCl, 0.1 % SDS, 0.5 % sodium deoxycholate, 1 % Triton X-100), 1 × protease cocktail (Sigma Aldrich, P8849), 1 mM PMSF (phenylmethylsulfonyl fluoride), 10 mM sodium azide, 10 mM sodium ascorbate, and 5 mM Trolox for 10 min at 4 °C. Lysates were clarified by centrifugation at 15,000 × g for 10 min at 4 °C. Then, the two T75 flask samples were combined (~3 mL).

Labeled peptide enrichment for transiently expressed APEXs. For removal of unreacted free desthiobiotin-phenol, 3 mL of cell lysates was placed on an Amicon filter (Merck Millipore, UFC801096) followed by centrifugation at 7500 × g for 15 min at 4 °C. PBS (phosphate-buffered saline) containing 1 mM PMSF and 1 × protease cocktail was added up to 4 mL followed by centrifugation three more times. Finally, the volume of the cell lysates was reduced to ~1 mL and transferred to an Eppendorf tube. Then, 300 µL of streptavidin beads (Pierce) was washed with PBS three times and added to the sample. The sample was rotated for 1 h at room temperature. The flow-through fraction was kept, and the beads were washed twice with PBS. After removing the PBS, 100 µL of denaturing solution (6 M urea, 2 M thiourea, 10 mM HEPES) was added. The solution was reduced using 20 µL of 100 mM DTT (dithiothreitol) in 50 mM ammonium bicarbonate (ABC) with shaking at 900 rpm for 60 min at 56°C using a Thermomixer (Eppendorf). Protein alkylation was performed by adding 35 µL of 300 mM iodoacetamide in 50 mM ABC with shaking at 900 rpm in the dark for 30 min. The final reaction volume was adjusted with 50 mM ABC to 1,000 µL. Then, 8 µL of 1 mg/mL trypsin gold in

acetic acid (Promega, V5280) was added. The solution was incubated at 37 °C with shaking at 900 rpm overnight. The supernatant was transferred to another Eppendorf tube, and 1 µL of formic acid was added to terminate the reaction. The beads were washed with PBS four times and eluted by boiling at 95°C for 10 min after adding 250 µL of 95 % formamide, 10 mM EDTA, pH 8.2. Then, 750 µL of 3 % acetonitrile/0.1 % formic acid (v/v) was added to make a total volume of 1 mL. The solution was desalted with Varian Bond ELUT (Agilent, 12109301) or home-made column.

Desalting method for transiently expressed APEX2 sample. In the triplicate experiments, different protocols for the desalting step were tested for method optimization. For transfected sample-1 (M1, L1, S1, U1), a home-made column was used. The end of a 200-µL Eppendorf tip was blocked with a 3M Empore C8 disk (3M Bioanalytical Technologies, Cat. No. 2214) and ~5 mg of POROS Oigo R2 reversed phase resin (Applied Biosystems, Cat. No. 1-1159-06) was added. The column was activated by sequential centrifugation at 1000 × g with 100 µL of 3 % acetonitrile/0.1 % formic acid (v/v), 100 µL of 100 % acetonitrile, and 200 µL of 3 % acetonitrile/0.1 % formic acid (v/v). Then, the sample was directly added to the column without dilution. The column was washed using 200 µL of 3 % acetonitrile/0.1 % formic acid (v/v) three times. The column was then eluted with 200 µL of 70 % acetonitrile/0. 1% formic acid (v/v) twice and then with 50 µL of 100 % acetonitrile. The eluted fraction was dried in a speed-vac and kept in the refrigerator. For transfected sample-2,3 (M2,3, L2,3, S2,3, U2,3), Varian Bond ELUT was used, which was activated with 1 mL 3 % acetonitrile/0.1 % formic acid, 1 mL 100% acetonitrile, and 2 mL 3 % acetonitrile/0.1 % formic acid (v/v). Then, the sample was added to the column for binding (× 2). The column was washed using 2 mL 3 % acetonitrile/0.1 % formic acid (v/v). It was then eluted with 1.4 mL 70% acetonitrile/0.1 % formic acid (v/v) and 500 µL of 100 % acetonitrile. The eluted fraction was dried in a speed-vac and kept in the refrigerator. For ER and Cytosol transfected samples (APEX2-KDEL and APEX2-NES), combined two methods. First, Bond ELUT method used. Samples were dissolved in the 0.1 % formic acid 180 µL and home-made column method was used.

Immunoprecipitation For immunoprecipitation, cells were prepared in wells of a six-well plate. After DBP labeling according to 'Desthiobiotin-phenol labeling in live cells' section, the cells were lysed with Cell Extraction buffer(Life technologies, FNN0011) containing 1× protease cocktail (Sigma Aldrich, P8849), and 1 mM PMSF (phenylmethylsulfonyl fluoride) for 30 min at 4 °C. Lysates were transferred to e-tube and vortexed for 2 min and lysates were clarified by centrifugation at 15,000 *g* for 10 min at 4 °C.

Dynabeads Protein G (Invitrogen, 10003D) 40 µl were incubated with 4 µg of anti-MICU1 (Abcam, ab102830), anti-MICU2 (Abcam, ab101465), anti-STOML2 (Abcam, ab191884), anti-NDUFB10 (Abcam, ab196019), anti-CHCHD3 (Sigma Aldrich, HPA042935) antibody during 30 min at room temperature. The beads were washed two times using PBS with 0.1% Tween 20. Then cell lysates were incubated with Protein G beads during 1 h. The beads were washed three times using PBS with 0.1% Tween 20 and eluted by boiling at 95 °C for 10 min after adding 2X protein loading buffer. Streptavidin-HRP

western blot analysis can be conducted as following 'Western blot analysis of desthiobiotin-phenol labeling' section.

Biochemical assay for NDUFB10 and STOML2 using Proteinase K. Mitochondria Isolation Kit for Cultured Cells (Thermo fisher, 89874) was used for HEK293T cell mitochondria isolation. Isolated mitochondria pellet was resuspended in 250 mM sucrose with 10 mM Hepes (pH 7.5). ~10 μg mitochondria were treated with different digitonin concentrations (0%-0.1%) or 1% Triton X-100 along with 50 μg/ml Proteinase K (Sigma Aldrich, P2308) at 4 °C during 15 min. 7 mM PMSF was added to stop the digestion and SDS protein loading buffer was added.

Solvent accessible surface area value calculation Solvent accessible surface area value can be obtained by PyMOL program using these commands.

PyMOL>set dot_solvent, on

PyMOL>set dot_density, 1

PyMOL>get_area resi X and chain X

If identical chains are shown within a PDB file, we obtained the average solvent accessible surface area over the identical chains.

Line scan analysis and correlation value calculation of biotinylated proteins of CLPB-APEX2 This analysis was followed by the reported protocol by Lee et al.[3] CLPB-APEX2, SCO1-APEX2(IMS), TOM20-APEX2(OMM), Matrix-APEX2 were transfected to HEK293T cell for 24 h. Cells were DBP labeled and lysed. Due to lower labeling intensity of CLPB-APEX2, CLPB-APEX2 sample was loaded three times more than other constructs for 10% SDS-PAGE gel running. Barcodes of streptavidin-HRP western blot images of **Supporting Figure 5c** was scanned and analyzed above 25 kDa using ImageJ software (National Institutes of Health, Bethesda, MD, USA) after background subtraction (ball-point size: 100 pt, sliding paraboloid) was applied in the software. The resulting graph is shown in **Supporting Figure 5d**. For quantification, we introduced the correlation index C_{ij} to quantify similarity between two barcodes *i* and *j*. For the given evenly spaced density values $\rho_0, \rho_1, \ldots, \rho_N$, $I_i(k)$ for a barcode *i* indicates the concentration with the mass density ranging ρ_{k-1} to ρ_k. Given a pair of the barcodes $I_i(k)$ and $I_j(k)$, the correlation C_{ij} is defined as shown in equation (1).

$$C_{ij} = \frac{\frac{1}{N}\sum_{k=1}^{N} I_i(k) I_j(k)}{\sqrt{\frac{1}{N}\sum_{k=1}^{N} I_i(k)^2}\sqrt{\frac{1}{N}\sum_{k=1}^{N} I_j(k)^2}} \qquad (1)$$

This equation (1) gives a greater or smaller value when two barcode shapes are more or less similar, respectively, and two identical barcodes results in a maximum value. The result is shown in **Supporting Figure 5e.**

Supporting Analysis and Discussion

Analysis of DBP-labeled Sites from Transiently Expressed APEXs

We performed three independent DBP-labeling experiments each for transiently expressed Matrix-APEX2, LACTB-APEX2, SCO1-APEX2, and untransfected HEK293T cells. From the analysis of DBP-labeled peptides of 12 independently labeled samples (three each of Matrix-APEX2, LACTB-APEX2, SCO1-APEX2 and untransfected cells), we identified 215 unique labeled sites, which were reproducibly found in each triplicate of APEX2-labeled samples. Interestingly, we found that Matrix-APEX2 and IMS-APEX2s labeled distinct sets of tyrosine residues, divided into five groups (Groups I–V) (**Supporting Figure 4, Supporting Dataset 2**). Group I sites (87 sites) were labeled only by Matrix-APEX2, and Group II sites were labeled by both LACTB-APEX2 and SCO1-APEX2 but not by Matrix-APEX2. Over 95% of Group I and over 85% Group II sites (60 sites) were mapped on the mitochondrial proteins with high mito-specificity (**Supporting Figure 4**).

We also found many overlapped labeled sites, which were observed in all transiently transfected APEX2 samples (Group V). Most of these labeled sites were mapped on the protein components (HNRNPA1, HNRNPA2B1, EIF5A) of the translational complex [4]. Abundant cytosolic proteins such as chaperone protein (HSPA1A) and cytoskeleton protein (ACTB) were also labeled in Group V (**Supporting Dataset 2**). Thus, we hypothesized that labeling these protein components occurred during the translation of APEX constructs and their translocation to mitochondria. Interestingly, from untransfected cells, we found only two DBP-labeled sites from one protein, namely, lanosterol demethylase or CYP51A1. CYP51A1 is an ER-localized cytochrome P450 protein, which is a heme enzyme.[5] We found two of its tyrosine residues (Y131 and Y145), which are very close to the heme residue, to be DBP-modified (**Supporting Figure 4d**).

Bioinformatics analysis of TMEM261

We further investigated the possibility of TMEM261 as an oncogene computationally, using COSMIC database (version 75) [6].Among 9,651 tumor samples with copy number alteration records, 48 pancreatic tumors showed a copy number amplification of TMEM261. However, among 987 breast tumor samples, there was no copy number alteration identified near TMEM261. Out of 8,650 tumor samples with gene expression data, we found that 20 pancreatic tumors (11.9% of total pancreatic tumor samples) and 86 breast tumors (7.8 % of total breast tumor samples) showed significant TMEM261 overexpression, speculating that this mitochondrial protein could have an important role in pancreatic and breast cancer. Several recent studies suggested the connection between mitochondria and pancreatic cancer through Kras [7], thus the role of TMEM261 in pancreatic cancer should be investigated in the future.

Supporting Results

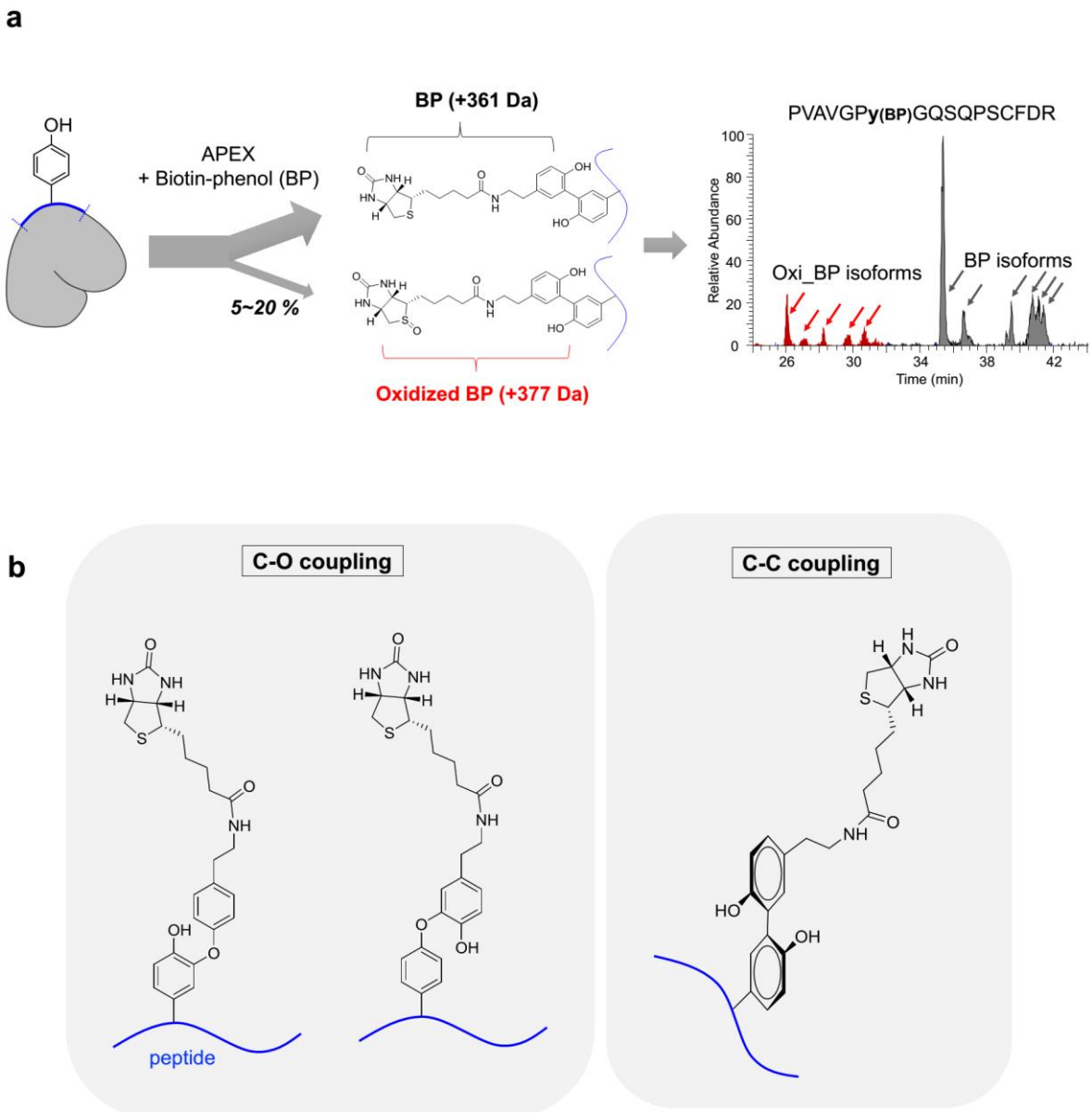

Supporting Figure 1. Drawback of conventional BP-labeling (a) Scheme of BP-labeling and an extracted ion chromatogram (XIC) of a BP-labeled peptide (PVAVGPy*GQSQPSCFDR from ROMO1_HUMAN) and its oxidized form. (b) Scheme of the labeled products from BP-labeling with the same mass but different retention times, via various bond formation between phenoxyl probe and tyrosine residue, e.g. C-C or C-O coupling.

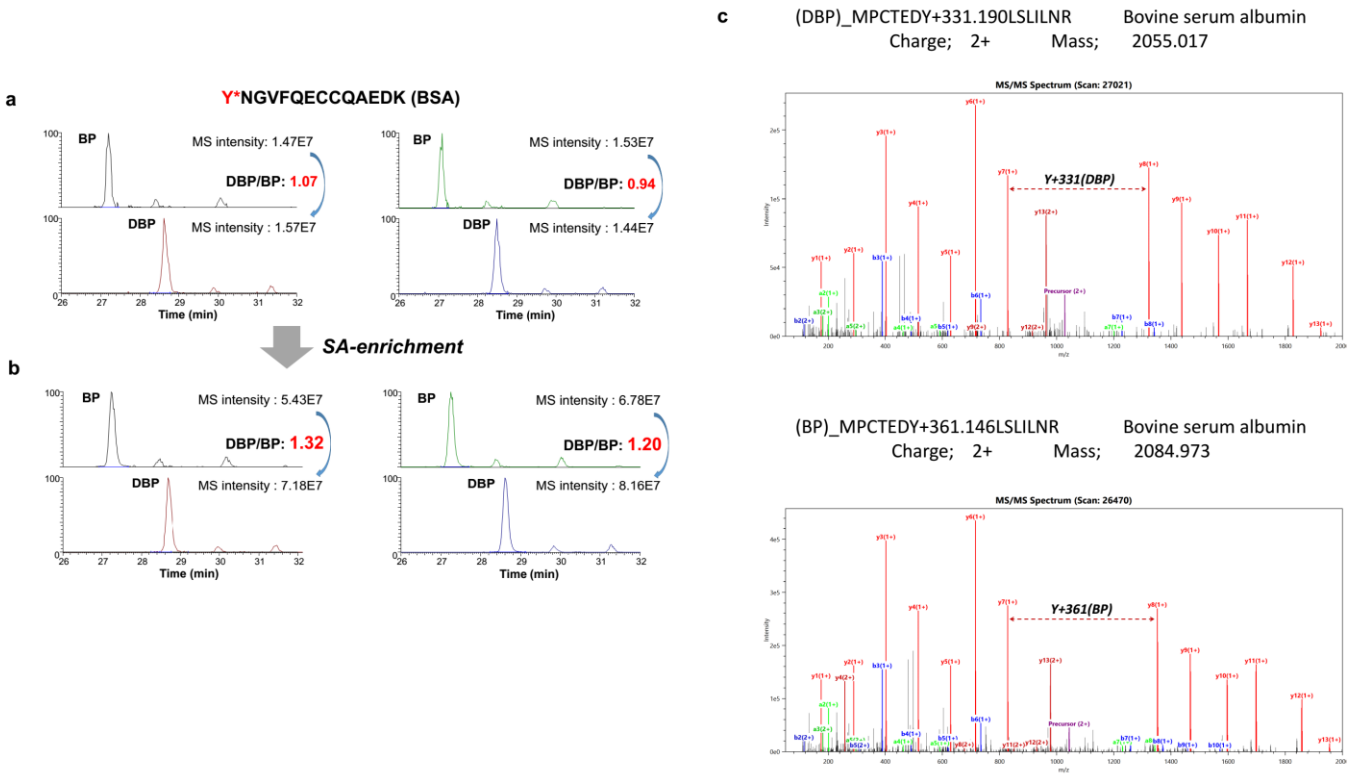

Supporting Figure 2. DBP-labeling vs. BP-labeling. Improved MS1 intensity of DBP-labeled peptide over BP-labeled peptide after enrichment by SA-beads in an equimolar mixture of DBP- and BP-labeled BSA; XIC from each replicate was displayed separately before (a) and after (b) SA-enrichment. (c) MS2 spectra of DBP (upper) and BP (lower) peptides labeled with the same BSA sequence (MPCTEDyLSLILNR) exhibited a highly similar pattern.

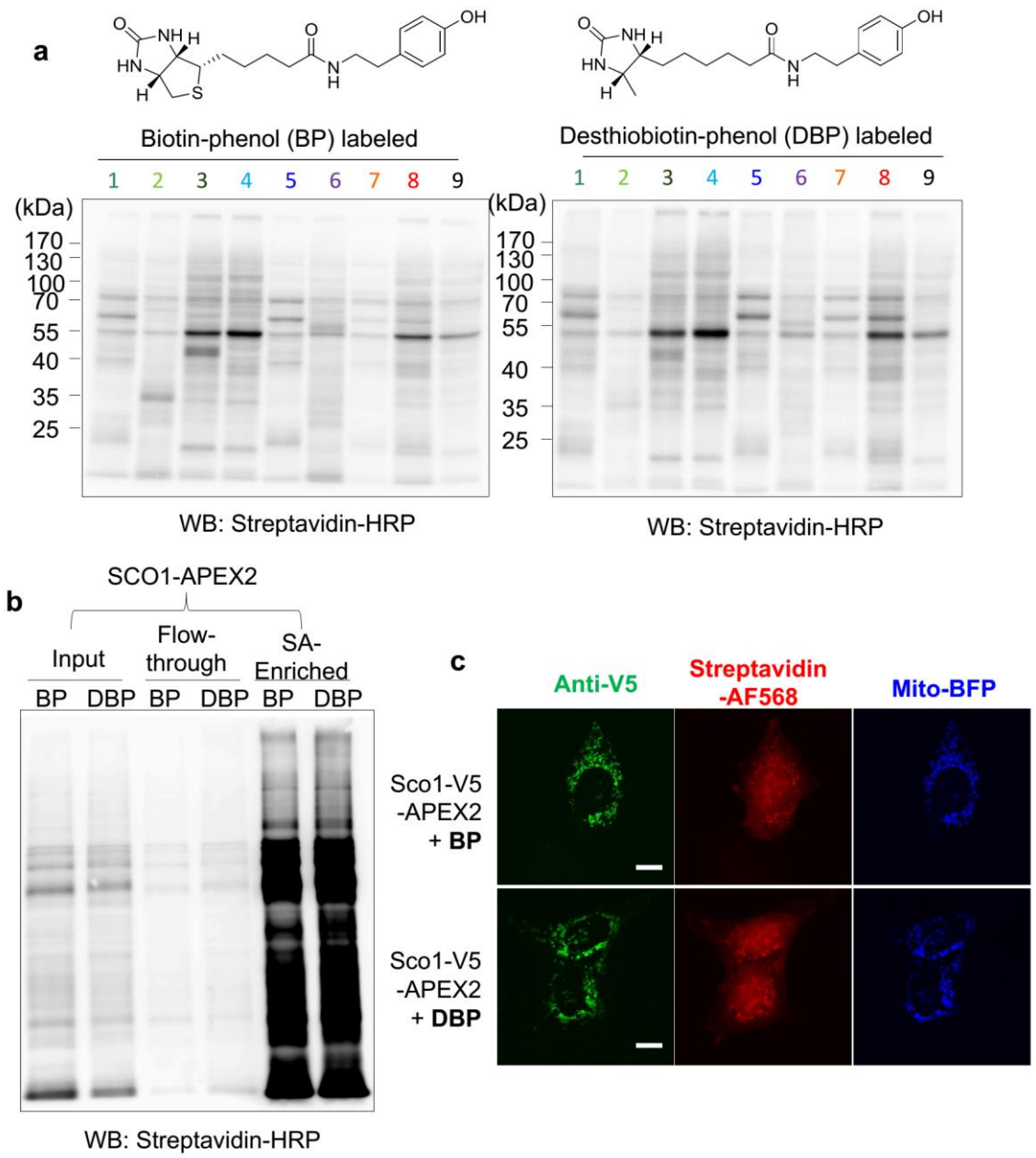

Supporting Figure 3. Similarity of DBP reactivity toward various subcellularly expressed APEX2. (a) Streptavidin (SA)-HRP western blot image of BP-labeled whole-cell lysate of various APEX constructs (1: MitoMatrix-APEX2, 2: LACTB-APEX2 (IMS), 3: Tom20-APEX2 (OMM), 4: APEX2-NES, 5: Pdk1-APEX2 (matrix), 6: SCO1-APEX2 (IMS), 7: TRMT61B-APEX2, 8: ATP5J-APEX2, 9: MGST3-APEX2)) (left), and SA-HRP western blot images of DBP-labeled whole-cell lysate of the same APEX constructs (right). (b) SA-bead enrichment test of DBP- and BP-labeled proteins by SCO1-APEX2. (c) Imaging assay of DBP- and BP-labeled proteins by SCO1-APEX2. Scale bar = 10 μm.

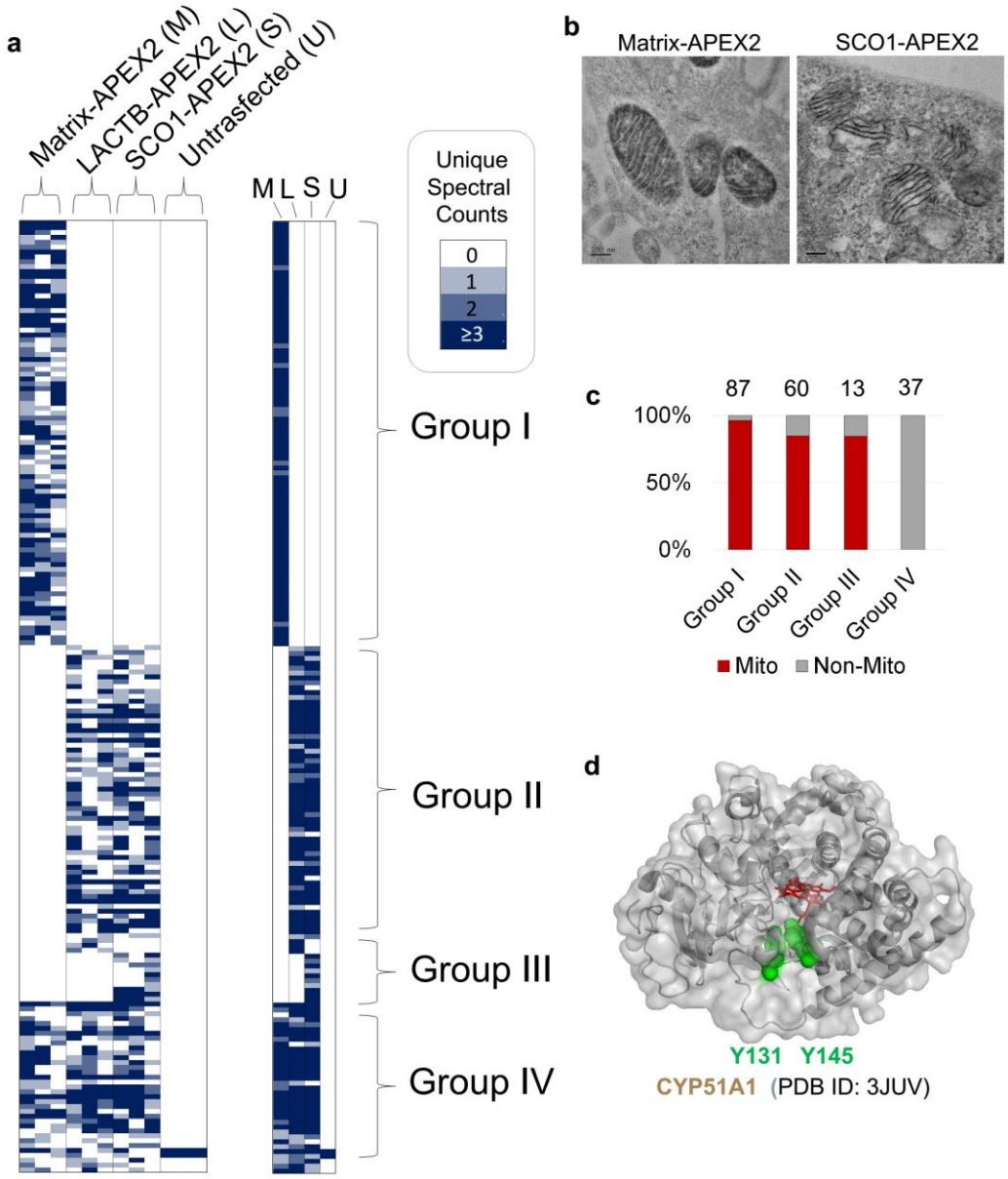

Supporting Figure 4. Identified DBP-labeled sites by transiently expressed APEX2. (a) Overview of 195 DBP-labeled sites of transiently expressed Matrix-APEX2, LACTB-APEX2, SCO1-APEX2, and untransfected cells. The table on the left shows the findings of 12 experiments, and the table on the right presents the overlap of each labeled site per triplicate experiment. Color intensity represents unique spectral counts of each labeled site per experiment for various APEXs. Detail information was shown in **Supporting Dataset 2**. We clustered four exclusively labeled sets (Groups I–IV) of DBP-labeled tyrosine residues (total 686 sites) from the three APEX2s results (**Supporting Dataset 2**). Group I sites were exclusively labeled only by Matrix-APEX2 (M), whereas Group II sites were labeled by both LACTB-APEX2 (L) and SCO1-APEX2 (S), but not by Matrix-APEX2. Group III sites were exclusively labeled either by LACTB-APEX2 or by SCO1-APEX2. Group IV sites were overlapped between Matrix-(M) and IMS-APEX2 (L or S). (b) Electron microscopic imaging of Matrix-APEX2 and SCO1-APEX2. Scale bar: 200 nm. (c) Mitochondrial specificity check of groups I to IV. The number of total labeled sites is depicted over the column. (d) The crystal structure of CYP51A1 (PDB ID: 3JUV) and its DBP-labeled tyrosine residues are shown in green, and heme is shown in red.

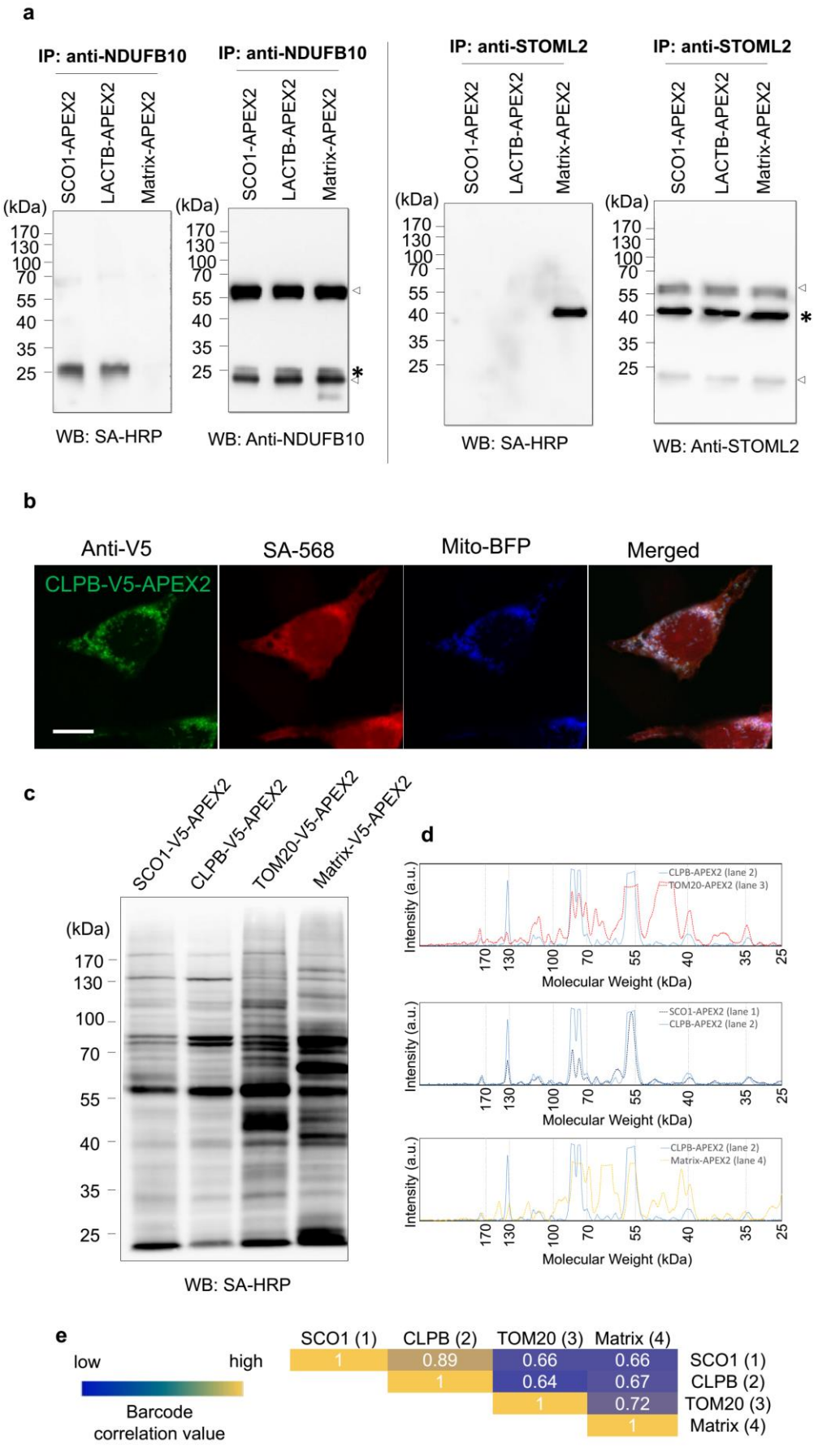
a
IP: anti-NDUFB10
IP: anti-NDUFB10
IP: anti-STOML2
IP: anti-STOML2
SCO1-APEX2
LACTB-APEX2
Matrix-APEX2
(kDa)
170
130
100
70
55
40
35
25
WB: SA-HRP
WB: Anti-NDUFB10
WB: SA-HRP
WB: Anti-STOML2
b
Anti-V5
SA-568
Mito-BFP
Merged
CLPB-V5-APEX2
c
SCO1-V5-APEX2
CLPB-V5-APEX2
TOM20-V5-APEX2
Matrix-V5-APEX2
WB: SA-HRP
d
Intensity (a.u.)
Molecular Weight (kDa)
CLPB-APEX2 (lane 2)
TOM20-APEX2 (lane 3)
SCO1-APEX2 (lane 1)
CLPB-APEX2 (lane 2)
CLPB-APEX2 (lane 2)
Matrix-APEX2 (lane 4)
e
low
high
Barcode correlation value
SCO1 (1)
CLPB (2)
TOM20 (3)
Matrix (4)
1
0.89
0.66
0.66
1
0.64
0.67
1
0.72
1

Supporting Figure 5. Follow-up study for NDUFB10, STOML2, and CLPB. (a) Immunoprecipitation assay by anti-NDUFB10 (left) and anti-STOML2 (right) in SCO1-, LACTB- and Matrix-APEX2 DBP-labeled samples. DBP-labeled NDUFB10 was only observed in IMS-APEX2 (left). DBP-labeled STOML2 was exclusively observed in Matrix-APEX2 sample. Isolated NDUFB10 and STOML2 are marked with an asterisk and the eluted heavy chain and light chain of antibody are marked by blank arrows. (b) Imaging of CLPB-V5-APEX2 labeling imaging; the green channel (anti-V5) is for enzyme expression pattern; red channel (SA-568), for the DBP labeling pattern; and blue channel, for the mitochondrial marker mito-BFP. Scale bar = 10 μm. (c) SA-HRP western blot of BP-labeled proteins from whole-cell lysates of SCO1-V5-APEX2 (IMS standard), CLPB-V5-APEX2, TOM20-V5-APEX2 (OMM standard), Matrix-V5-APEX2 (mitochondrial matrix standard) (d) line-scan analysis graph of the SA-HRP western blot image (c); x-axis: molecular weight, y-axis: intensity (a.u.) (e) Table of calculated barcode correlation value between the line scan analysis graphs for each APEX2-labeled sample (d). Correlation analysis heat map (blue: low, yellow: high)

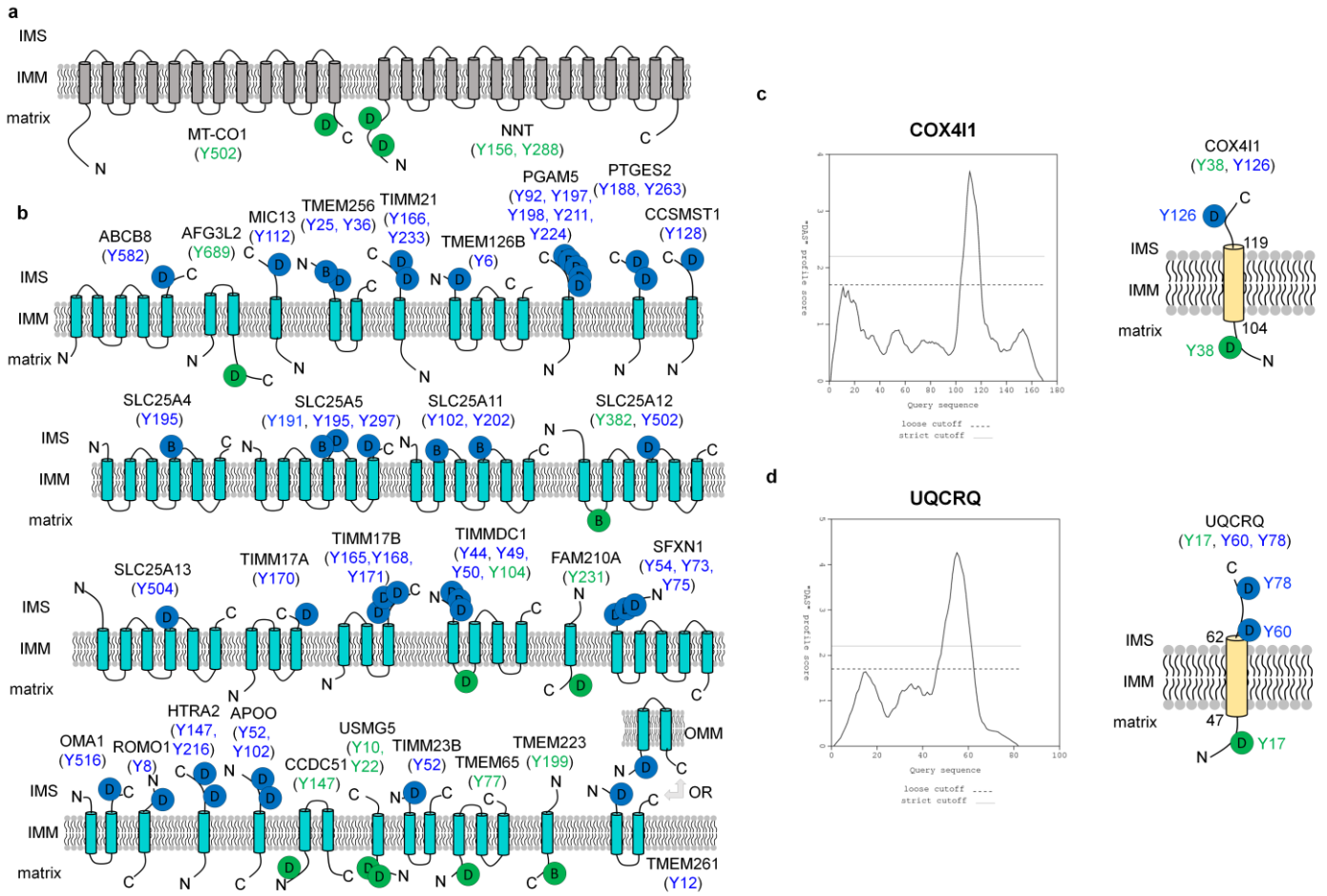

Supporting Figure 6. Identified IMM-TM proteins by labeled sites (a) Confirmed IMM-TM protein topology by our labeled sites (b) Proposed IMM-TM protein topology by our labeled site result. The proposed TM direction is shown in blue. DBP-labeled sites by Matrix-APEX2 are marked by green circles with 'D' and either DBP- or BP-labeled sites by IMS-APEX2 are marked with blue circles with 'D' or 'B' respectively. Detailed information is shown in the **Supporting Dataset 3** and **7** (c–d) Proposed membrane topology of (c) COX4I1 and (d) UQCRQ with the predicted TM domains (right) from Dense Alignment Surface (DAS)-TM prediction analysis[8] (left). Horizontal lines on the DAS-TM plots indicate a "strict" 2.2 DAS score cutoff and a "loose" cutoff at 1.7, which represent the number of matching segments and the actual location of the transmembrane segment, respectively.

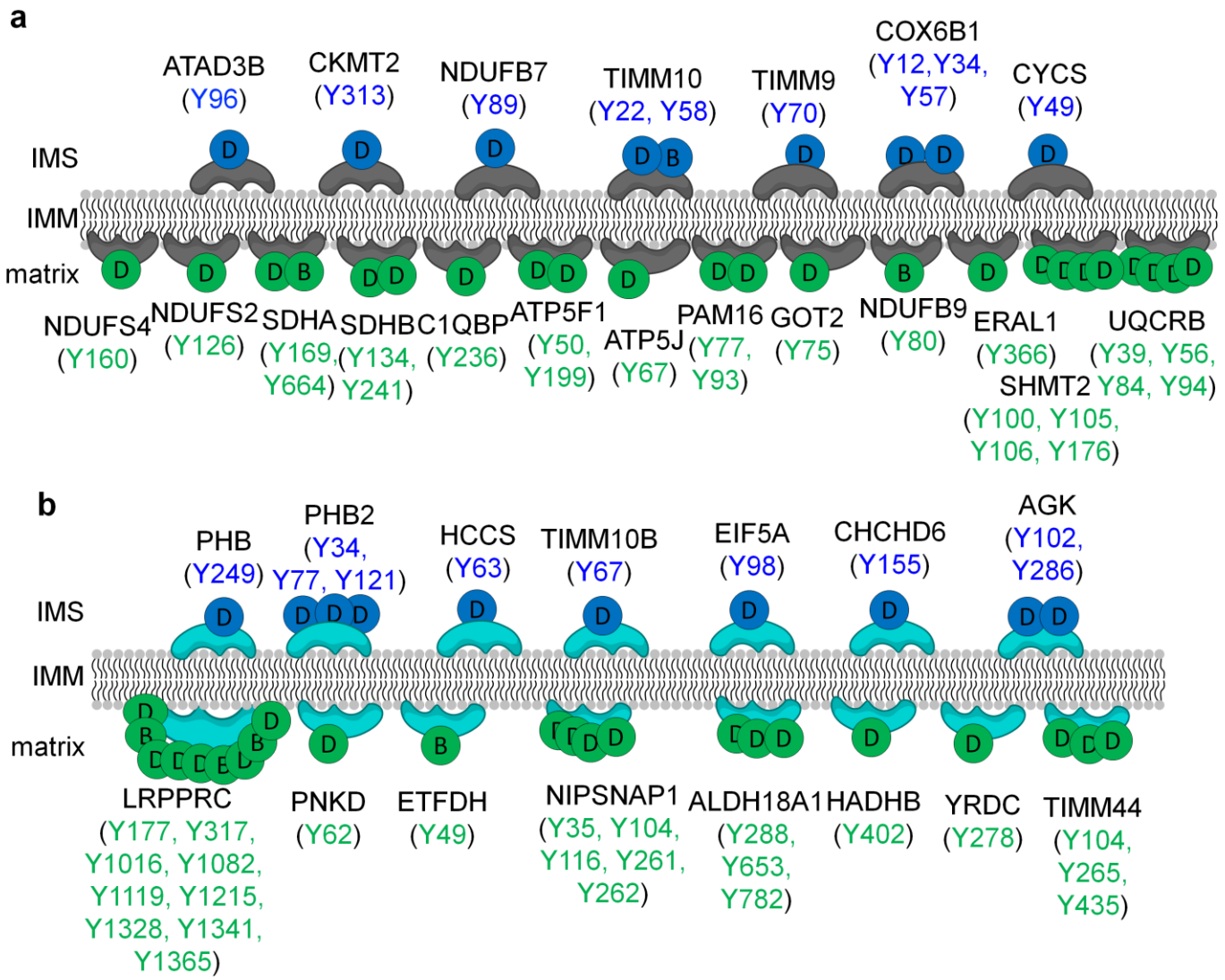

Supporting Figure 7. Identified peripheral membrane proteins at IMM by labeled sites (a) Confirmed peripheral protein direction at IMM by our labeled sites (b) Proposed direction of peripheral proteins at IMM by our labeled site result. DBP-labeled sites by Matrix-APEX2 are marked by green circles with 'D' and DBP-labeled sites by IMS-APEX2 are marked with blue circles with 'D'. Detailed information is shown in the **Supporting Dataset 3** and **7**.

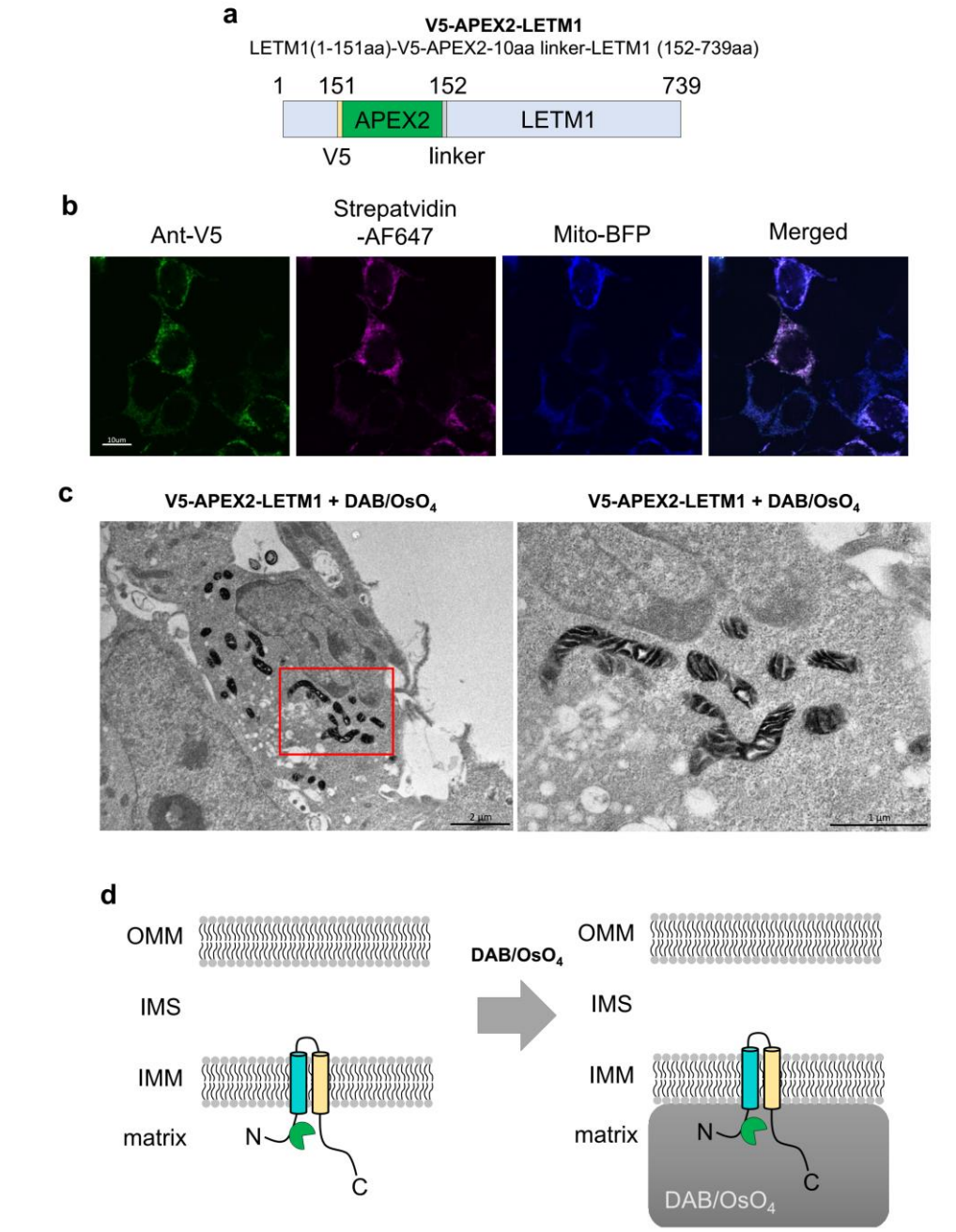
a
V5-APEX2-LETM1
LETM1(1-151aa)-V5-APEX2-10aa linker-LETM1 (152-739aa)
1
151
152
739
APEX2
LETM1
V5
linker
b
Ant-V5
Strepatvidin -AF647
Mito-BFP
Merged
c
V5-APEX2-LETM1 + DAB/OsO4
V5-APEX2-LETM1 + DAB/OsO4
d
OMM
IMS
IMM
matrix
N
C
DAB/OsO4
e
Query sequence
loose cutoff
strict cutoff
f
Proposed topology of LETM1
232
413
IMS
IMM
204
421
matrix
APEX-EM confirmed (151-152)
D
Y422
Y141
Y598

Supporting Figure 8. Follow-up study for topology mapping of LETM1. (a) Construct map of V5-APEX2-LETM1. V5-APEX2 gene was inserted between 151 and 152 aa of LETM1 gene. (b) V5-APEX2-LETM1 labeling imaging; the green channel (anti-V5) is for enzyme expression pattern; the Cy5 channel (SA-AF647) is for the DBP labeling pattern; and the blue channel is for the mitochondrial marker mito-BFP. (c) Electron microscopic imaging of V5-APEX2-LETM1. The right image is an expanded view (scale bar: 1 μm) of inset red box in the left EM image (scale bar: 2 μm). (d) Schematic representation of mitochondrial matrix DAB staining of V5-APEX2-LETM1. (e) LETM1 TM domain analysis with the Dense Alignment Surface (DAS)-TM prediction program[8] revealed two TM domains over a strict cut-off value (2.2 DAS score). (f) Proposed LETM1 membrane topology (e), APEX-EM results (c), and DBP-labeled sites by Matrix-APEX2 (Y141, Y422, Y598).

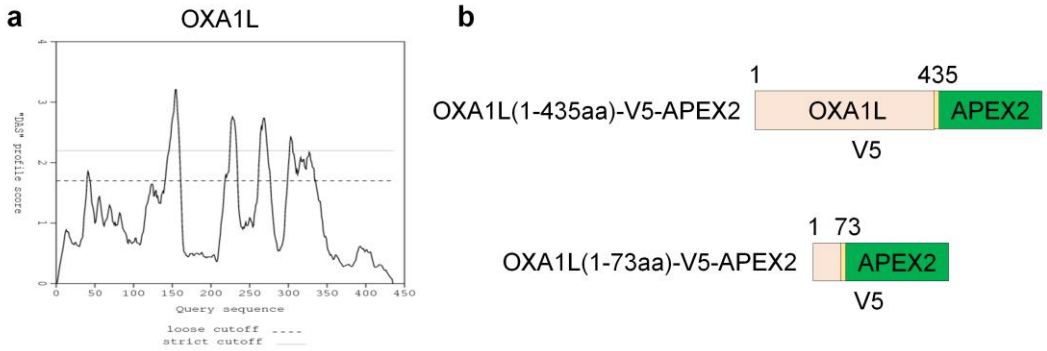

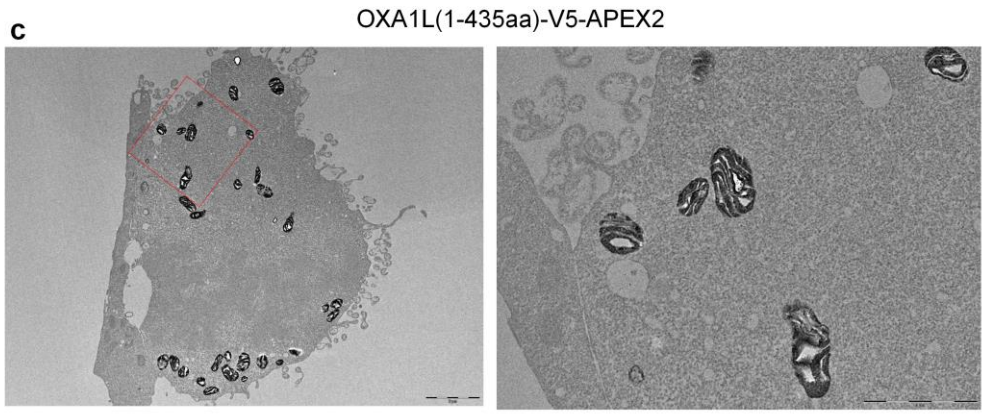

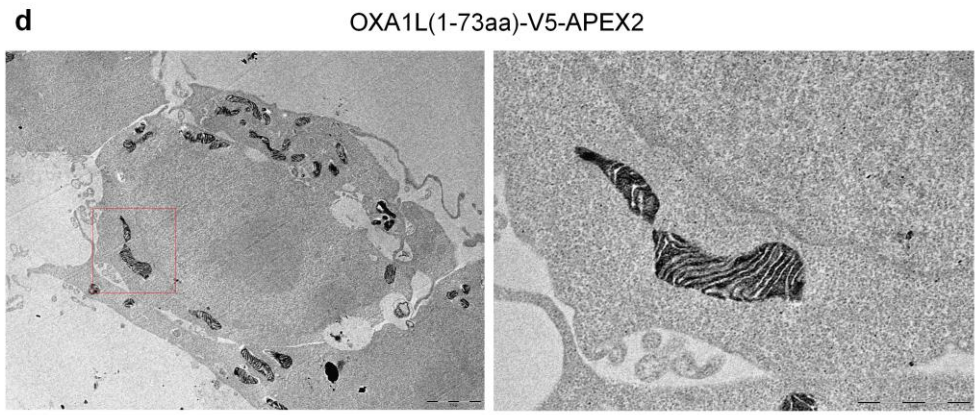

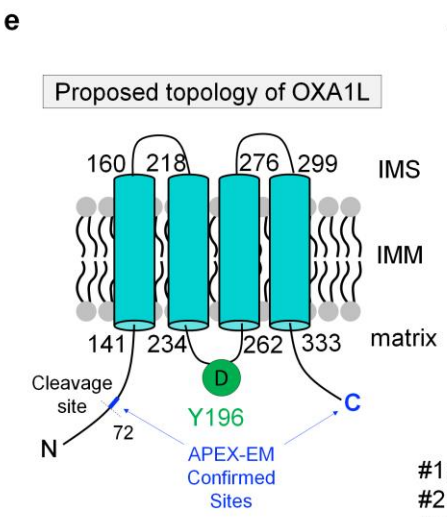

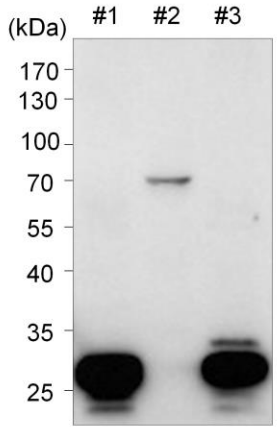

#1: OXA1L(1-73aa)-V5-APEX2 (processed MW : 29kDa)
#2: OXA1L(1-435aa)-V5-APEX2 (processed MW : 69kDa)
#3: Matrix-V5-APEX2 (processed MW : 29kDa)

Supporting Figure 9. Follow-up study for OXA1L topology mapping. (a) OXA1L TM domain analysis revealed 4 TM domains over a strict cut-off value (2.2 DAS score). (b) Construct map of OXA1L(1-435 aa)-V5-APEX2 and OXA1L(1-73 aa)-V5-APEX2, where the V5-APEX2 gene was inserted after aa 435 or 73 of OXA1L, respectively. Electron microscopic imaging of OXA1L(1-435aa)-V5-APEX2 (c) and OXA1L(1-73 aa)-V5-APEX2 (d). The right image is an expanded view (scale bar: 1 μm) of the inset red box in the left EM image (scale bar: 2 μm) (e) Proposed OXA1L membrane topology with 4 predicted TM domains from the prediction analysis (a), APEX-EM results (c and d), and DBP-labeled sites by Matrix-APEX2 (Y196). (f) Expressed size of OXA1L(1-73 aa)-V5-APEX2 (lane 1) and OXA1L(1-435aa)-V5-APEX2 (lane 2) by anti-V5 western blot. Matrix-V5-APEX2 (lane 3) was used as a control for processed size. The size of each construct matched with that expected after cleavage of the N-terminal mitochondrial matrix targeting signal peptide (1-72 aa).

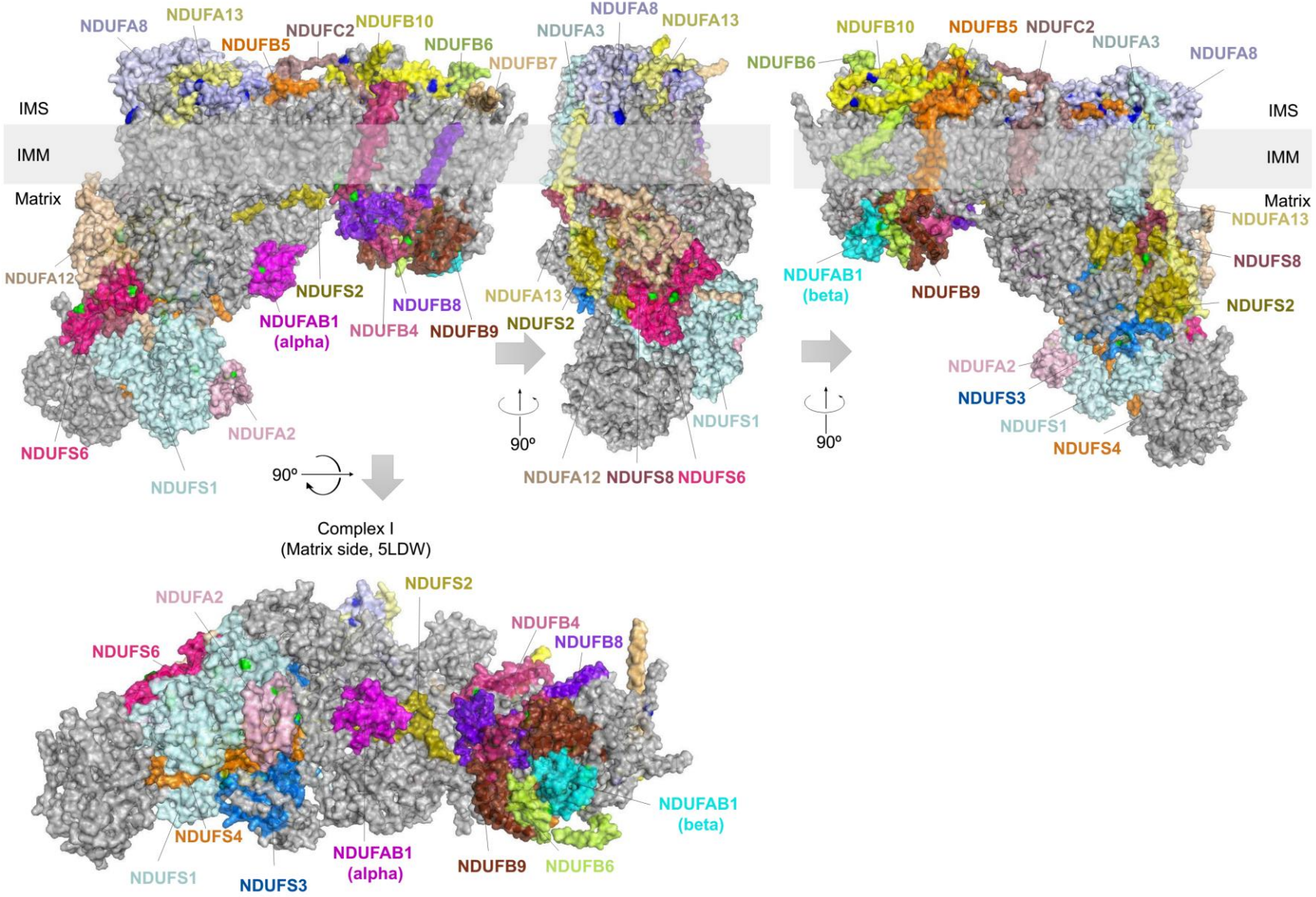
NDUFA8
NDUFA13
NDUFB5
NDUFC2
NDUFB10
NDUFB6
NDUFB7
IMS
IMM
Matrix
NDUFA12
NDUFS2
NDUFAB1
(alpha)
NDUFB8
NDUFB4
NDUFB9
NDUFA2
NDUFS6
NDUFS1
90°
NDUFA3
NDUFA8
NDUFA13
NDUFA13
NDUFS2
NDUFS1
NDUFA12
NDUFS8
NDUFS6
NDUFB10
NDUFB5
NDUFC2
NDUFA3
NDUFA8
NDUFB6
IMS
IMM
Matrix
NDUFA13
NDUFS8
NDUFS2
NDUFAB1
(beta)
NDUFB9
NDUFA2
NDUFS3
NDUFS1
NDUFS4
Complex I
(Matrix side, 5LDW)
NDUFA2
NDUFS2
NDUFB4
NDUFB8
NDUFS6
NDUFAB1
(beta)
NDUFS4
NDUFAB1
(alpha)
NDUFB9
NDUFB6
NDUFS1
NDUFS3

Supporting Figure 10. Expanded view of MS-identified subunits and labeled sites on Complex I. EM structures of Complex I including supernumerary subunits (PDB ID: 5LDW)[9], were shown at different axis. The identified subunits either by Matrix-APEX2 and IMS-APEX2 were colored with various colors. The labeled tyrosine residues by Matrix-APEX2 were colored in green and labeled residues by IMS-APEX2 were colored in blue. Detailed information of the labeled sites and labeled subunits of Complex I were shown in **Supporting Dataset 6**.

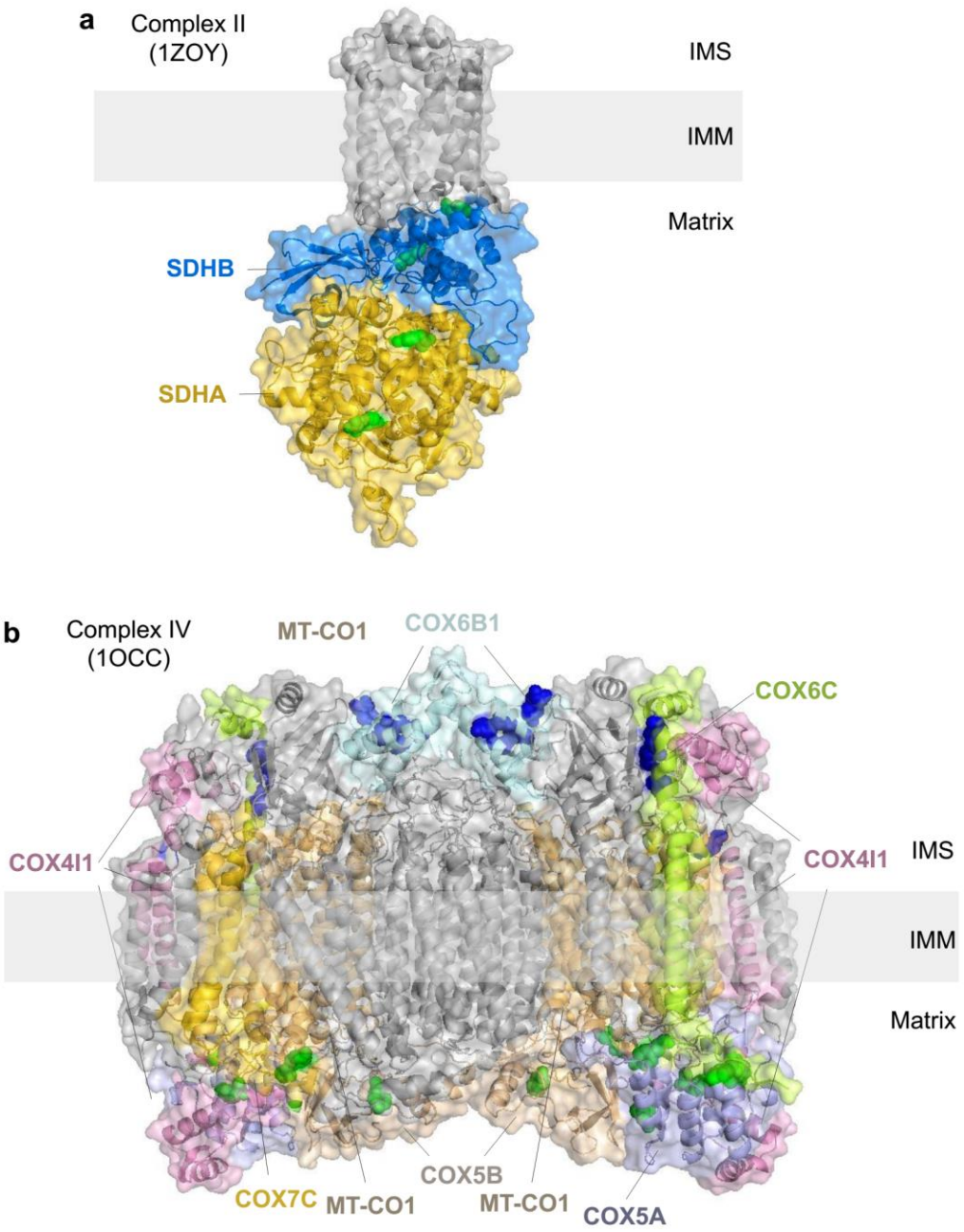

Supporting Figure 11. Expanded view of MS-identified subunits and labeled sites on Complex II and Complex IV. Crystal structures of Complex II (PDB ID: 1ZOY)[10] and Complex IV (PDB ID: 1OCC)[11] were shown. The identified subunits either by Matrix-APEX2 and IMS-APEX2 were colored with various colors. The labeled tyrosine residues by Matrix-APEX2 were colored in green and labeled residues by IMS-APEX2 were colored in blue. Detailed information of the labeled sites and labeled subunits of these complexes shown in **Supporting Dataset 6**.

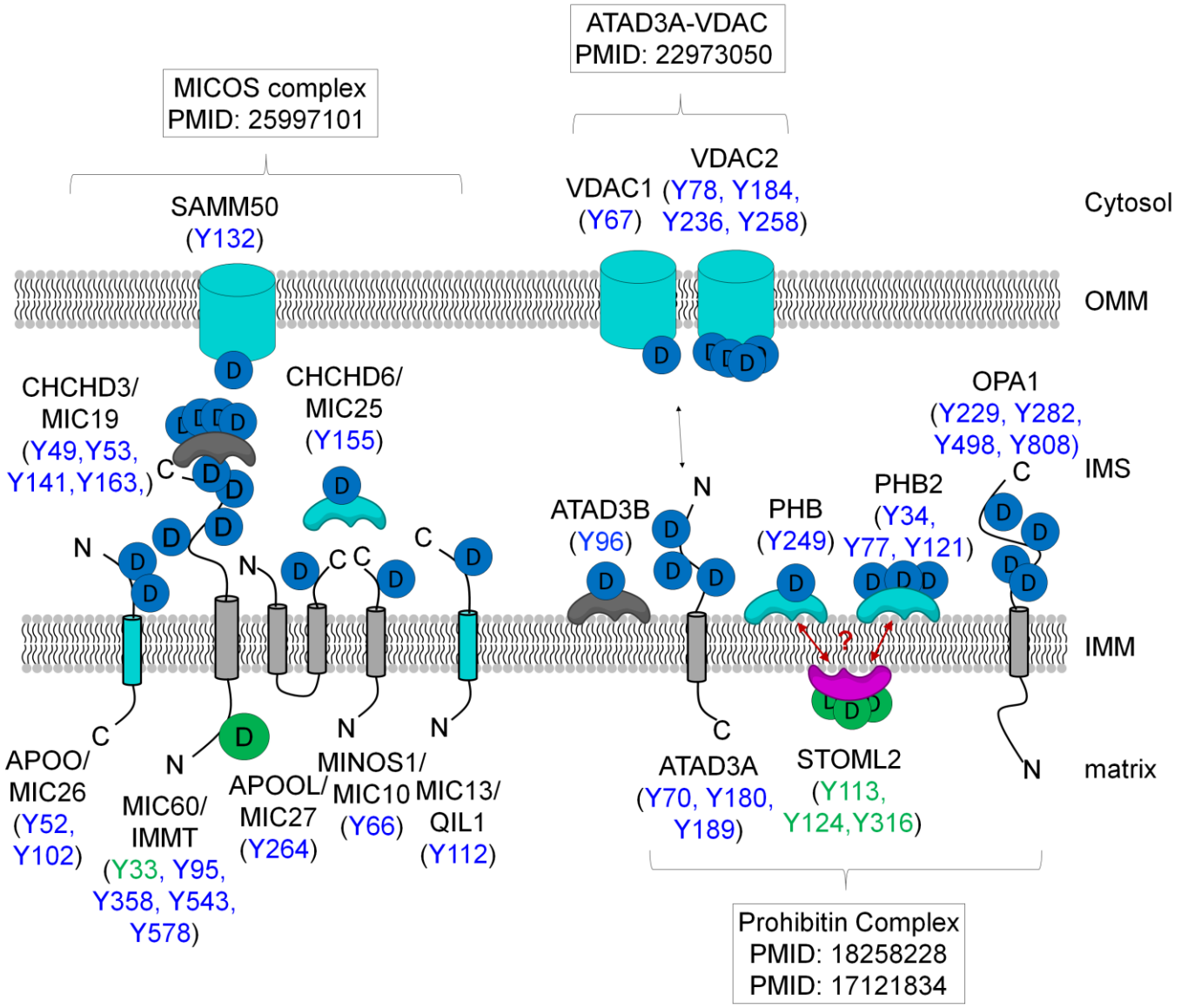

Supporting Figure 12. Proposed topology of protein-protein interaction of identified proteins. Figure legend is shown in the following pages.

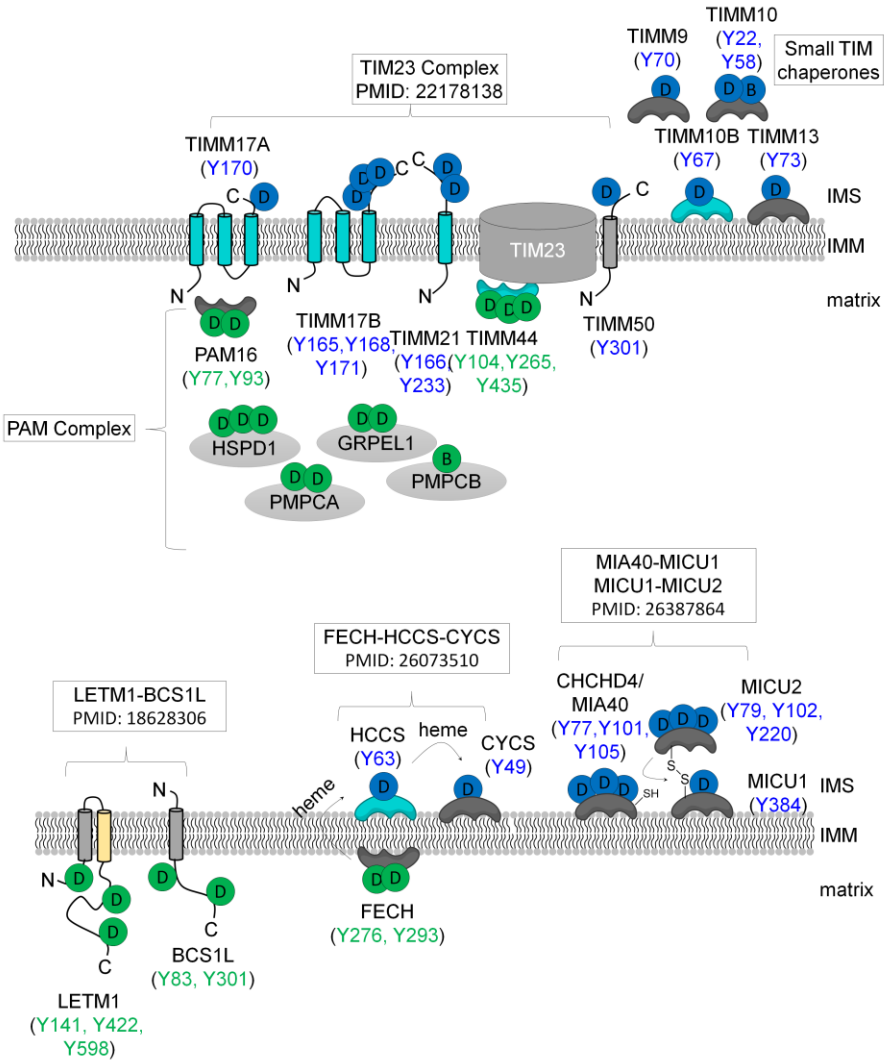
TIM23 Complex
PMID: 22178138
TIMM9
(Y70)
TIMM10
(Y22,
Y58)
Small TIM
chaperones
TIMM17A
(Y170)
TIMM10B
(Y67)
TIMM13
(Y73)
IMS
IMM
matrix
TIM23
TIMM17B
(Y165,Y168,
Y171)
TIMM21
(Y166)
TIMM44
(Y104,Y265,
Y435)
TIMM50
(Y301)
PAM16
(Y77,Y93)
PAM Complex
HSPD1
GRPEL1
PMPCB
PMPCA
MIA40-MICU1
MICU1-MICU2
PMID: 26387864
FECH-HCCS-CYCS
PMID: 26073510
LETM1-BCS1L
PMID: 18628306
CHCHD4/
MIA40
(Y77,Y101,
Y105)
MICU2
(Y79, Y102,
Y220)
HCCS
(Y63)
heme
CYCS
(Y49)
MICU1
(Y384)
FECH
(Y276, Y293)
BCS1L
(Y83, Y301)
LETM1
(Y141, Y422,
Y598)

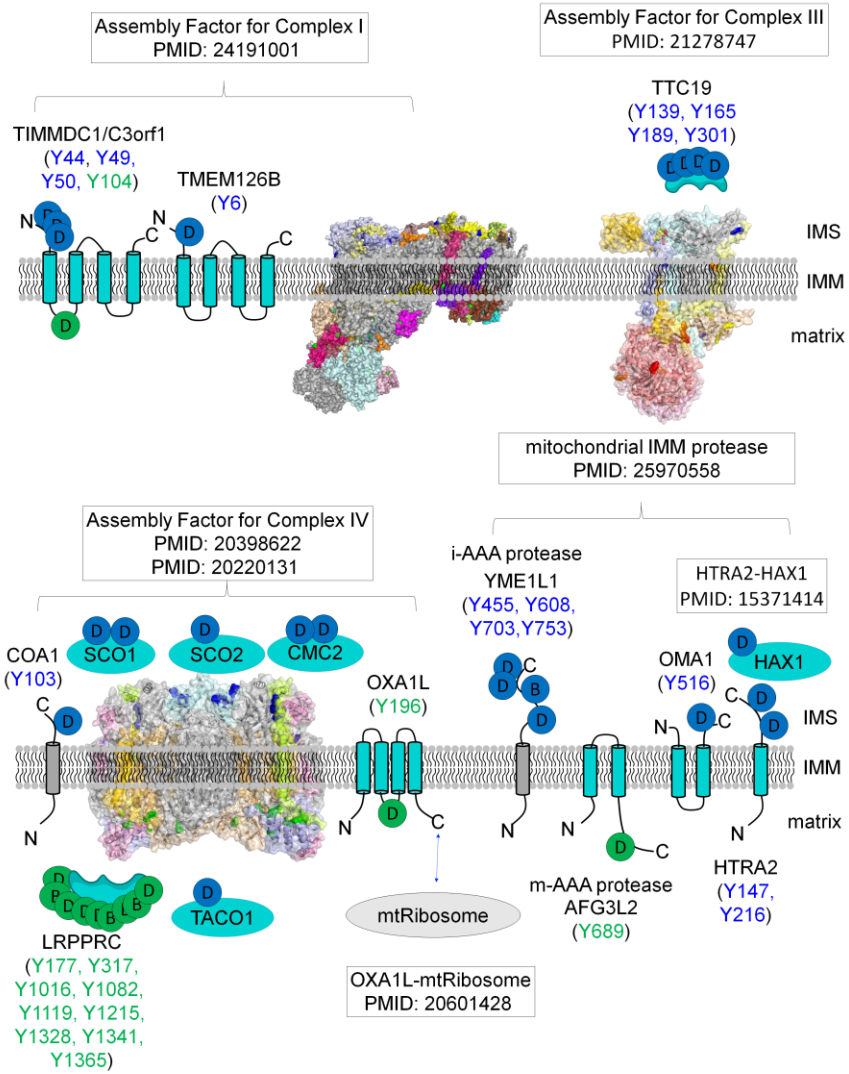
Assembly Factor for Complex I
PMID: 24191001
Assembly Factor for Complex III
PMID: 21278747
TIMMDC1/C3orf1
(Y44, Y49,
Y50, Y104)
TMEM126B
(Y6)
TTC19
(Y139, Y165
Y189, Y301)
IMS
IMM
matrix
mitochondrial IMM protease
PMID: 25970558
Assembly Factor for Complex IV
PMID: 20398622
PMID: 20220131
i-AAA protease
YME1L1
(Y455, Y608,
Y703,Y753)
HTRA2-HAX1
PMID: 15371414
COA1
(Y103)
SCO1
SCO2
CMC2
OXA1L
(Y196)
OMA1
(Y516)
HAX1
HTRA2
(Y147,
Y216)
TACO1
LRPPRC
(Y177, Y317,
Y1016, Y1082,
Y1119, Y1215,
Y1328, Y1341,
Y1365)
mtRibosome
m-AAA protease
AFG3L2
(Y689)
OXA1L-mtRibosome
PMID: 20601428

Supporting Figure 12 (Continued). Proposed topology of protein-protein interaction of identified proteins. Proposed topology of several mitochondrial macromolecular complex at IMM (e.g. MICOS complex, TIM/PAM complex, PHB complex) and reported mitochondrial protein interactions (e.g. Accessory subunits of Complex I, III, IV, LETM1-BCS1L, HCCS-FECH, MIA40-MICU) were shown. The proposed TM direction is shown in blue. The proposed new TM domain is shown in yellow. Matrix-orphan and IMS-orphan proteins are colored in blue. Reference for each mitochondrial protein complex are shown as Pubmed ID (PMID).

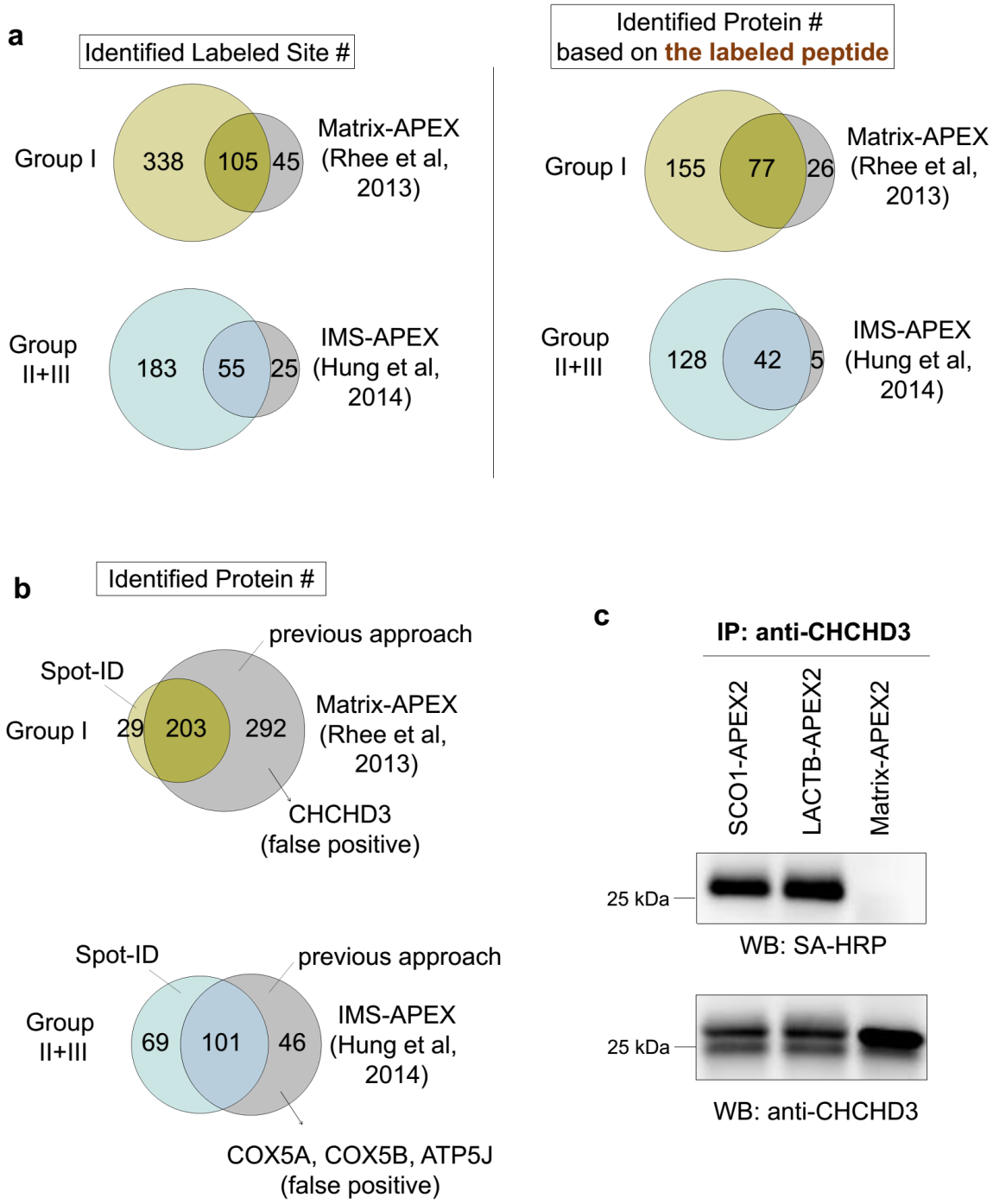

Supporting Figure 13. Comparative analysis with previous mapped data. Figure legend is shown in the following page.

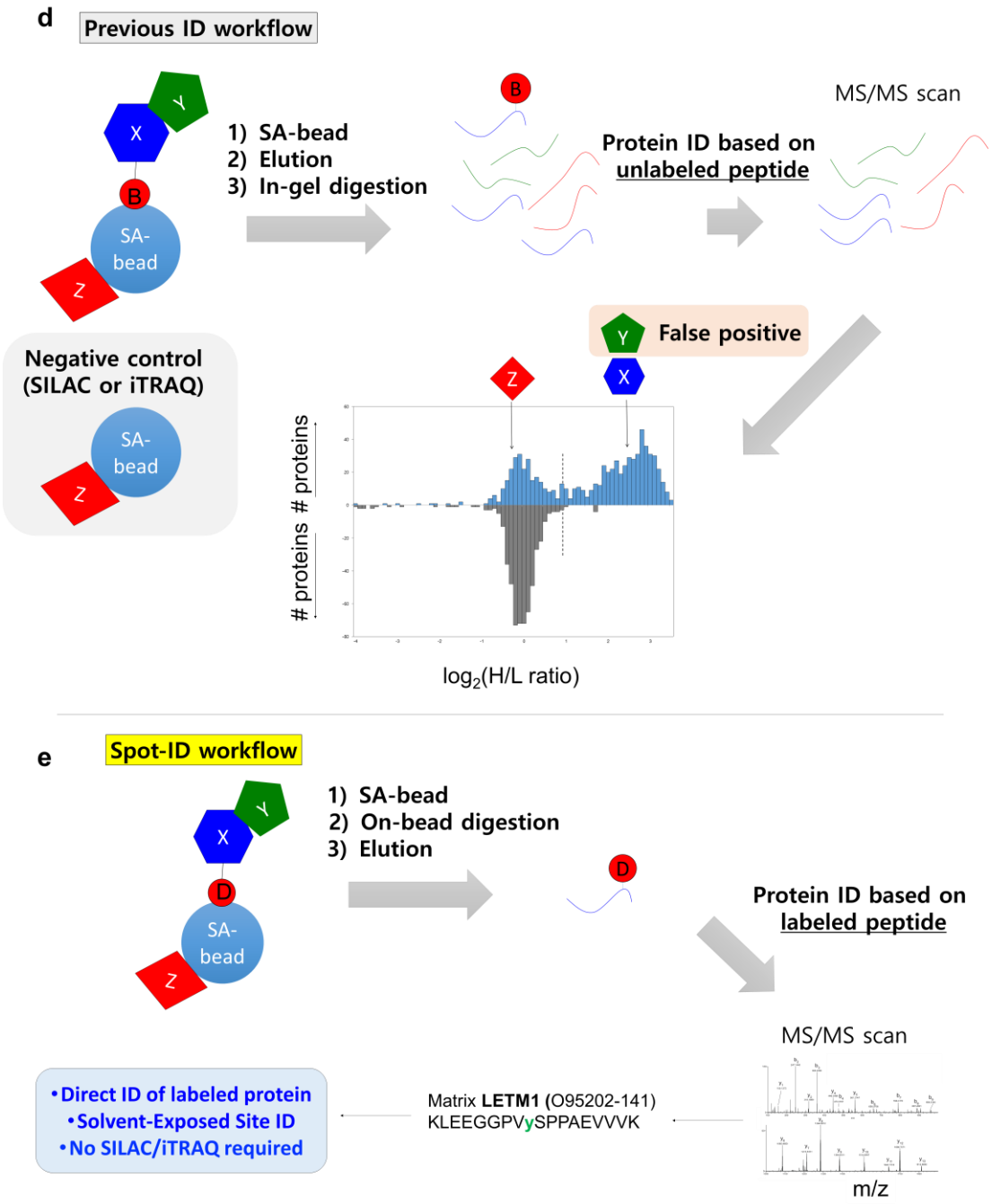

Supporting Figure 13 (Continued). Comparative analysis with previous mapped data (a) Overlaps of the identified DBP-labeled sites and the identified BP-labeled sites in previous studies (left). Overlaps of the identified proteins based on the DBP-labeled sites and the identified proteins based on the BP-labeled sites in previous studies. (b) Overlaps of the proteins identified by our new approach (Spot-ID) and the proteins identified by the previous approach based on the unlabeled peptide in previous studies. (c) Immunoprecipitation assay by using anti-CHCHD3 in SCO1-, LACTB-, and Matrix-APEX2 DBP-labeled samples. DBP-labeled CHCHD3 was only observed in IMS-APEX2s (WB: SA-HRP), Total CHCHD3 was similarly enriched in all of the samples (WB: anti-CHCHD3). (d) Scheme of previous protein ID method by unlabeled peptide (upper). (e) Scheme of current Spot-ID method (below) by labeled peptide.

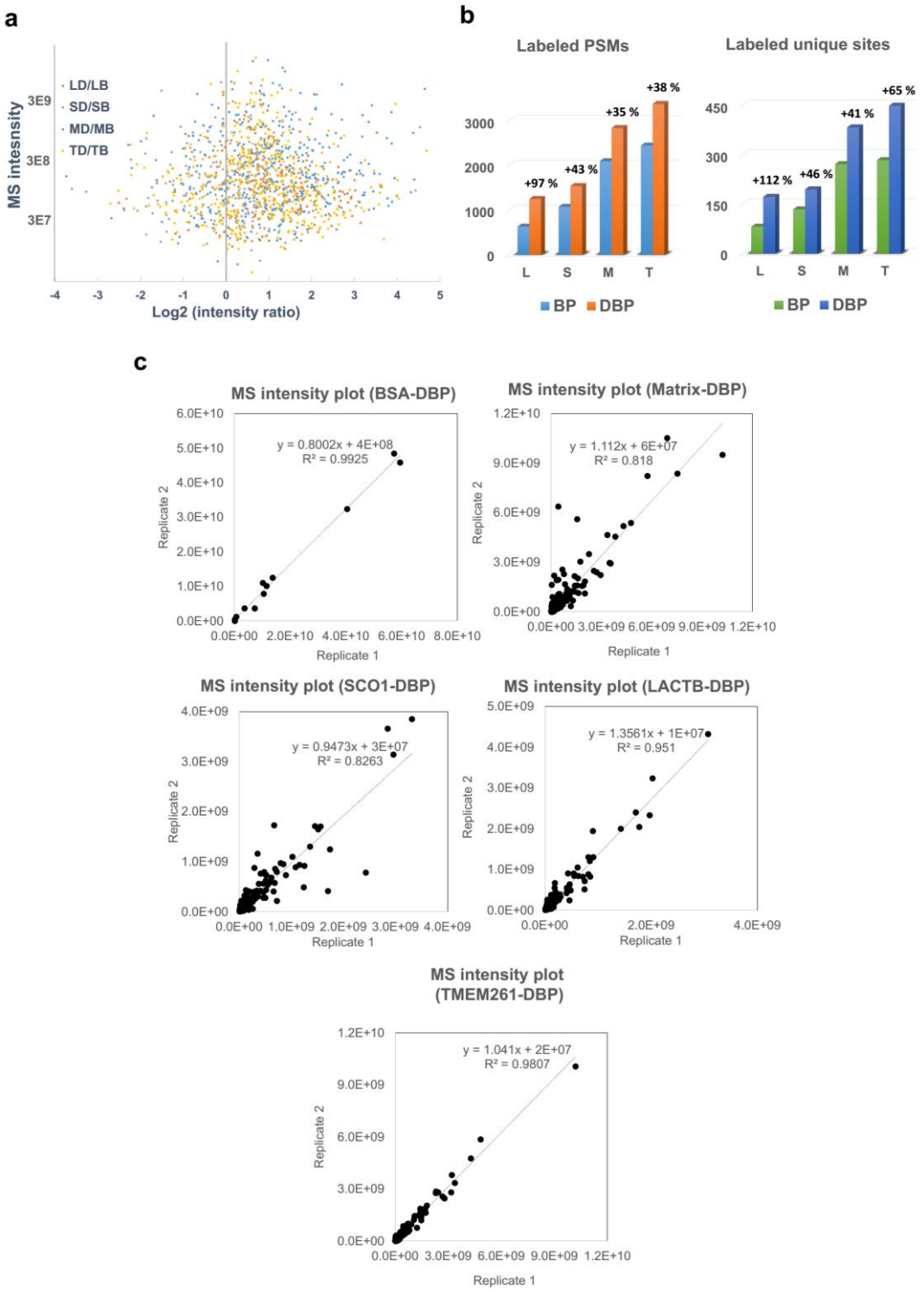

Supporting Figure 14. Scatter plot of MS1 intensity versus intensity ratio of (a) DBP-/BP-labeled peptides and (b) histograms of labeled PSMs and unique labeled sites from human HEK293T cell lines expressed by Matrix-APEX2 (M), LACTB-APEX2 (L), SCO1-APEX2 (S), and TMEM261-V5-APEX2 (T). (c) Reproducibility plots of DBP-labeled peptides between replicate mass samples.

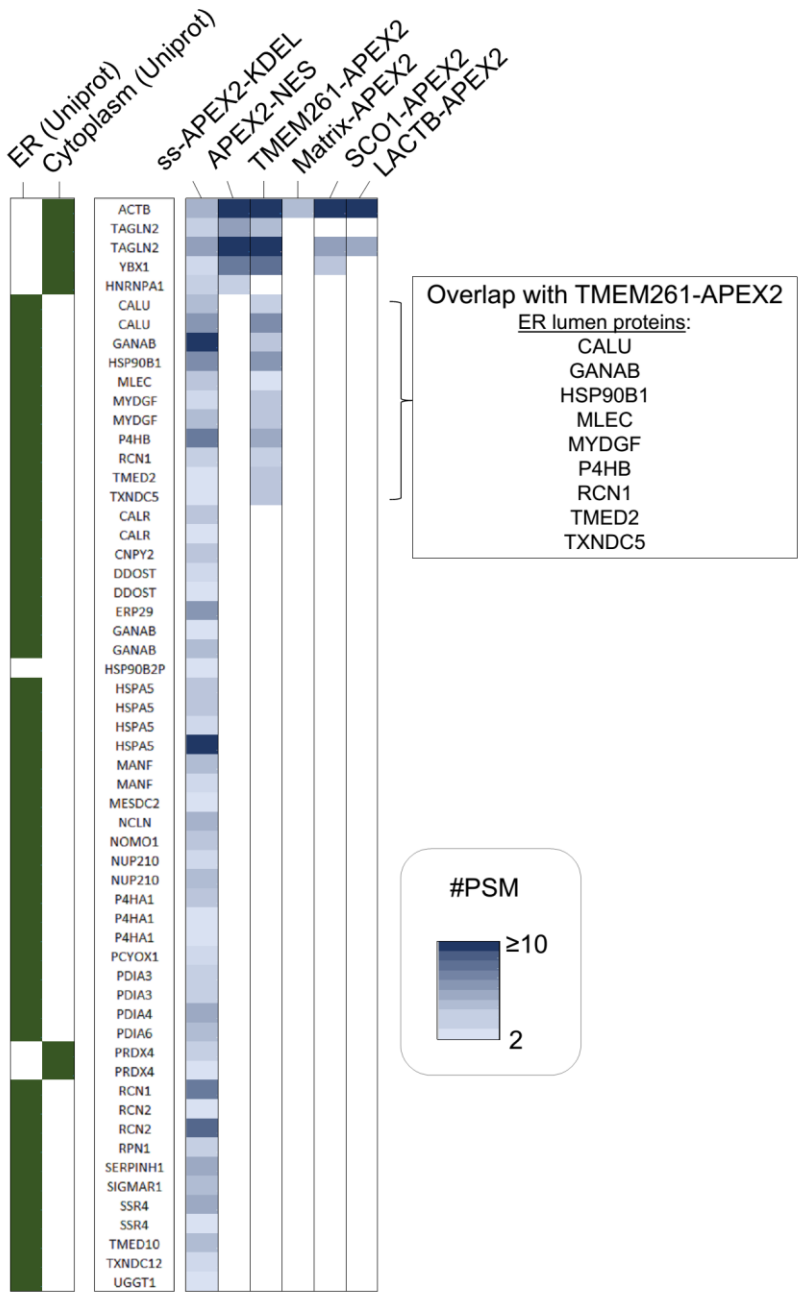

Supporting Figure 15. ER luminal proteome mapping by ss-APEX2-KDEL construct. Overview of 57 DBP-labeled sites by transiently expressed ss-APEX2-KDEL in HEK293T cells. The MS analysis of these labeled sites of ss-APEX2-KDEL were conducted by LTQ-Orbitrap Elite (CID). The table shows the findings for each reproducibly labeled site per biological replicate experiment. The color intensity represents number of peptide spectra match of the labeled peptides per unique labeled site over the replicate experiment. Each labeled site was matched to previous subcellular organelle annotation (e.g. ER and cytoplasm). Detailed information is shown in the **Supporting Dataset 5**.

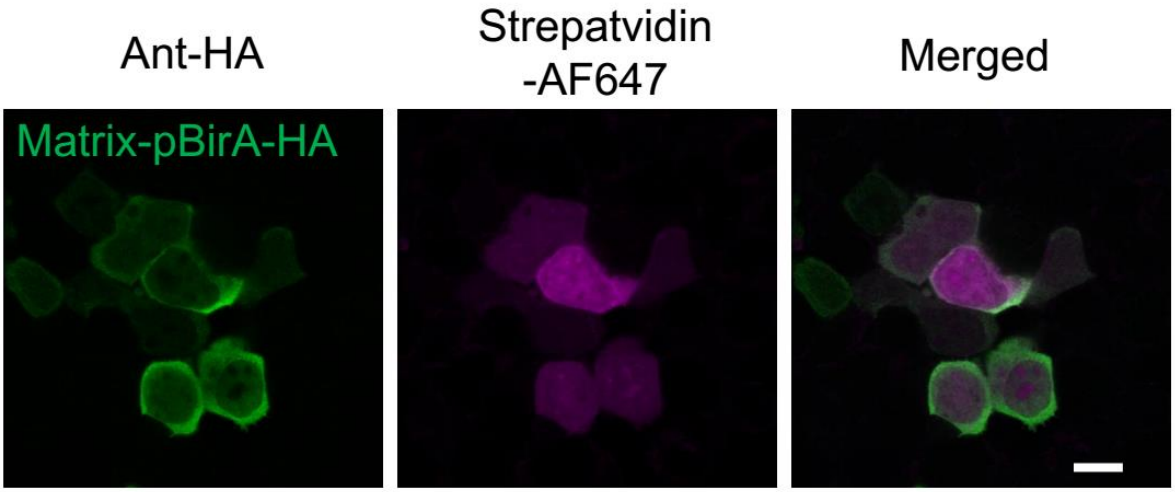

Supporting Figure 16. Imaging assay of Matrix-pBirA-HA construct. Matrix-pBirA-HA was transiently expressed in HEK293T cells by Lipofectamine transfection. After 24 h, cells were fixed and permeabilized. Subcellular localization of Matrix-pBirA-HA was visualized by anti-HA immunofluorescence and its biotinylated pattern was visualized by Streptavidin-AF647. Scale bar = 10 μm.

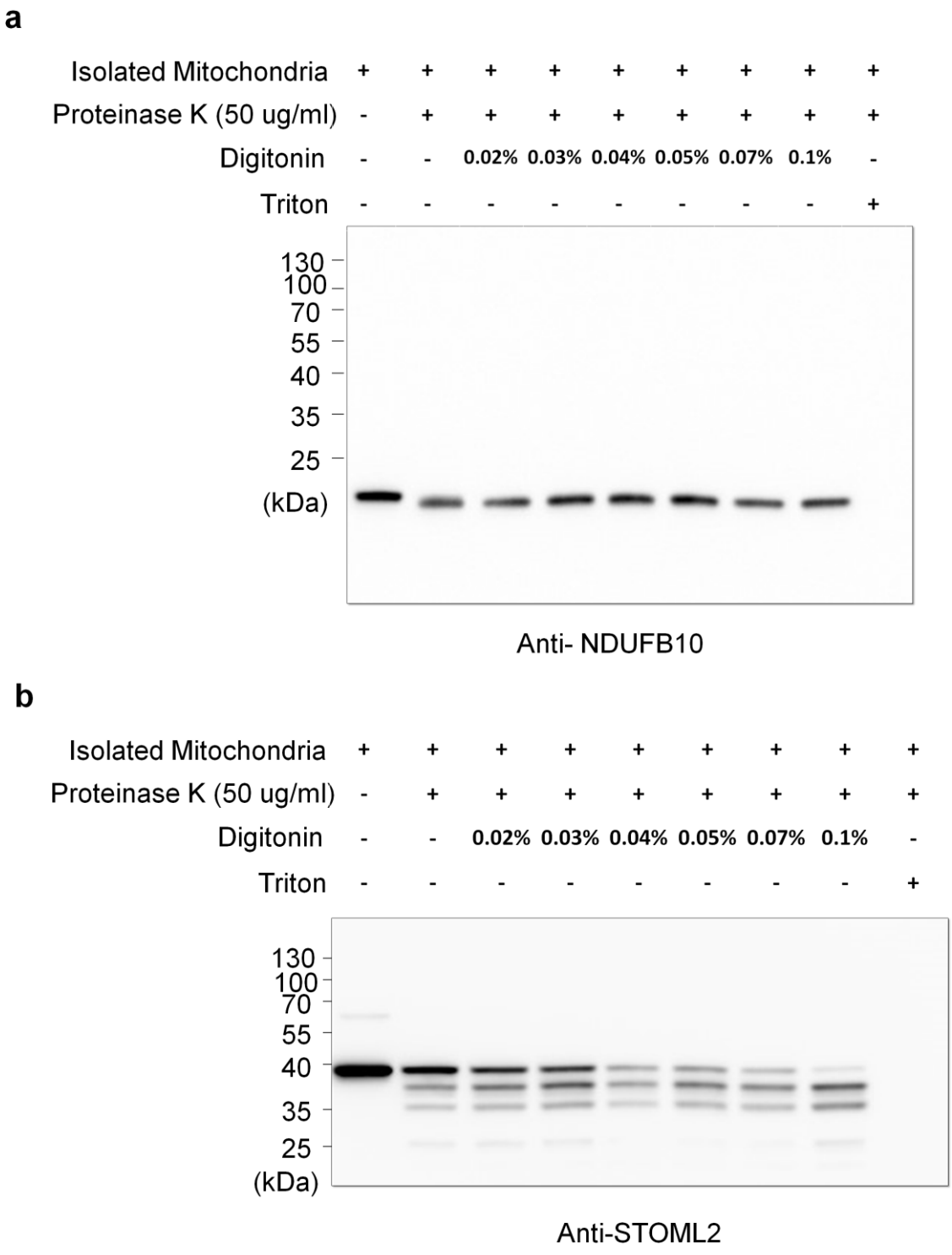

Supporting Figure 17. Proteinase K digestion assay for NDUFB10 and STOML2. Localization analysis was performed according to (Sato and Mihara, 2010). HEK-293T cell crude mitochondria were isolated by Mitochondrial isolation kit (Thermo Fisher). After isolation, the mitochondrial pellet was resuspended in 280mM sucrose with 10mM Hepes buffer (pH 7.2). Isolated mitochondria (10 µg per condition) were treated with different digitonin concentrations (0%-1%) or 1% Triton X-100 along with 50 ug/ml Proteinase K (PK) on the ice for 15 min.

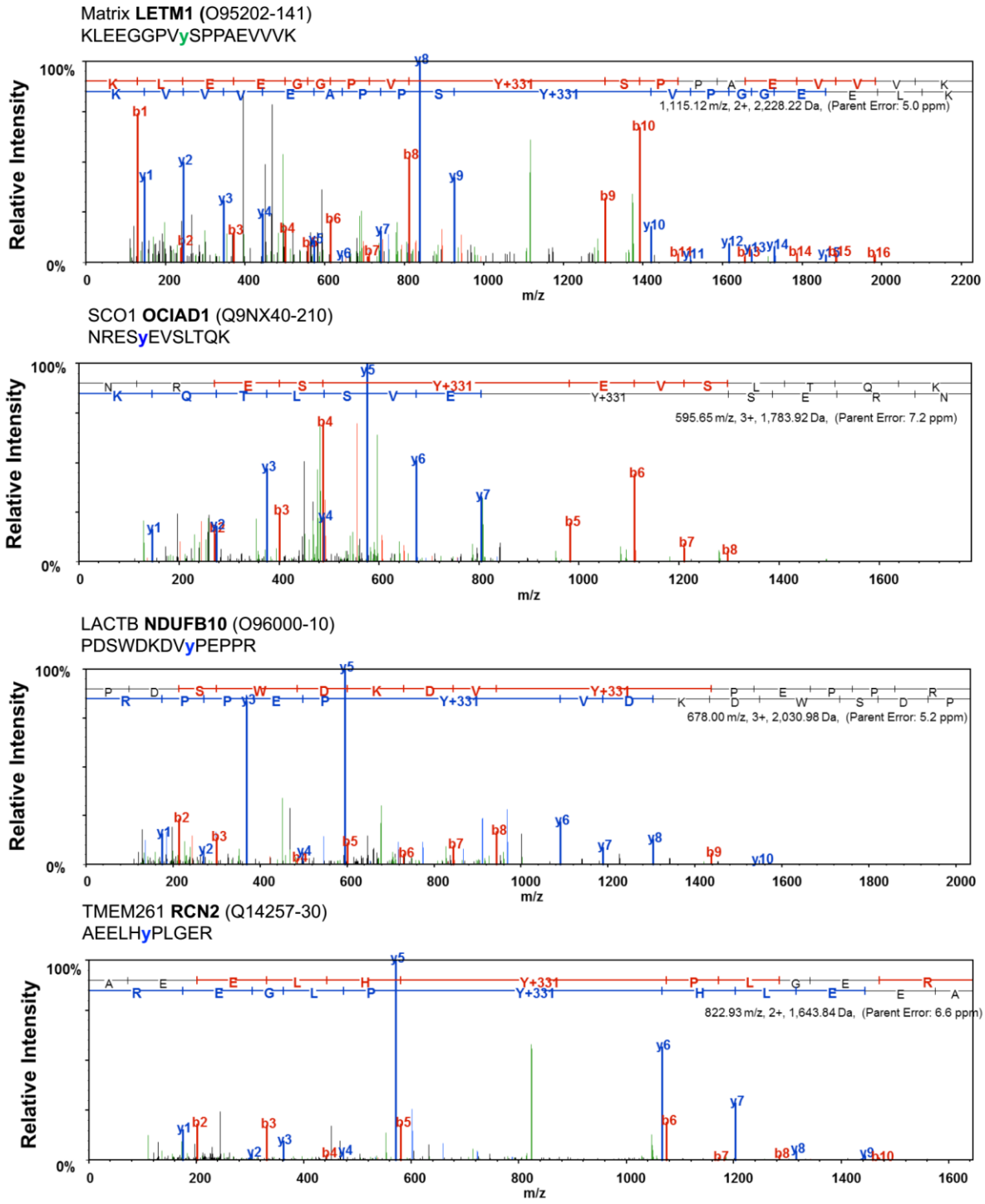

Supporting Figure 18. MS/MS spectra of DBP-labeled peptides. MS/MS spectra of DBP-modified peptide from LETM1 (by Matrix-APEX2), OCIAD1 (by SCO1-APEX2), NDUFB10 (by LACTB-APEX2), and RCN2 (by TMEM261-APEX2) were shown.

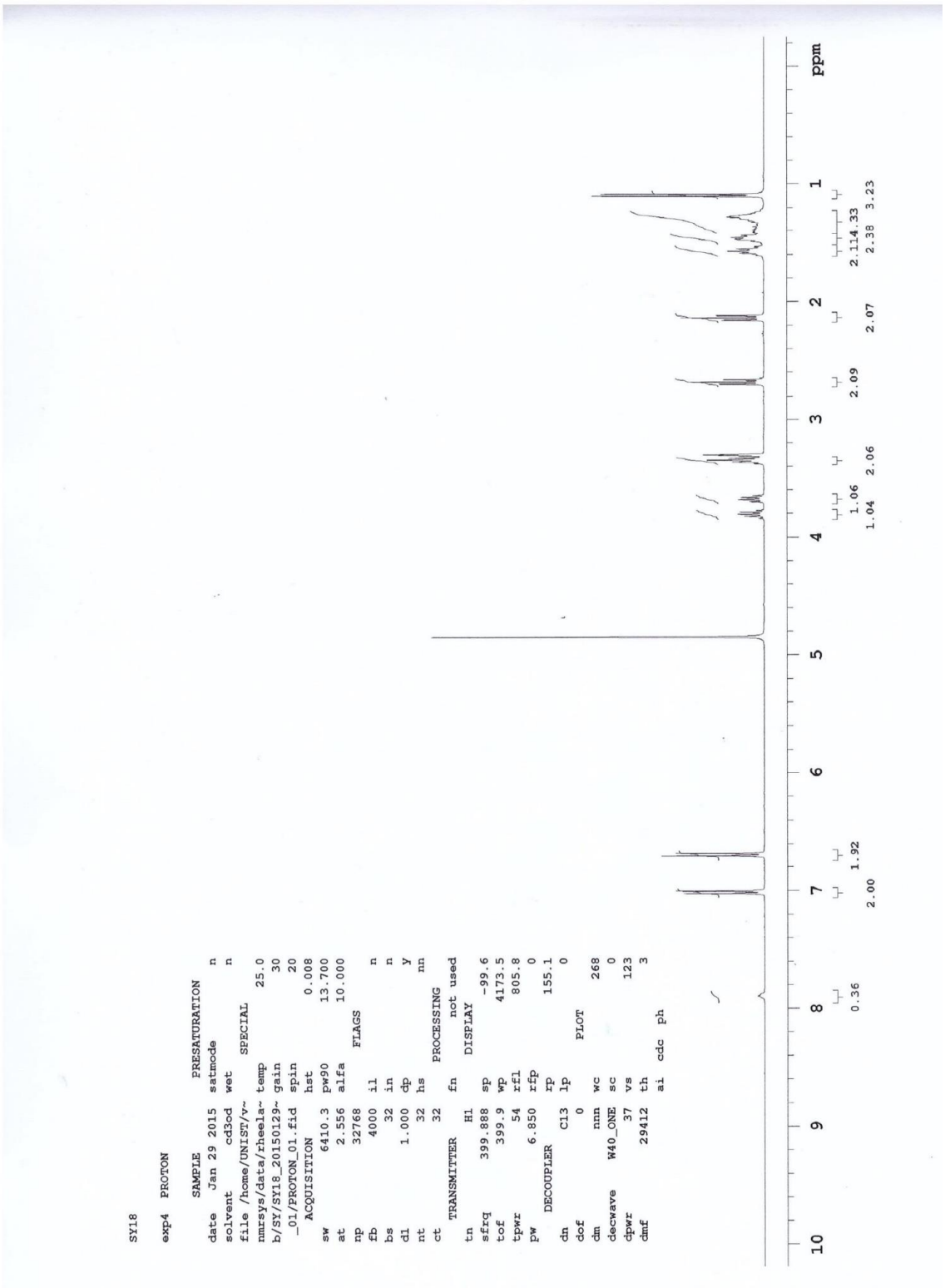

Supporting Figure 19. ^{1}H NMR spectrum of Desthiobiotin phenol (in CD_3OD)

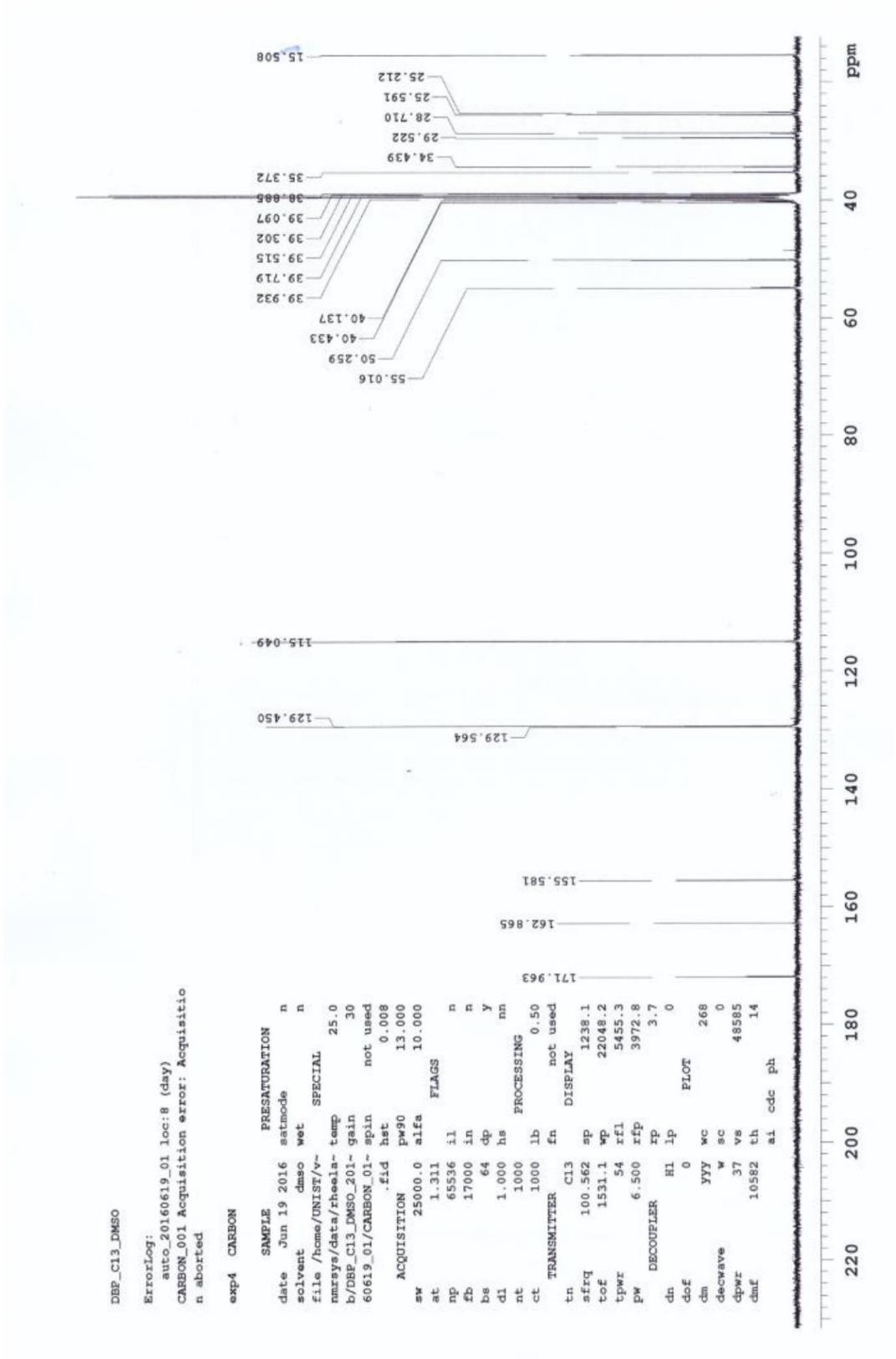

Supporting Figure 20. ^{13}C NMR spectrum of Desthiobiotin phenol (in d_6-DMSO)

References in Supporting Information.

(1) Claros, M. G.; Vincens, P. *Eur. J. Biochem.* **1996**, *241*, 779.

(2) Petersen, T. N.; Brunak, S.; von Heijne, G.; Nielsen, H. *Nat. Methods* **2011**, *8*, 785.

(3) Lee, S. Y.; Kang, M. G.; Park, J. S.; Lee, G.; Ting, A. Y.; Rhee, H. W. *Cell reports* **2016**, *15*, 1837.

(4) Dreyfuss, G.; Kim, V. N.; Kataoka, N. *Nat. Rev. Mol. Cell Biol.* **2002**, *3*, 195.

(5) Mukha, D. V.; Usanov, S. A. *FEBS J.* **2011**, *278*, 469.

(6) Forbes, S. A.; Beare, D.; Gunasekaran, P.; Leung, K.; Bindal, N.; Boutselakis, H.; Ding, M.; Bamford, S.; Cole, C.; Ward, S.; Kok, C. Y.; Jia, M.; De, T.; Teague, J. W.; Stratton, M. R.; McDermott, U.; Campbell, P. J. *Nucleic Acids Res.* **2015**, *43*, D805.

(7) Bryant, K. L.; Mancias, J. D.; Kimmelman, A. C.; Der, C. J. *Trends Biochem. Sci.* **2014**, *39*, 91.

(8) Cserzo, M.; Wallin, E.; Simon, I.; von Heijne, G.; Elofsson, A. *Protein Eng.* **1997**, *10*, 673.

(9) Zhu, J.; Vinothkumar, K. R.; Hirst, J. *Nature* **2016**, *536*, 354.

(10) Sun, F.; Huo, X.; Zhai, Y. J.; Wang, A. J.; Xu, J. X.; Su, D.; Bartlam, M.; Rao, Z. H. *Cell* **2005**, *121*, 1043.

(11) Tsukihara, T.; Aoyama, H.; Yamashita, E.; Tomizaki, T.; Yamaguchi, H.; ShinzawaItoh, K.; Nakashima, R.; Yaono, R.; Yoshikawa, S. *Science* **1996**, *272*, 1136.